論文 / 著書情報
Article / Book Information

題目(和文)	画像転写ベルト系の振動抑制のためのモデル化と制御
Title(English)	Modeling and Control for Vibration Attenuation in Image Transfer Belt System
著者(和文)	YuJie
Author(English)	Jie Yu
出典(和文)	学位:博士（学術）, 学位授与機関:東京工業大学, 報告番号:甲第9918号, 授与年月日:2015年3月26日, 学位の種別:課程博士, 審査員:山浦　弘,伊能　教夫,大熊　政明,山北　昌毅,中島　求
Citation(English)	Degree:, Conferring organization: Tokyo Institute of Technology, Report number:甲第9918号, Conferred date:2015/3/26, Degree Type:Course doctor, Examiner:,,,,
学位種別(和文)	博士論文
Type(English)	Doctoral Thesis

DOCTORAL DISSERTATAION

Modeling and Control for Vibration Attenuation in Image Transfer Belt System

A thesis submitted for the degree of

Doctor of Philosophy in Mechanical and Control Engineering

December, 2014

Jie Yu

Supervisor: Professor Hiroshi Yamaura

東京工業大学
Tokyo Institute of Technology

Department of Mechanical and Control Engineering

Graduate School of Science and Engineering

Tokyo Institute of Technology

Acknowledgements

I would like to express my deepest gratitude to Professor Hiroshi Yamaura at Department of Mechanical and Control Engineering, Graduate School of Science and Engineering, Tokyo Institute of Technology, who provided me this opportunity to conduct this research. Plenty of his penetrating questions and guidance led me to deeper understanding and investigation of this topic. Additionally, his help with internship in Japanese corporation, attending conferences, and life in Japan is highly appreciated.

I would like to show my great appreciation to Assistant Professor Hara of this laboratory. Although period spent with him is not long, I learnt a lot from him during discussions. His advice for experimental design and review of some papers of mine contributed much to this work.

I would like to declare my gratitude to former Assistant Professor Huang at Department of Mechanical and Control Engineering, Tokyo Institute of Technology. His suggestions and guide on control theory and motor actuation enlightened me when facing some difficulties.

I would like to say a lot of thanks to my labmates including people who already graduated. Their names are not list here due to lack of space. Life and study shared with their are quite joyful. And without their help this work can not be conducted smoothly.

I would like to thank all my friends for their generous help and advice. Conversations, visits and play with them made life more colourful. I also want to show my appreciations to people who cared and helped me a lot in Japan.

Meanwhile, I would like to thank the Japanese Government (Mobusho) for providing scholarship during my doctoral study.

Part of this research is carried out cooperating with Fuji Xerox Co., Ltd. And I would like to express special appreciations to fellows who gave extremely useful advice and help during this research and internship.

Last but not the least, I want to dedicate this work and my deepest love to my parents for their selfless support and love. They went through all the hardness with me both in research and life. I might be a piece of work sometimes, but they never abandon me and help me find the confidence. Their wisdom inspire me to investigate the world and carry on with my dream. And let the more loving one be me this time.

Contents

List of Figures

List of Tables

Chapter 1

Introduction

1.1 Background

1.1.1 History of Printing

Modern society is consuming enormous printing products nowadays, from standard size books, newspapers to increased size commercial posters. It is quite fair to say that printing and its derivatives possess significant positions in the history of culture communication in human society since they have realized promoting literacy among the masses [1].

The history of printing actually can go back to a very early time when the procedure is simply the duplication of images by means of stamps, for example, round seals for rolling an impression into clay tablets in the early Mesopotamian civilization. The early principles of printing vary in different parts of the world to meet needs of people in different eras. Ancient China and Egypt used small seals and larger blocks, Europe and India printed on cloth like silk otherwise [2].

During the early century from 2^{nd} to 12^{th}, the East Asia took the lead in invention of printing which is a striking achievement of Buddhists. The world earliest known printed document is a sutra printed on a single sheet of paper in Korea in 750[1]. And it is closely followed in Japan during 768 that the empress commissioned a huge edition of a lucky charm prayer. Following in 868, the world earliest known printed book is a scroll in Chinese, discovered in a cave at

[1]Part of the informations are referred to website: http://www.historyworld.net

Dunhuang [3]. In Chinese publishing history, printing from wood blocks between 10^{th} and 11^{th} century were used for scholar officials [4]. However this kind of printing technology requires enormous investment of labour that inspired the movable type achieved in Korea in early 11^{th}.

More than six centuries after its invention in the East Asia, the technique of printing from wood blocks is introduced in Europe in about 1400 [5]. However it is not until the 15^{th} century then the technical advances are made in Germany rapidly. Johann Gutenberg (1400-1468) of Mainz, Germany is thought to be the key figure in the history of European printing. One of his achievements is the development of the printing press which is capable of applying a rapid but steady downward pressure. More significant are Gutenbergs skills with mental that enables him to master the complex stages in the manufacturing. The most well-known printouts could be the Gutenberg Bible which was printed simultaneously on six presses during the middle 1450 [6].

The first printing process to achieve a fully tonal effect is pioneered in the late 1650 by prince Rupert of the Rhine [7]. It is immediately given a name reflecting its ability to print halftones, the mezzotint. With this technology, printers of the 17^{th} and 18^{th} centuries can reproduce in fairly large numbers at a cost which remains high but still much less than the previous oil copies. In 1798, Alois Senefelder makes a discovery of profound significance in the history of artist's prints and later of commercial printing too and names it as lithography. This technique pioneered the next stage which is the chromolithograph that can print in several colours. The chromolithograph is a characteristic feature of the 19^{th} century commercial printing. The expansion of books and newspaper businesses in Britain and mechanical technologies enlightens the rotary printing press and offset printing during 1900 [8]. The former style curve the image to be printed around a cylinder that is also referred as rotary drum. The latter transfers the inked image from a plate to a rubber blanket, then to the printing surface. These two techniques are still widely applied in the newspapers industry nowadays with several improvements.

The key technique that allows most of the people access to massive and fast printing is xerography which is also called electrophotography (EP) based on its characteristic. This dry photocopying technique is invented by Chester Carlson

in 1938, for which he was awarded U. S. Patent 2,297691 in October, 1942 [9]. It is now used in most photocopying machines, and led to laser printing and printers. The development of computer provides the realizing chance to inkjet printing around 1951. This price varied type of printer recreates digital images by propelling droplets of ink onto printing substrates, and led to the massive products in digital printing with xerography.

Another technique invention that is now discussed most is the 3D printing. This additive manufacturing is the various process for printing a three-dimensional object developed in 1980 [10]. Unlike the other printing techniques mentioned above, the 3D printing is not limited in media industry but provided with promising applications in industrial robot, automobile, construction, and even medical.

To make readers more clearer about the chronicle of printing development, Table 1.1 lists name, approximate period, and inventors of most of the printing technologies. Moreover Fig. 1.1 shows images of some of the significant ones.

Table 1.1: Part of some techniques in printing history

technique	year	inventors
woodblock printing	200 CE	unknown
movable type	1040	Korean
printing press	1450	Johann Gutenberg
mezzotint	1650	prince Rupert of the Rhine
lithography	1798	Alois Senefelder
chromolithography	1837	Godefroy Engelmann
rotary press	1843	Richard March Hoe
offset printing	1875	Robert Barclay
xerography	1938	Chester Carlson
inkjet printing	1951	unknown, developed by Epson, HP and Canon
3D printing	1984	Chuck Hull

Some of the inventors are remained ambiguous in Table 1.1, like the movable style. It is inspired by Chinese but realized in Korea. Also the inventors list here are based on the patents declaration although some of the original ideas are not from them. The concept of inkjet printing originated in the 19^{th} century, but it was not until late 1970 then the computers that can reproduce digital images

haven been developed. This is mainly conducted by Epson, Hewlett-Packard (HP), and Canon.

(a) royal inscription of naram-sîn, printing block

(b) the Diamond Sutra, woodblock printing

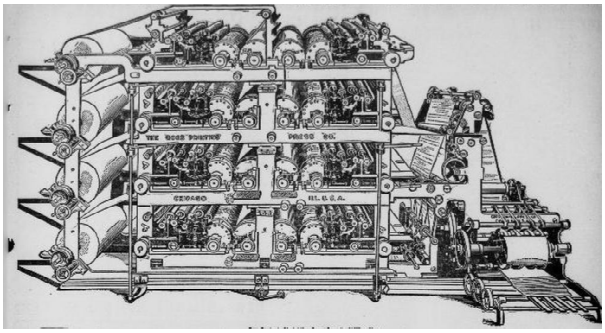

(c) the herald's two great printing presses, rotary printing

(d) phaser 7800 in Fuji Xerox products, xerography

Figure 1.1: Images of some of the significant printing technologies and their products

The printing in Fig. 1.1 (a)[1] actually appears around 2291 to 2254 BC in Sumer. The intricate frontispiece of the Diamond Sutra shown in Fig. 1.1 (b)[2]

[1]Source from website http://archaicwonder.tumblr.com
[2]Source from Wikipedia

is the known as the world's earliest dated printed book, now exhibited in British Museum. Fig. 1.1 (c)[1] was originally printed in the Los Angeles Herald on December 17, 1905 as a company illustration probably. And Fig. 1.1 (d)[2] is obviously one production from Fuji Xerox Co., Ltd, named as Phaser 7800 which won the Australian Business Awards 2012.

1.1.2 Xerography and Image Transfer Belt

As introduced previously, history of xerography is less than one hundred years. However the invention is quite unique that combines electrostatic printing with photography. The original process of the inventor Carlson's work was recorded as cumbersome, requiring several manual processing steps [11]. Improvements have been applied to the original process, and it finally evolved into six fundamental stages: charging, exposing, developing, transferring, fusing and cleaning [12]. Fig. 1.2 depicts detailed movements of the six stages inside one xerography printer or copier.

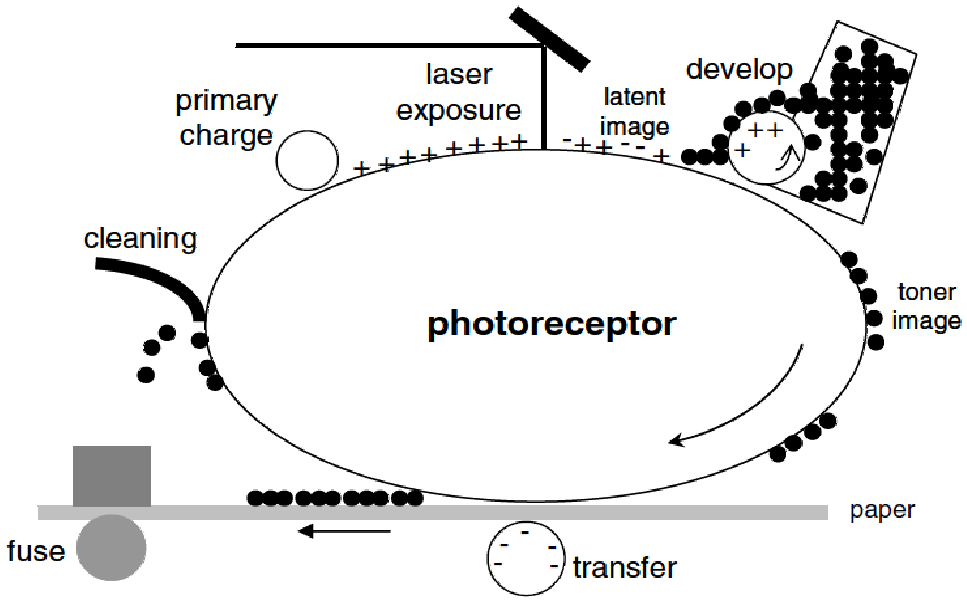

Figure 1.2: Six stages in one cycle of xerography

[1]Source from Wikipedia
[2]Source from Fuji Xerox. Co., Ltd homepage

Before explaining each stage, there are several terminologies need to illustrate first:

photoreceptor: a flexible belt or drum consists of a thin layer of photoconductive material which becomes more electrically conductive due to the absorption of electromagnetic radiation. This allows the photoreceptor remain insulating in the dark, but become conducting when exposed to light [13].

toner: pigmented power used to develop the image. Toner particles made of colorant and plastic resin have precisely controlled electrostatic properties and range from about five to ten micrometers in diameter [14].

Then the procedure is explained as following:

charging: A high direct-current (DC) voltage will charge the surface of the photoreceptor averagely, creating an electric field across it [15].

exposure: a laser beam with a polygon mirror to reflect the beam is used to expose the image on the photoreceptor. The areas of the photoreceptor exposed to light are selectively discharged, causing a reduction in the electric field leaving the darker areas retain their charge. During this stage, the printed image information is carried onto photoreceptor and denoted as latent image.

developing: the electric field from charge toner associated with charge pattern of the image on photoreceptor exerts an electrostatic force on toner, which adheres to the image. The formed power image is called toner image.

transferring: the toner image is transferred from photoreceptor onto paper which is charged with polarity opposite to toner.

fusing: toner comprising the image is melted and bonded to paper by passing the paper through a pair of rollers providing both heat and pressure.

cleaning: the residual toner is removed from photoreceptor preparing for the next print cycle.

When concerning to colour printing, this cycle is conducted and synchronized for four times according to the modern colour printing techniques [16–18]. Each cycle forms different monochrome toner image which are cyan (C), magenta (M), yellow (Y) and black (K). Colour dots in each toner image are precisely adjusted before developing by the upper microprocessor [19]. Superposition of these toner images produces full-colour printouts through various position and density of colour dots [20–24].

To achieve massive colour printing in a short period, image transfer belt is introduced into colour printing process. Instead of transferring the toner image directly to paper or other printing medium, each monochrome toner image is firstly adheres onto an intermediate transfer belt (ITB) where the superposition is carried out [25]. The full-colour toner image is then applied onto final printing medium [26–28].

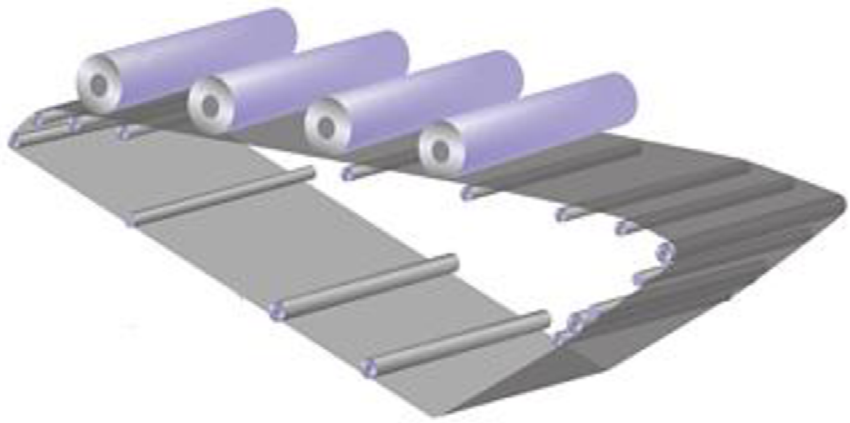

Figure 1.3: Image transfer belt with photoreceptors

Fig. 1.3[1] is a typical image transfer belt with four photoreceptors posed above the belt. This kind of apparatus first appeared in United States Patent No. 4,684,238 with a rough prototype invented by Henry R. Till, and others in August, 1987 [29]. The original purpose of this belt is simply providing an intermediate receiver from a photoconductive member to a copy sheet, according to the authors. And no full-colour printing application seems involved in the patent. Yet like the authors claimed, "While this invention has been described in conjunction with a specific embodiment thereof, it is evident that many alternatives, modifications, and variations will be apparent to those skilled in the art", the image transfer belt unit has been through plenty of improvements and now appearing in most of the large-scale, high-speed printers and copiers.

[1]Source from Fuji Xerox Co., homepage

1.2 Review

1.2.1 Studies on Intermediate Transfer Belt (ITB) and Belt Misalignment Control

Additional parts have been placed onto image transfer belt after its appearance in full-colour printers. And one of the most considered issues is belt tension adjustment [30–33].

David P. Bujese first described a belt tension apparatus in U. S. Patent No. 5,285,244 as a combination of belt tensioning roller and an air cylinder functioning as an actuator to alter tensile force applied on the belt [34].

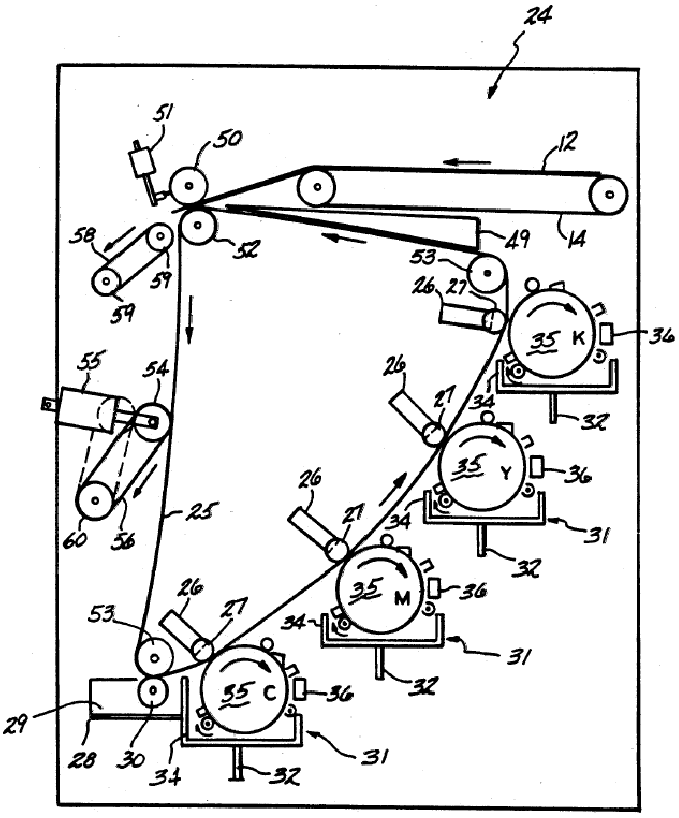

Figure 1.4: Invention of David P. Bujese from U. S. Patent No. 5,285,244

Fig. 1.4 is part of the description from David's work. The tension apparatus is located above the belt on the left side numbered as 54, 55. Air cylinder 55

provides actuating torque to tension roller 54 that contacts with ITB 25. The belt is thus adjustable maintained in constant tension or may be adjusted to provide the slack to permit replacement of the conductive ITB. Also in his invention, the tension roller 54 is designed for another usage that is driving the belt cleaning web 56 with the idler roller 60 to wipe out the useless toner from ITB. This kind of tension roller is employed in many ITB designs though the air cylinder has been redesigned and replaced by other apparatus.

In David's invention, the belt is directly rotating around the four toners that may lead to the scattering of toner. One cause of this phenomenon is so-called pre-transferring that refers the transfer of toner from the photoconductive element to the belt occurring at a position upstream of the nip between the element and the belt in the direction of movement of the element. This problem first came up in U. S. Patent No. 6,212,351 B1 and was deal with a unique solution by Katsuya Kawagoe, and others [35].

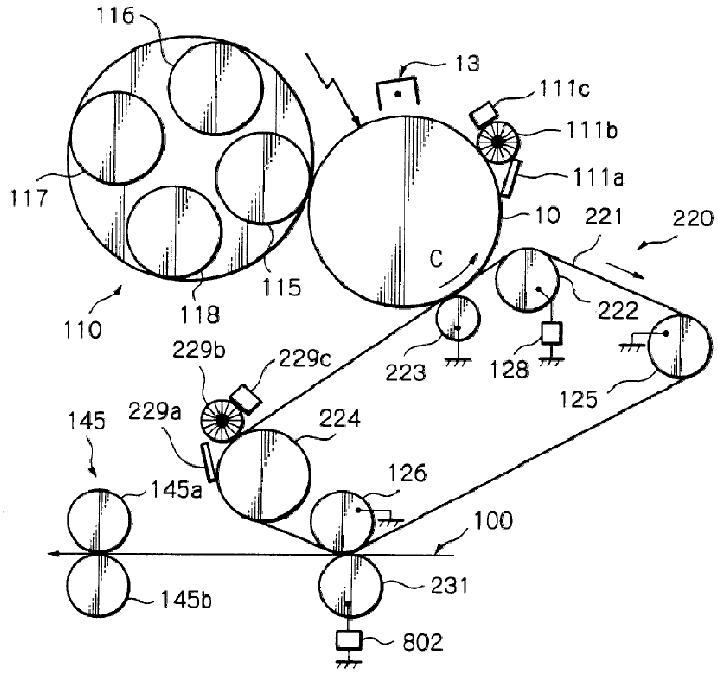

Figure 1.5: Invention of Katsuya Kawagoe, and others from U. S. Patent No. 6,212,351 B1

Fig. 1.5 presents the alternative path of ITB in Kawagoe's proposal. In their

work, there is an additional image carrier 10 to prevent the pre-transferring from the toner to the belt. Therefore the belt is not wrapped around the discharging member involved in the exposure stage. It prevents the belt from curling along the circumference of the discharging member even when left unused over a long time, since a curled belt would vary the image transfer condition and would thereby bring about a defective image ascribable to irregular image transfer. Also they applied the tension roller 125 in the designing but not mentioned much about the tensioning torque provider.

Another representative modification on the image transfer belt is recorded in U. S. Patent No. 8,064,797 B2 submitted by Shinichi Sugiyama [36]. The belt is still positioned along with the photoreceptor. An operation member is located on the support frame with three different positions to adjust the tensile force applied on the belt. The first position of this operation member is shown in Fig. 1.6.

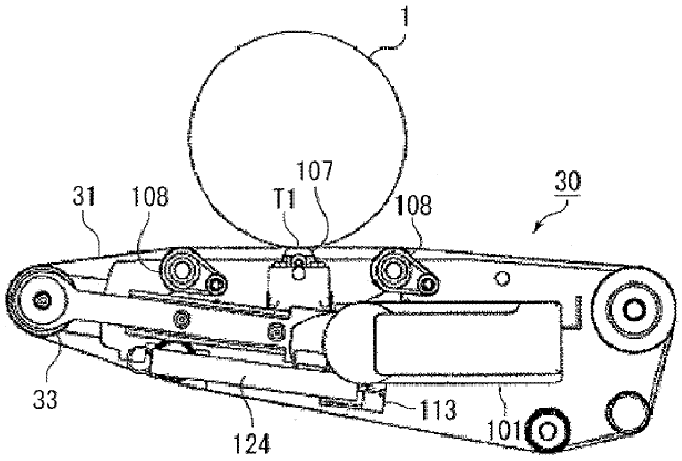

Figure 1.6: Invention of Shinichi Sugiyama from U. S. Patent No. 8,064,797 B2, the first position

In his design, to avoid the actuator part, the transfer roller 107 press-contacts the photosensitive drum 1 via ITB 31 to form a primary transfer portion that sandwiches the belt contacting the toner image on the photosensitive drum. To release and adjust the tensile force, a slider 113 latched with one end of a spring 124 is held to be movable linearly on a slide rail mounted on the frame along with the operation lever 101. The other end of the spring 124 is connected to

the tension roller 33 that is part of the belt supporters. As a result, the tension roller 33 applies a tensile force to ITB 31 by the biasing force of the spring 124. The tensile force applied to ITB 31 can be released by linearly moving the slider 113 inwards against the biasing force of the spring 124 to reduce protrusion of the tension roller 33. And the large operation lever 101 is used as a handle for both pulling out and carrying the belt unit. In Fig. 1.6, the lever 101 is turned horizontally right to a press-contact position that allows the tight contact between ITB 31 and the photosensitive drum 1. When the lever 101 is turned vertically down to the separate position, the slider 113 applies a predetermined tensile force to the belt through the spring 124 that separate the belt and the photosensitive drum 1. At this working status, no toner image can be transferred onto the belt. Again when the lever 101 is turned horizontally left to the release position, the tensile force applied to the belt is reduced making it easily be removed from the whole intermediate transfer unit. As described in the inventor's manuscript, this single operation unit allows a user manipulate it with a small force manually. Therefore, even a user who is not skilled can clean and check the intermediate transfer belt in a short time.

The primary idea of unseparated steering system is recorded in U. S. Patent 7,957,682 B2 applied by David A. DeHollander and others in 2008 [37]. The improved intermediate transfer belt with one or more steering ribs ascertains the image forming processes making the same. As David A. DeHollander mentioned, there could be some researches explaining about a separate steering ribs apparatus. This will not be discussed in detail. However if the readers are interested, the materials written in the DeHollanders patents could be a good reference.

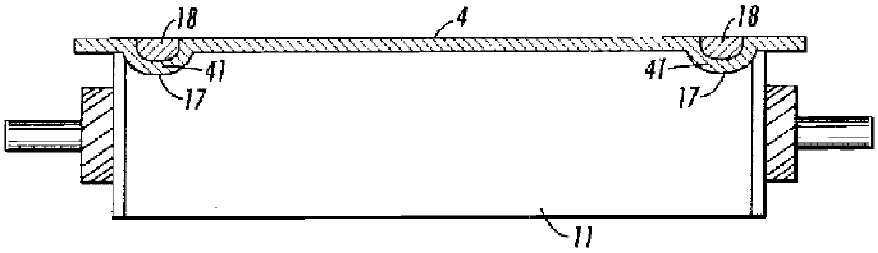

Figure 1.7: Invention of David A. DeHollander and others from U. S. Patent No. 7,957,682 B2, the belt with steering ribs

Fig. 1.7 is the cross sectional view showing an embodiment including a drive roller 11 and the intermediate transfer belt 4. The steering ribs 41 are formed into the belt while the receiving grooves 17 are embedded with the drive roller. This kind of additional ribs and grooves can prevent the belt from a zig-zag movement which leads to irregular toner image transferring especially during full-colour printing. Additionally, the inventor mentioned about several other similar embodiments, like alternating the material of drive roller and belt.

Multiple belt-steering in large scale was thoroughly described in U. S. Patent No. 7,920,814 B2 submitted by Mark A. Atwood and his co-workers in 2011 [38]. In their description, the embodiments with actuators named steering rollers could maintain alignment of an endless belt. Fig. 1.8 (a), and Fig. 1.8 (b) are related to this large steering system.

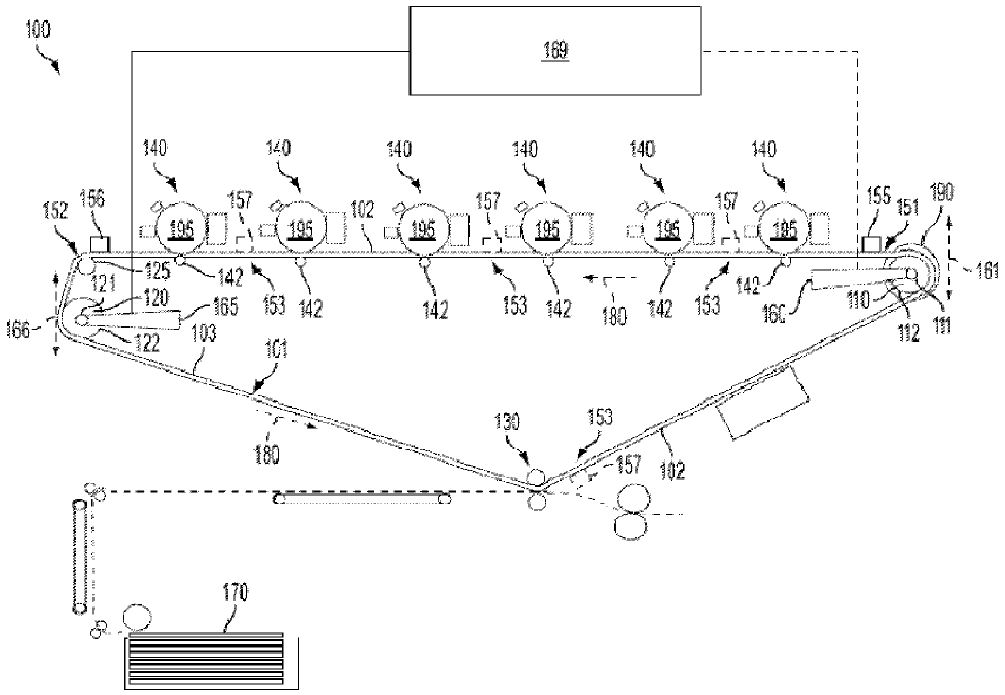

(a) a printing apparatus in the embodiments

In Fig. 1.8 (a), the steering roller 110 and second steering roller 120 are used to ensure lateral alignment of the endless belt 101. The mechanism 160, 165 of these steering rollers graphed in Fig. 1.8 (b) can be controlled in response to sensor measurements. To be more specific, the sensor 155 and 156 in Fig. 1.8

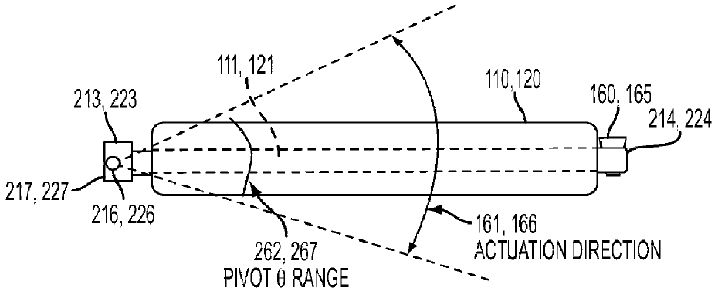

(b) cross section view of a steering roller

Figure 1.8: Invention of Mark A. Atwood and others from U. S. Patent No. 7,920,814 B2

(a) detects the lateral edge of the belt 101 and send the information back to the controller 169. Then, the controller can determine a second pivot angle for moving the steering roller 110, 120 to return the lateral edge of the belt to the desired position. This multiple belt steering system can control lateral alignment of the intermediate transfer belt maintaining the belt edge alignment more uniformly around the belt circumference. Hence the colour-to-colour registration and image on paper registration are improved.

It is not difficult to draw the conclusion that concerning to design for image transfer belt, location, assemble and alignment about the belt attract most of the attentions [39–45]. Furthermore, most of the investigations started from the structure design based on manufacturing principles. When coming to alignment concerning, the real time sensors and actuators on line became the choice of most engineers. The fact that few of the mechanical description about this image transfer belt unit has been written, inspired the author to consider about modelling the apparatus from mechanical components. In fact, the motions of pulley and belt system have been studied for over decades and the general idea of modelling them is based on the force-motion relationship.

In study of T. C. Kraver, G. W. Fan, and J. J. Shah, the vibration component of tensioner-arm was the focus. However the modelling between belt span and the pulley could be applied to the image transfer belt [46].

Consider the simplest pulley-belt model in Fig. 1.9

The pulley angular rotation, velocity and acceleration are denoted as θ, $\dot{\theta}$, and

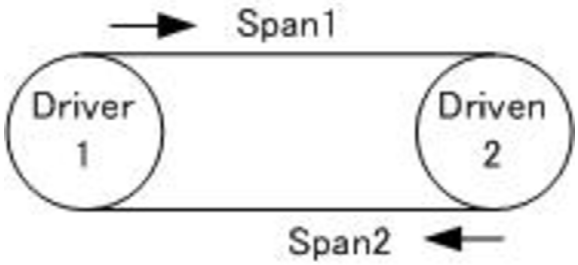

Figure 1.9: Simple pulley-belt system

$\ddot{\theta}$, respectively. According to Barker and Yang's research [47, 48], the belt spans $n(n = 1, 2)$ can be modelled as linear springs with constant K_n in parallel with a dash pot with damping D_n. K_n is a function of belt elastic modulus K_b and belt length L_n:

$$K_n = \frac{K_b}{L_n} \ . \tag{1.1}$$

D_n may be linked with K_n through an experimentally determined damping constant β:

$$D_n = \beta K_n \ . \tag{1.2}$$

The tension force F_n in each span could be calculated from

$$F_n = K_n(R_{n+1}\theta_{n+1} - R_n\theta_n) + D_n(R_{n+1}\dot{\theta}_{n+1} - R_n\dot{\theta}_n) \ . \tag{1.3}$$

Torque balance of driven pulley mass moment of inertia M_n to applied vibration belt tension at the belt cord radius R_n is given by:

$$M_n\ddot{\theta}_n = R_n(F_n - F_{n+1}) \ . \tag{1.4}$$

Although the linear spring model has been improved in the following researches, this kind of thinking is suitable for the image transfer belt considering the main elements are rollers and belt.

1.2.2 Studies on Halftone Banding and Control Design for it in Xerographic Printing

Halftone banding is one of the typical banding artifacts appearing in printing image. It commonly reflects as periodic light and dark streaks across a printed page perpendicular to the process or print direction [49–51].

Studies on sources of the halftone banding in xerographic printing can go back to early 1990s. In Robert P. Loce, William L. Lama and Martin S. Maltz's work, it is mentioned that when there is vibratory motion of the photoreceptor or wobble in the polygon mirror, the raster lines on the photoreceptor will not be evenly spaced [51]. This raster line is also known as the scanline in other researchers'literary works [52–55].

The reason why velocity of the photoreceptor is generally not constant in time in xerographic printing, is the modulation by dynamic errors of gears, timing belts, and motors indirectly. The problem is illustrated in Fig. 1.10 (a), and (b).

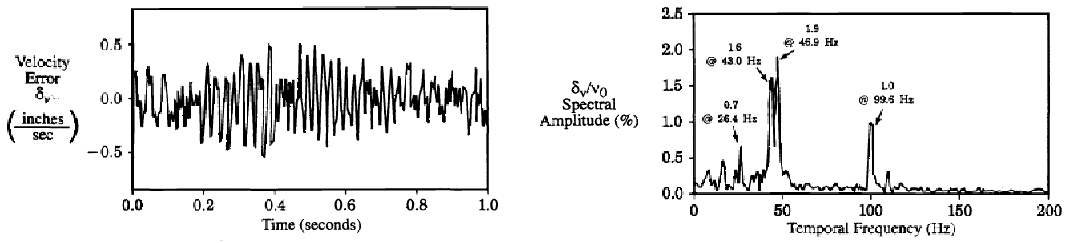

(a) measurement of photoreceptor velocity error for a prototype xerographic printer with a nomial velocity of 8.1 $in./s$

(b) frequency spectrum of photoreceptor velocity error with four major frequency components

Figure 1.10: Measured photoreceptor velocity variations in Robert P. Loce, William L. Lama and Martin S. Maltz's work

According to their research, the raster spacing error leads to exposure modulation in halftone image regions, and the exposure modulation at the spatial frequency of vibration is proportional to the fractional velocity error, but is relatively independent of system parameters. They also developed a first-order, geometry-based printing model to calculate reflectance modulation induced by the vibration. This model allows the following investigators to examine the dependence of halftone banding on various imaging parameters from a purely

geometric perspective, without complicating the situation with higher order xerographic effects. The mathematical description of this model can be referred to their work.

As robust control theory and convex optimization bloomed in late 1990s, reducing the vibration through optimal and robust control for system came into engineer's vision. According to the control technology report at Xerox Corporation, the development of modern control technologies applied to xerography reached to a peak around 2004 [56–60]. Among many researchers, Cheng-Lun Chen, George T. C. Chiu and J. P. Allebach have made the thorough investigations about laser printing system [61–78].

Researches from Cheng-Lun Chen have close connection to the model uncertainty, banding artifact reduction, and modern control method. The researchers approached from different parts of the laser printer. For example, considering the underactuated motor/gear problem, he provided a mathematical description to explain and ascertain that the print quality of a xerography prints depends largely on the performance of the image formation system, which consists of the motor/gear transmission and the laser/polygon mirror subsystems. Also the researcher mentioned that the velocity variation of the photoconductive drum and the intermediate transfer belt induce scanline spacing variation that cause the most common banding artifact. Although in this paper, the speed of intermediate transfer belt is not included into the controller design, the design process illustrated a general way to solve control design problem involved in both the exposure and developing stage of xerography printing. Also uncertainties caused by the underactuated motor/gear system are considered in the design.

Fig. 1.11 is the scheme of the generic design framework for the colour xerography printing system in the study of Cheng-Lun Chen and his co-workers [69]. The proposed strategy is to compose a feedback control system for the motor that aiming at reducing disturbances affecting the transfer belt velocity, and followed by designing a nonlinear feedforward control algorithm that modulates the laser intensity to compensate for disturbances that affect the latent images on the photoconductive drum. This kind of dual-controllers architecture is not often seen from the previous research. Also the feedback controller is set to be designed though the frame is a dual-controllers structure. The control strategy is selected

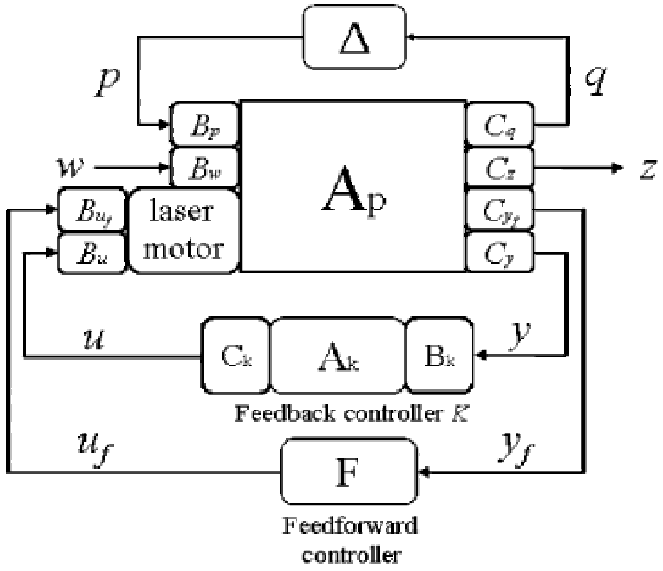

Figure 1.11: Generic design framework for colour xerography printing system in the work of Cheng-Lun Chen and others

mainly to maintain the system robust performance, and compensate the disturbance affect by the feedforward controller. Additionally the human visual system is used in the design for a filter.

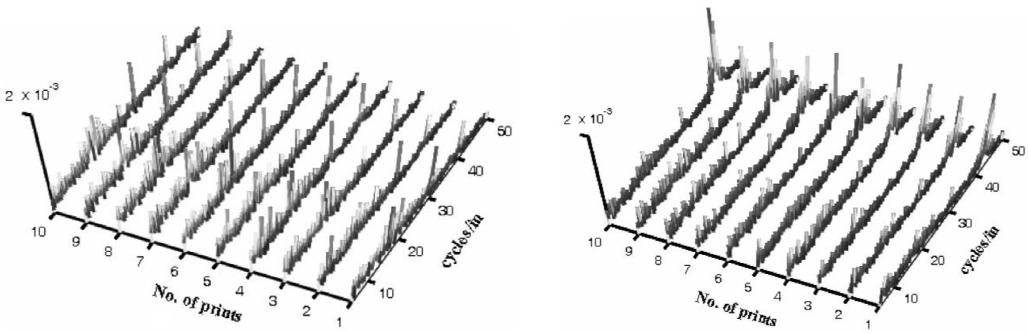

(a) before compensation

(b) after being compensated only by feedback controller

The dual-controllers design resulted in a satisfying response in the measured reflectance on the printed page shown in the Fig. 12 (c). The results before compensation and after being compensated by using only feedback control are depicted in Fig. 1.12 (a), and Fig. 1.12 (b), respectively.

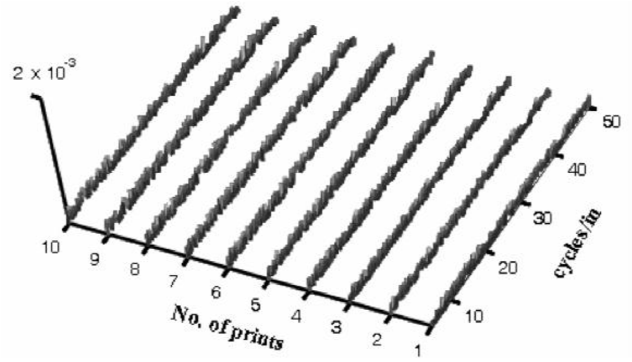

(c) after being compensated by the dual-controllers

Figure 1.12: measured reflectance results from the work of Cheng-Lun Chen and others

It is clearly to observe that with the dual-controllers design, the reflectance related to image quality is improved significantly. To readers who want to see the actual printing result, can refer the paper mentioned here. They exhibited the actual printed images before and after compensation that the difference of banding artifact level can be clearly observed by human visual.

Another successful control design for halftone banding reduction is also proposed by Cheng-Lun Chen, and George T. C. Chiu [69]. In this work, they advised a two-degree of freedom control structure based on the internal model principle and H_∞ robust control theories. Also the human contrast sensitivity function (CSF) is incorporated into the shaping filter for specifying the desired loop transfer function. Fig. 1.13 depicts the control structure as a sequential design.

The lower loop in the control scheme is designed following the robust control theories leading to a stabilizing controller for the system and achieves some performance specification. The upper loop is to synthesize a repetitive controller for the resulting closed-loop system since photoconductive drum rotates repetitively that might be affected by periodic disturbances.

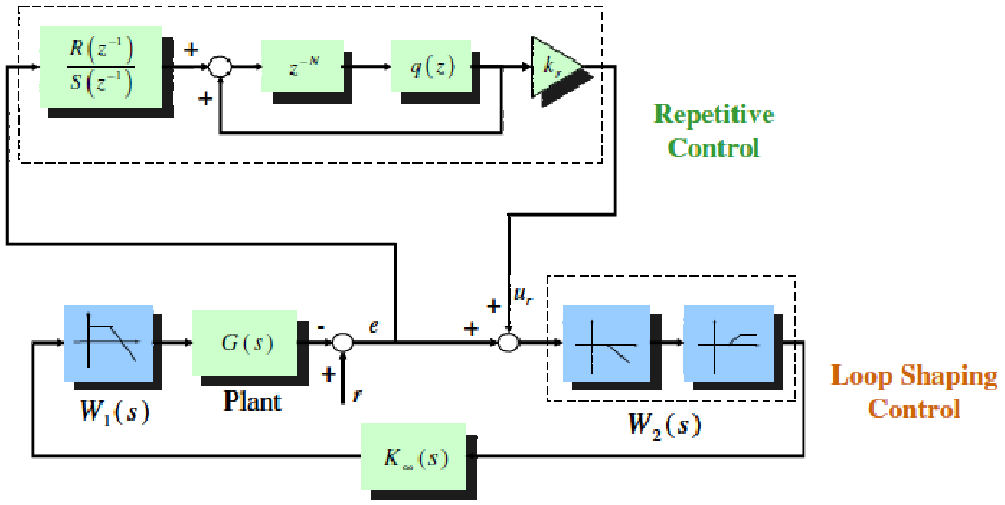

Figure 1.13: Control structure for the two-degree-of-freedom control system in Cheng-Lun Chen, and George T. C. Chiu's work

The block $W_1(s)$ is a pre-filer for the looping shaping containing the modified human contrast sensitivity information which is described as following:

$$|CSF(j2\pi f_t)| = 2.174 k_p(\phi^a - \phi^b), \tag{1.5}$$

with

$a = -0.0013 v_d$, $b = -0.0050 v_d$

$$\phi = \begin{cases} \frac{f_t}{e^{\omega_0 r_0}}, f_t \geqslant f_{max} \\ \frac{f_{max}}{e^{\omega_0 r_0}}, f_t < f_{max} \end{cases} \quad f_{max} = \frac{ln(a/b)}{b-a}$$

where k_p and v_d are adjustable gain coefficient and viewing distance, respectively. Also the frequency conversion is based on nominal vales of $\omega_0 = 3.1416$ rad/s and $r_0 = 0.0150$ m. The proposers emphasized that from the viewpoint of feedback control design, a certain amount of low frequency gain is needed to maintain an acceptable steady state regulation performance that is the reason why the modified contrast sensitivity function is applied instead of the real human contrast sensitivity. The differences between the modified contrast sensitivity and the filter used in the design are pictured in Fig. 1.14 (a), and Fig. 1.14 (b), with

different k_p and v_d value, respectively.

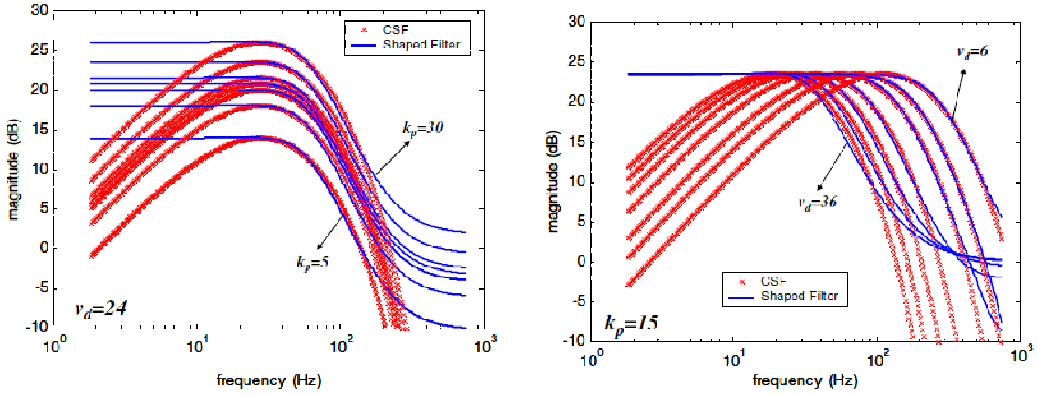

(a) different k_p value (b) different v_d value

Figure 1.14: Modified contrast sensitivity functions, and approximating filters used in Cheng-Lun Chen, and George T. C. Chiu's work

The loop shaping part follows the solving a four-block optimization problem, and a modified repetitive controller is used in the upper loop proposed by Guo. And the results of the velocity of photoconductive drum and the reflectance before compensation and after this two-degree-of-freedom controller compensation are shown in Fig. 1.15

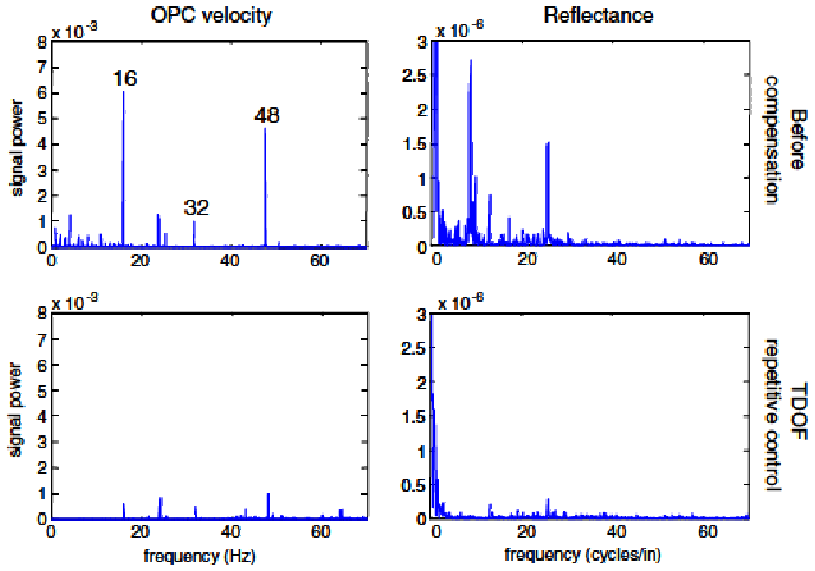

Figure 1.15: Experimental results before and after implementing the two-degree-of-freedom controller in Cheng-Lun Chen, and George T. C. Chiu's work

It is obviously seen that this dual-layers control architecture achieved a satisfying reduction in reflectance that is closely related to the halftone banding. The actual printing image before compensation and after compensation can be found in their paper.

Many other successful applications of control design can be found in the references. Yet most of them are focusing on regulating velocities of laser beam and photoreceptor in exposure and developing stage. It is led the question that even though misalignment in intermediate transfer belt has caught attention from industry, it has not been discussed thoroughly through the control design and this fact inspired the motivation of this research.

1.2.3 Studies on Optimal and Robust Control

Optimal control theory is a mature mathematical discipline with numerous applications in both science and engineering [79–81]. A general optimization problem in continuous time can be described in the following form:

$$max\ or\ min \int_0^T F(x(t), u(t), t)dt \tag{1.6}$$

subject to

$$\begin{aligned}
&\dot{x}_i = Q_i(x(t), u(t), t),\ i = 1, ..., n;\\
&x_i(0) = x_{i0},\ i = 1, ..., n;\\
&x_i(T) \geqslant 0,\ i = 1, ..., n;\\
&u(t) \in \Upsilon,\ \Upsilon \in \mathbb{R}^m
\end{aligned}$$

where,

$x(t)$ is a n-vector of state variables $x_i(t)$. These describes the state of the system at any point in time. $\dot{x}_i$ means dx_i/dt.

$u(t)$ is a m-vector of control variables. These are the choice variables in the optimization problem.

$F(\cdot)$ is a twice continuously differentiable objective function.

$Q_i(\cdot)$ are twice continuously differentiable transition functions for each state variable.

The optimization problem is also constraint by the subject to part, that are:
(1) the transition equations for each state variables. It describes how the state variable evolve over time.
(2) the initial conditions for each state variable. In this description, x_{i0} are constants.
(3) the terminal conditions for each state variable. This is often required as approaching to zero for disturbance rejection purpose.
(4) the feasible set for control variables.

The approaches to solve such kinds of optimization problem are developed and varied. One of them that is frequently mentioned in literatures is known as *dynamic programming* (DP). As in the reference from Emanuel Todorov [82], DP relies on the following obvious fact: if a given state-action sequence is optimal, and we were to remove the first state and action, the remaining sequence is also optimal (with the second state of the original sequence now acting as initial state). This is the *Bellman optimality principle*. The choice of optimal actions in the future is independent of the past actions which led to the present state. The optimal value function $F(\cdot)$ is an extremely useful quantity and is the heart of this method for optimization.

When combined with specific control design, the optimal value function can be cast into difference expressions corresponding to various control targets. Some of them are conclude as following:

LQR optimal problem:

Consider a linear system with input u, described as:

$$\dot{x}(t) = Ax(t) + Bu(t) \tag{1.7}$$

with the state initial value $x(0) = x_0$, the linear quadratic regulator (LOR) demands a full state feedback gain K as $u(t) = Kx(t)$ reconstructing the closed-loop system as:

$$\dot{x}(t) = (A + BK)x(t) \tag{1.8}$$

with the same state initial value.

The optimal cost function has the form:

$$\begin{aligned} F(\cdot) &= \int_0^\infty (x(t)^{\mathrm{T}} Q x(t) + u(t)^{\mathrm{T}} R u(t)) dt \\ &= \int_0^\infty x(t)^{\mathrm{T}} (Q + K^{\mathrm{T}} R K) x(t) dt \end{aligned} \tag{1.9}$$

where Q and R are positive definite matrices for the adjusting to achieve desired control performance. It is obvious that this kind of regulator design require that the state is fully accessible and controllable.

H_2 optimal control problem

Consider a system with a state space description as :

$$\dot{x}(t) = Ax(t) + Bu(t) y(t) = Cx(t) + Du(t) \tag{1.10}$$

the transfer function or matrices G from control variables $u(t)$ to output variables $y(t)$ can be derived as:

$$G(s) = C(sI - A)^{-1} B + D \tag{1.11}$$

where s is the Laplace operator. The H_2 norm of this transfer function or matrices is defined as:

$$\|G\|_2^2 = \frac{1}{2\pi} \int_{-\infty}^{\infty} Trace(G(j\omega)^{\mathrm{H}} G(j\omega)) d\omega \tag{1.12}$$

where $G(j\omega)$ is the frequency response function or matrices, and $G(j\omega)^{\mathrm{H}}$ is its Hermitian transpose. The meaning of this H_2 norm is that when the input signal is white noise, it reflects the energy of the outputs affected by the input. So if there is a designed controller K minimizes the H_2-norm of the plant, it will minimize the variance of the plant under the influence of coloured noise with a given density. The formation of this problem and the controller K will be studies in the next few chapters.

H_∞ optimal control problem

The system description can refer to the one in the H_2 optimal control problem. The difference is that finding a controller K to minimize the H_∞ norm of G that

is expressed as:

$$\|G\|_\infty = sup\frac{\|Gu(t)\|_2}{\|u(t)\|_2} \tag{1.13}$$

subject to any $u(t)$

The H_∞ norm provides a complete parametrization of the space of causal bounded linear time-invariant operators. And the ideal of the control design is to minimize the maximum energy of the outputs concerning to the inputs, and often used as one of the indices for the robustness of a system.

Also there are many other optimal problems description, like mixed H_2/H_∞ control problem, mixed sensitivity H_∞ control problem and so on. In these kind of design, controllers are required that not only reaches some minimum or maximum value of the optimal functions, but also satisfy a list of constraints. The linear matrix inequalities (LMIs) is often used to solve them combined with DP, and the general formation is

$$f(x) = f_0 + \sum_{i=1}^{m} x_i f_i > 0 \ , \tag{1.14}$$

where $x \in \mathbb{R}^m$ is the variable, and $f_i = f_i^{\mathrm{T}} \in \mathbb{R}^{n\times n},\ i = 0, ..., m$ are the given constraint matrices [83].

The approach to solve the specific control problem with LMIs is included in the next following chapters.

1.3 Purpose of the Work

In this research, the vibration attenuation problems of intermediate transfer belt in image transfer belt system against to loading disturbance which is specified as loading torque of printing medium, are considered. To our knowledge, study directly related to belt variations arose by loading disturbance, and control design for suppression, had not been conducted until now, although speed control for actuating motor in belt driving system has been thoroughly studied for a long time.

It can be seen, from the previous researches, the tensioner part is extremely necessary to image transfer unit for applying and adjusting tensile force on intermediate transfer belt. However this tensioner part could also be one of the factors leading to belt variation when loading disturbance is functioning on the system. Meanwhile the relevancy between them has not yet been studied. Moreover it is clearly to see that belt misalignment control designs in previous researches are concentrated on controllers for laser beam actuator in exposure stage. Also the knowledge of belt vibration is barely based on sensor measurement with no mathematical description, which is difficult for controller design from theoretical approach and leaves system vulnerable to noise and uncertainty. Speed control is often used in actuation system for intermediate transfer belt, nevertheless this could only cover speed variation problem of the actuating motor. Belt variation has not yet been included in control objectives and it aroused our interest.

Therefore, the main purpose of this work is to:

- Establish the mathematical model for image transfer belt including the tensioner part to investigate the effects from loading disturbance on belt variation. Study how far the system uncertainty could affect conventional passive control method.

- Design new control methods for image transfer belt system to resist loading disturbance aiming at attenuating belt vibration considering both optimization problem and system robustness concern.

1.4 Outlines of the Thesis

This thesis mainly deals with modelling study of image transfer belt system and optimal H_2, optimal H_∞, mixed H_2/H_∞ control along with their applications for the established image transfer belt system model. The remainder of the thesis is organized as follows.

- Chapter 2

  In this chapter, a simplified mechanical model, called four-rollers-belt (FRB) system with and without the tensioner part is studied to figure out the effect from tensioner on belt variation. Meanwhile, to ascertain the applicability of this simplified model, the multi-rollers-belt system which originated from the real equipment is set as comparison and studied along with the FRB system. Also in order to explain the necessity of active control method, limitation on passive control method by flywheel under system uncertainty disturbance is presented. Numerical simulation results are given in this chapter to prove the proposed model and inefficiency of the previous control method.

- Chapter 3

  An optimal state feedback controller based on H_2 norm is proposed for the model established in chapter 2. The control design procedure is explained in detail including how to solve stabilization problem for open-loop system, and minimization problem on H_2 norm of transfer function from loading disturbance on system outputs. Several combinations of outputs including speed of different driven rollers, and tensioner displacement are selected to find out the optimal constrain for attenuation on belt vibration. Also to testify the effectiveness of proposed controller, several numerical simulations are exhibited and compared in this chapter too.

- Chapter 4

  An optimal output feedback controller based on H_∞ norm is designed in this chapter to stabilize image transfer belt system and endow strong robustness

on belt variation. Procedure to obtain the desired controller are conducted and a mathematical model for real loading disturbance is proposed. Numerical simulation results including comparison between conventional PID speed controller and optimal H_∞ controller, system performance with and without uncertainty by the proposed controller are conducted to exhibit the effectiveness of this design.

- Chapter 5

  An optimal output feedback controller based on mixed H_2/H_∞ norm is investigated in this chapter to take advantage from both of these two norms. The control architecture is explained with how to pick up constraints on outputs. Various selections and combinations between outputs with different constraints and optimization settings are studied thoroughly in numerical simulations, in order to figure out the most promising design for system. And results ascertain the efficiency of this mixed norm control design.

- Chapter 6

  In the end, the conclusions of this thesis are summarized in this chapter.

Chapter 2

Study of Mechanical Model for Image Transfer Belt System and Passive Control Method for it

2.1 Introduction

As explained in Chapter 1, the belt span can be modeled as ideal spring due the tension of the belt itself. This leads to the mathematical description of a general image transfer belt system with several driven rollers. Also, as introduced previously, it is necessary to have tensioner part which usually is a spring involved in the belt to regulate the tensile force applied on the belt. However the affect from it on the belt variation under loading disturbance has not yet been included in the previous research. This chapter will deal with this issue from establishing a general mathematical model to describe the image transfer belt system and the variations in the belt. Although the general model is started with the ignorance of damping, the Rayleigh damping model is proposed to make the compensation. Comparisons between system with and without the tensioner are conducted to reflect the necessity of modeling the tensioner.

Also number of the driven rollers in image transfer belt system is minified to four for simplification in control design. The investigation between this four rollers model and multi rollers one certified its availability.

In the authors previous work [84], the passive control using flywheel and dynamic vibration absorber showed some effectiveness. This leads to the question about how they work with uncertainties from the system modeling itself. And it will be answered in this chapter.

The organization of this chapter is as follows: Section 2.1 juxtaposes and shows the influence on the belt variation between with and without the tensioner part, by starting from the general mathematical description of belt-roller drive system. Section 2.2 ascertains the applicability of the minified four-rollers-belt system by comparing with the multi rollers one. The necessity of including the uncertainties in system parameters is explained with the passive control results in Section 2.3. The summary for this chapter is drawn in Section 2.4.

2.2 Modeling of Image Transfer Belt System with and without Tensioner

2.2.1 Mechanical Descriptions of Belt Span and Rollers Rotation

As described previously, the image transfer unit consists of a long seamless image transfer belt, several rollers and a tensioner part to adjust the tensile force applied on the belt. To obtain the motion equations of the image transfer unit, the remodeling of a belt is studied first.

Considering only in the printing direction, a belt span with horizontal and axial extension can be described to a piece of ideal spring moving only in the horizontal way shown in Fig. 2.1.

The stiffness of the ideal spring can be calculated from:

$$k = \frac{EA_b}{l} \ , \tag{2.1}$$

where E refers the *Young's* modulus of the belt material, A_b is the area of the belt span, and l means the span's length.

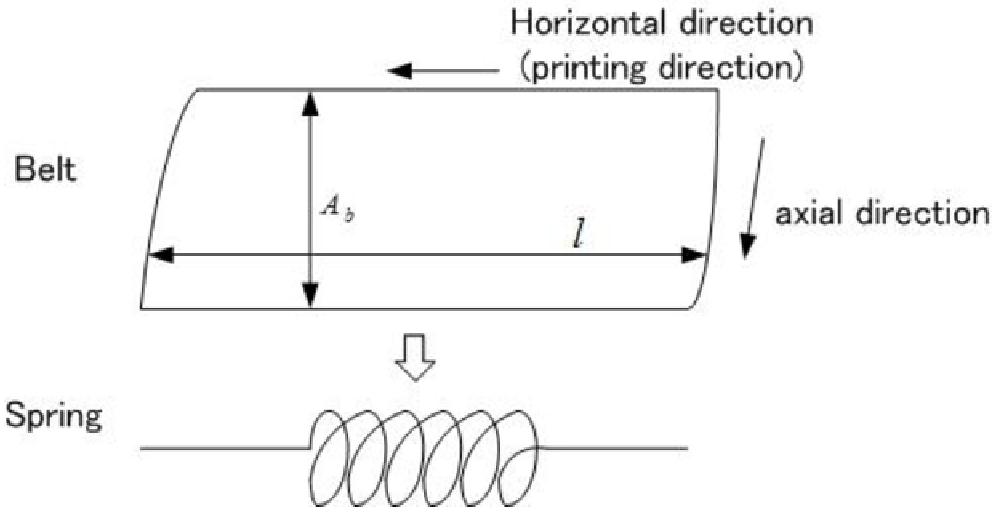

Figure 2.1: The remodeling for a belt span to a ideal spring

The rollers driving two belt spans is pictured in Fig. 2.2, and without losing the generality the rollers are numbered clockwise.

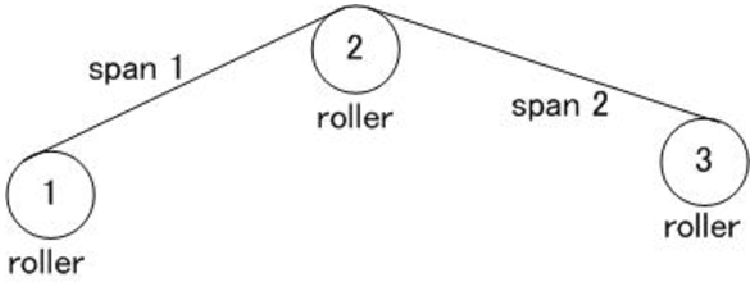

Figure 2.2: Model of three rollers driving two belt spans

Assuming that the contact slip between roller and belt can be ignored, then the tensile force in span 1 and span 2 can be derived from:

$$\begin{aligned} T_1 &= (\theta_1 r_1 - \theta_2 r_2) k_1 \\ T_2 &= (\theta_2 r_2 - \theta_3 r_3) k_2 \ , \end{aligned} \tag{2.2}$$

where the θ, r represent each roller's rotation angular and radius, respectively. k is the stiffness of the each span calculated from Eq. (2.1), and T_1, T_2 are the tensile force in each belt span.

The rotational equation of No. 2 roller is described as:

$$\begin{aligned} I_2\ddot{\theta}_2 &= (T_2 - T_1)r_2 \\ &= (\theta_2 r_2 - \theta_3 r_3 k_2 r_2 - (\theta_1 r_1 - \theta_2 r_2)k_1 r_2 \ . \end{aligned} \tag{2.3}$$

I_2 is the inertia of the roller with number two, and $\ddot{\theta}_2$ means its rotational angular acceleration. Eq. (2.3) is the basic formula to describe a rotation roller between two belt spans, and will be mentioned in the following study.

As mentioned in Introduction, misalignment of belt is simply detected by sensor in xerographic printing, therefore it is necessary to establish the mathematical model for it. Two indices are defined here to describe the variation in belt related to image transferring process depicted in Fig. 2.3 (a), and Fig. 2.3 (b).

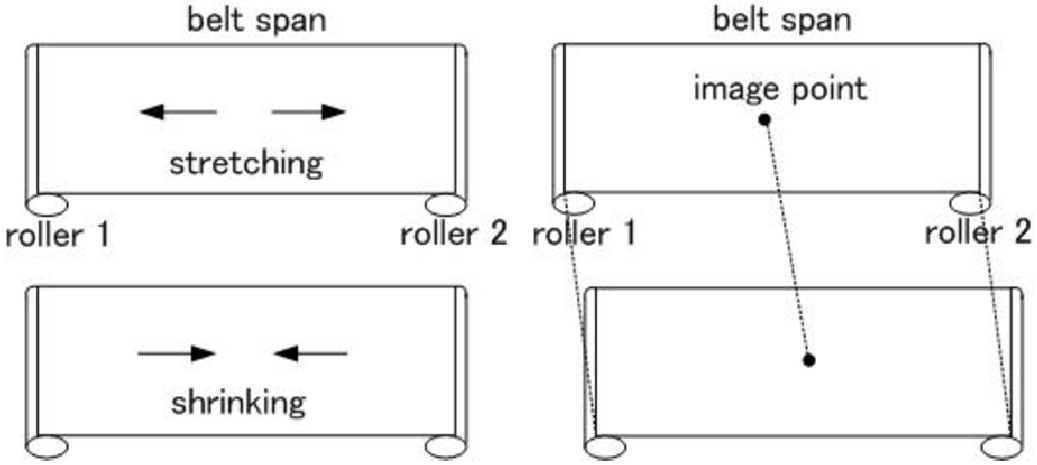

(a) stretching displacement (b) absolute displacement

Figure 2.3: Two types of variation in belt span

Due to the tensile force, the belt span can stretch or shrink like a spring, and figure 2.3 (a) reflects this kind of variation named as the stretching displacement (SD). Also because of the speed variation of the driven rollers, the original location where the toner image is transferred is misaligned showing in figure 2.3 (b). It is called the absolute displacement (AD). And the mathematical descriptions can

be derived as:

$$\begin{aligned} SD &: \theta_1 r_1 - \theta_2 r_2 \\ AD &: \frac{1}{2}(\theta_1 r_1 + \theta_2 r_2) \end{aligned} \tag{2.4}$$

Notice that the number of each roller in Eq. (2.4) should be adjusted accordingly.

2.2.2 Comparisons of System Behavior with and without Tensioner

Though the realization method varies, the basic tensioner part in the image belt unit can also be described as an ideal spring. The effects from this part to the belt variation have not been investigated yet as mentioned in the introduction part. Therefore it is necessary to establish two models with and without the tensioner and compare them.

Consider these two models graphed in Fig. 2.4 (a), and Fig. 2.4 (b):

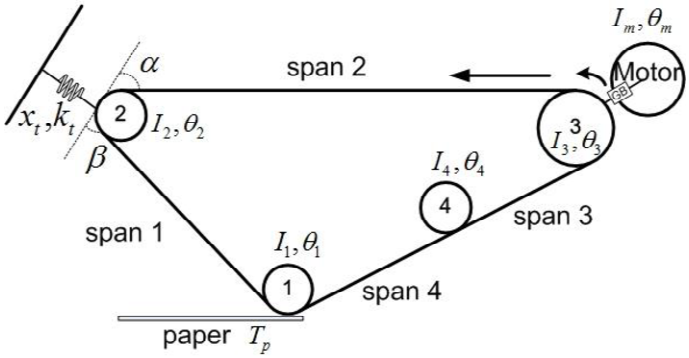

(a) with the tensioner

The rollers and belt spans are numbered clockwise in both models, and I_i, θ_i represent each rollers inertia and rotation angle separately. k_i which is not labeled in the figure means each belt spans stiffness calculated from Eq. (2.1). The belt span labelled No. 2 is where the toner image be transferred, and is of the investigation. The only difference between these two models is the tensioner part connected to the roller with number 2. The tensioner is modeled as a spring

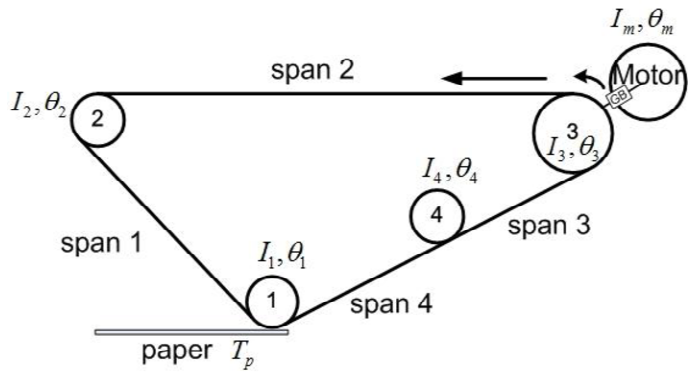

(b) without the tensioner

Figure 2.4: Two types of modeling for image transfer belt

with stiffness k_t, and displacement x_t. And the stretching angels related to the horizontal direction are denoted as α, and β.

The inputs to this kind of image transfer belt are the loading torque T_p from roller No. 1, and the motors output torque T_m from roller No. 3. Gear ratio is denoted as m, and the rotational stiffness and frictional coefficient of the motor are k_m, b_m. Also motor's rotational angle is written as θ_m. Based on Eq. (2.3), the equations of motion for these two models are derived as following:

For the system with tensioner:

$$
\begin{aligned}
I_1\ddot{\theta}_1 &= -(\theta_1 r_1 - \theta_4 r_4)k_4 r_1 + (\theta_2 r_2 - \theta_1 r_1 + x_t \sin\beta)k_1 r_1 + T_p \\
I_2\ddot{\theta}_2 &= -(\theta_2 r_2 - \theta_1 r_1 + x_t sin\beta)k_1 r_2 + (\theta_3 r_3 - \theta_2 r_2 + x_t \sin\alpha)k_2 r_2 \\
I_3\ddot{\theta}_3 &= -(\theta_3 r_3 - \theta_2 r_2 + x_t sin\alpha)k_2 r_3 + (\theta_4 r_4 - \theta_3 r_3)k_3 r_3 + k_m(\frac{\theta_m}{m} - \theta_3) \\
I_4\ddot{\theta}_4 &= -(\theta_4 r_4 - \theta_3 r_3)k_3 r_4 + (\theta_1 r_1 - \theta_4 r_4)k_4 r_4 \\
I_m\ddot{\theta}_m &= k_m(\theta_3 - \frac{\theta_m}{m}) - b_m\dot{\theta}_m + T_m \\
m_2\ddot{x}_t &= -k_t x_t - (\theta_2 r_2 - \theta_1 r_1 + x_t \sin\beta)k_1 \sin\beta - (\theta_3 r_3 - \theta_2 r_2 + x_t \sin\alpha)k_2 \sin\alpha \ ,
\end{aligned}
\tag{2.5}
$$

where m_2 represents the mass of the roller connected with the tensioner. Now the expressions of stretching displacement and absolute displacement in span 2

are adjusted as:

$$\begin{aligned} SD &: \theta_3 r_3 - \theta_2 r_2 + x_t \sin\alpha \\ AD &: \frac{1}{2}(\theta_3 r_3 + \theta_2 r_2 + x_t \sin\alpha) \ . \end{aligned} \tag{2.6}$$

For the system without tensioner:

$$\begin{aligned} I_1\ddot{\theta}_1 &= -(\theta_1 r_1 - \theta_4 r_4)k_4 r_1 + (\theta_2 r_2 - \theta_1 r_1)k_1 r_1 + T_p \\ I_2\ddot{\theta}_2 &= -(\theta_2 r_2 - \theta_1 r_1)k_1 r_2 + (\theta_3 r_3 - \theta_2 r_2)k_2 r_2 \\ I_3\ddot{\theta}_3 &= -(\theta_3 r_3 - \theta_2 r_2)k_2 r_3 + (\theta_4 r_4 - \theta_3 r_3)k_3 r_3 + k_m(\frac{\theta_m}{m} - \theta_3) \\ I_4\ddot{\theta}_4 &= -(\theta_4 r_4 - \theta_3 r_3)k_3 r_4 + (\theta_1 r_1 - \theta_4 r_4)k_4 r_4 \\ I_m\ddot{\theta}_m &= k_m(\theta_3 - \frac{\theta_m}{m}) - b_m\dot{\theta}_m + T_m \ . \end{aligned} \tag{2.7}$$

And the variations in span 2 are:

$$\begin{aligned} SD &: \theta_3 r_3 - \theta_2 r_2 \\ AD &: \frac{1}{2}(\theta_3 r_3 + \theta_2 r_2) \ . \end{aligned} \tag{2.8}$$

Since the damping factor is out of the consideration during the establishment of the equations of motion, it is reasonable to introduce the Rayleigh damping model into Eq. (2.5), and Eq. (2.7). The Rayleigh damping model describes that the damping matrix in a system can be calculated from experimental data, reflected as a linear combination of the mass and stiffness matrices of the system. The procedures are explained in Appendix A. In general, the equations of motion for these two models can be written in the following matrix form as:

$$\mathbf{M}\ddot{x} + \mathbf{C}\dot{x} + \mathbf{K}x = \mathbf{P}_1 T_p + \mathbf{P}_2 T_m \ , \tag{2.9}$$

where:

- when with tensioner, $x = \left[\theta_1, \theta_2, \theta_3, \theta_4, \theta_m, x_t\right]^{\mathrm{T}}$, $\mathbf{M}, \mathbf{C}, \mathbf{K} \in \mathbb{R}^{6\times6}$, and $\mathbf{P}_1, \mathbf{P}_2 \in \mathbb{R}^{6\times1}$.
- when without tensioner, $x = \left[\theta_1, \theta_2, \theta_3, \theta_4, \theta_m\right]^{\mathrm{T}}$, $\mathbf{M}, \mathbf{C}, \mathbf{K} \in \mathbb{R}^{5\times5}$, and $\mathbf{P}_1, \mathbf{P}_2 \in \mathbb{R}^{5\times1}$.

The parameters of the system used in the calculation are list in Table 2.1.

Table 2.1: Parameters of image transfer belt system

parameter	symbol	value
belt length	l_i $(i = 1 \sim 4)$	0.2 m
belt area	A_b	3.6×10^{-5} m^2
$1^{st}, 2^{nd}, 4^{th}$ roller's radius	r_i $(i = 1, 2, 4)$	0.014 m
3^{rd} roller's radius	r_3	0.01675 m
$1^{st}, 2^{nd}, 4^{th}$ roller's inertia	I_i $(i = 1, 2, 4)$	6.45×10^{-5} kgm^2
3^{rd} roller's inertia	I_3	1.32×10^{-4} kgm^2
tensioner angular	$\alpha,\ \beta$	45 deg
belt *Young's modulus*	E	3.4×10^3 MPa
2^{nd} roller's mass	m_2	1 kg
tensioner stiffness	k_t	1.38×10^4 N/m
shaft torsional stiffness	k_m	39 N $\cdot$ m/rad
motor inertia	I_m	3.6×10^{-6} kgm^2
motor vicious coefficient	b_m	1×10^{-4} N $\cdot$ m $\cdot$ s/rad
gear ratio	m	5

Based on Eq. (2.9), the frequency responses from the loading torque T_p considered as one of the disturbances to the system on the belt variations are obtained and the magnitude of them are demonstrated in Fig. 2.5 (b), and (c). Additionally, the affects on number 3^{rd} roller driven by the motor is also included and its magnitude of frequency response is displayed in Fig. 2.5 (a). due to the request of maintaining steady rotation for the whole system.

Blue line indicates the results from the system with tensioner, and red line represents the ones without tensioner. It is obviously that one additional peak around 523 rad/sec (83.3 Hz) appears in all of the three results from the system with tensioner. And the magnitude of stretching displacement at this frequency in system with tensioner could not be ignored. Although the magnitude values of this peak in stretching displacement and absolute displacement are not large, the toner image quality could receive considerable misalignment since in full color printing, the process of toner image transferring will be carried out four times.

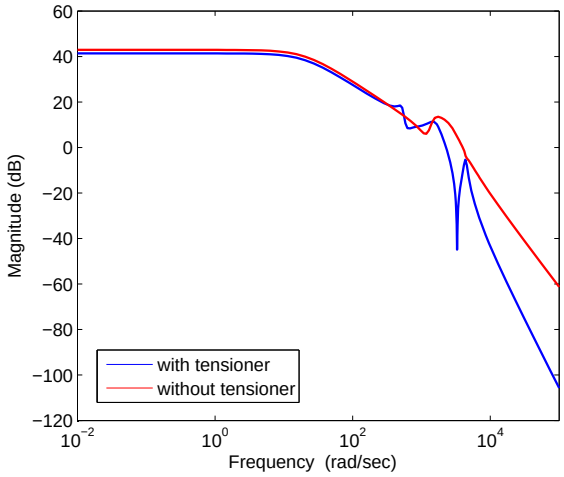

(a) number 3^{rd} roller's rotational speed

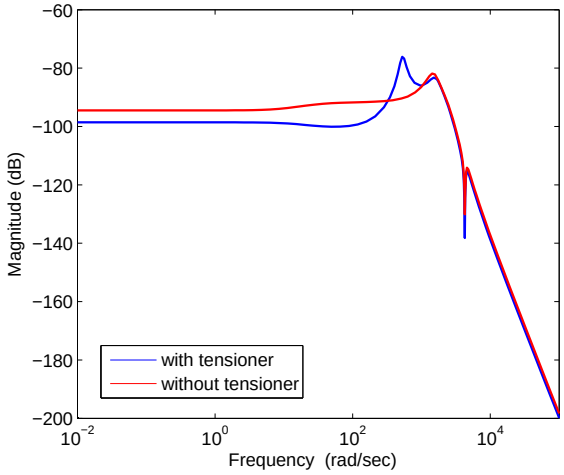

(b) stretching displacement

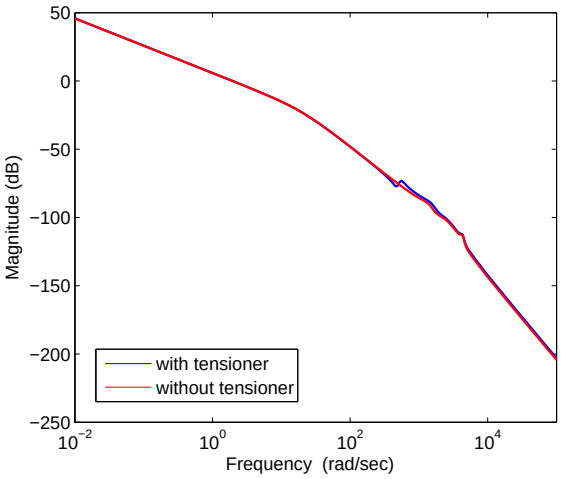

(c) absolute displacement

Figure 2.5: Magnitude of frequency responses from T_p to the system

Also the affects from the loading torque to the tensioner displacement is examined and shown in Fig. 2.6. And the results indicated that the peak around 523 rad/sec is caused by the vibration in the tensioner. Therefore the conclusion that the tensioner part in image transfer belt system should not only be included, but also emphasized to attenuate the belt variations.

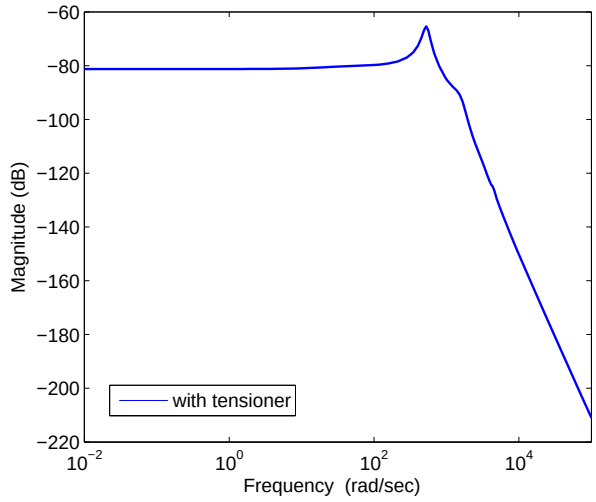

Figure 2.6: magnitude of frequency response from T_p to the tensioner displacement x_t

2.3 Comparisons of Four-Rollers-Belt Model and Multi-Rollers-Belt Model

In xerographic printing, the image transfer belt system contains a large long belt and multiple rollers. As investigated in Section 2.1, only four rollers and four belt spans are considered in the mathematical model. So it is considerable to find out that whether it is proper to apply the four rollers one in the following study. Also whether the effect from the tensioner part plays important role in the belt variation in the large belt system is considered in this section.

Consider a system graphed in Fig. 2.7 which consists of 15 rollers and 15 belt spans.

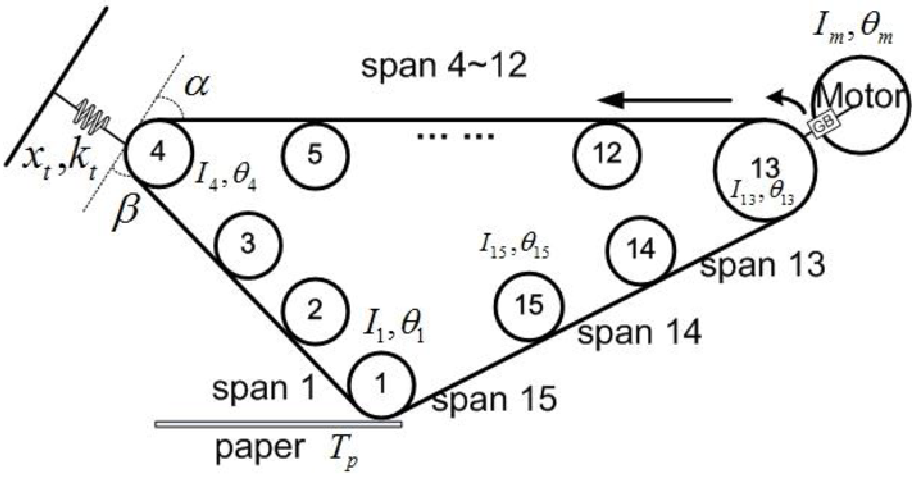

Figure 2.7: Multi-rollers-belt system

The tensioner is connected to the 4^{th} roller, and the motor drives the 13^{rd} roller through a gear box. The paper is still carried to the belt by the 1^{st} roller. The toner image transferring is conducted on the upper layer labelled span 4 to 12 along with the rollers numbered from 5 to 12 which are not shown in the picture for simplification, and the location is not specified in this model. Based on Eq. (2.3), the equations of motion for this multi-rollers-belt system are established as:

$$
\begin{aligned}
I_1\ddot{\theta}_1 &= -(\theta_1 r_1 - \theta_{15} r_{15})k_{15} r_1 + (\theta_2 r_2 - \theta_1 r_1)k_1 r_1 + T_p \\
I_2\ddot{\theta}_2 &= -(\theta_2 r_2 - \theta_1 r_1)k_1 r_2 + (\theta_3 r_3 - \theta_2 r_2)k_2 r_2 \\
I_3\ddot{\theta}_3 &= -(\theta_3 r_3 - \theta_2 r_2)k_2 r_3 + (\theta_4 r_4 - \theta_3 r_3 + x_t \sin\beta)k_3 r_3 \\
I_4\ddot{\theta}_4 &= -(\theta_4 r_4 - \theta_3 r_3 + x_t \sin\beta)k_3 r_4 + (\theta_5 r_5 - \theta_4 r_4 + x_t \sin\alpha)k_4 r_4 \\
I_5\ddot{\theta}_5 &= -(\theta_5 r_5 - \theta_4 r_4 + x_t \sin\alpha)k_4 r_5 + (\theta_6 r_6 - \theta_5 r_5)k_5 r_5 \\
&\vdots \\
I_i\ddot{\theta}_i &= -(\theta_i r_i - \theta_{i-1} r_{i-1})k_{i-1} r_i + (\theta_{i+1} r_{i+1} - \theta_i r_i)k_i r_i \ , (i = 6 \sim 12) \\
&\vdots
\end{aligned}
$$

$$
\begin{aligned}
I_{13}\ddot{\theta}_{13} &= -(\theta_{13}r_{13} - \theta_{12}r_{12})k_{12}r_{13} + (\theta_{14}r_{14} - \theta_{13}r_{13})k_{13}r_{13} + k_m(\frac{\theta_m}{m} - \theta_{13}) \\
I_{14}\ddot{\theta_{14}} &= -(\theta_{14}r_{14} - \theta_{13}r_{13})k_{13}r_{14} + (\theta_{15}r_{15} - \theta_{14}r_{14})k_{14}r_{14} \\
I_{15}\ddot{\theta_{15}} &= -(\theta_{15}r_{15} - \theta_{14}r_{14})k_{14}r_{15} + (\theta_1 r_1 - \theta_{15}r_{15})k_{15}r_{15} \\
I_m\ddot{\theta}_m &= k_m(\theta_{13} - \frac{\theta_m}{m}) - b_m\dot{\theta}_m + T_m \\
m_4\ddot{x}_t &= -k_t x_t - (\theta_4 r_4 - \theta_3 r_3 + x_t \sin\beta)k_3 \sin\beta - (\theta_5 r_5 - \theta_4 r_4 + x_t \sin\alpha)k_4 \sin\alpha \ ,
\end{aligned}
\tag{2.10}
$$

For simplification, the equation of motion for the 6^{th} to 12^{th} roller are generalized as the i^{th} roller. And the mass of the roller connected to the tensioner is denoted as m_4. It is obviously that the items with x_t are switched to the $3^{rd}, 4^{th}, 5^{th}$ equations. Again, the Rayleigh damping model is added in Eq. (2.10) which is similar to Appendix A, and the matrix form of the compensated Eq. (2.10) is expressed as:

$$
\mathbf{M}_{multi}\ddot{x}_{multi} + \mathbf{C}_{multi}\dot{x}_{multi} + \mathbf{K}_{multi}x_{multi} = \mathbf{P}_{multi1}T_p + \mathbf{P}_{multi2}T_m \ , \tag{2.11}
$$

where $x_{multi} = \left[\theta_1, \theta_2, \theta_3, \theta_4, ..., \theta_{15}, \theta_m, x_t\right]^{\mathrm{T}}$, $\mathbf{M}_{multi}, \mathbf{C}_{multi}, \mathbf{K}_{multi} \in \mathbb{R}^{17\times17}$, and $\mathbf{P}_{multi1}, \mathbf{P}_{multi2} \in \mathbb{R}^{17\times1}$.

To approach the real equipment, the lengths of each belt span are different leading to variant belt stiffness, and they are listed in Table 2.2

Table 2.2: Length of each belt span

No. of the span	length	No. of the span	length
1	0.105 m	9	0.218 m
2	0.229 m	10	0.111 m
3	0.583 m	11	0.211 m
4	0.055 m	12	0.173 m
5	0.033 m	13	0.035 m
6	0.034 m	14	0.159 m
7	0.100 m	15	0.354 m
8	0.416 m		

Again the expressions of belt variations should be adjusted. Since which belt

span is the exact location for tone image transferring is not fixed, the upper layer of the belt which includes the span from 4 to 12 is set to be the object. The stretching displacement is showing the stretching or shrinking displacement of the belt that leads the cancellation in the mathematical expression from each span. However the absolute displacement does not follow this rule. Without losing the generality, the average absolute displacement from span 4 to span 12 is set to the one used to make comparison. And the mathematical of these two indices are as following:

$$\begin{aligned}
\textbf{SD}: &(\theta_5 r_5 - \theta_4 r_4 + x_t \sin\alpha) + (\theta_6 r_6 - \theta_5 r_5) + ... + (\theta_{13} r_{13} - \theta_{12} r_{12}) \\
&= \theta_{13} r_{13} - \theta_4 r_4 + x_t \sin\alpha \\
\textbf{AD}: &\frac{1}{9}\left[\frac{1}{2}(\theta_5 r_5 + \theta_4 r_4 + x_t \sin\alpha) + \frac{1}{2}(\theta_6 r_6 + \theta_5 r_5) + ... + \frac{1}{2}(\theta_{13} r_{13} + \theta_{12} r_{12})\right] \\
&= \frac{1}{18}(\theta_{13} r_{13} + \theta_4 r_4 + x_t \sin\alpha) + \frac{1}{9}(\theta_5 r_5 + ... + \theta_{12} r_{12}) \ .
\end{aligned} \tag{2.12}$$

The comparisons between this multi-rollers-belt system and the one in Section 2.1 named as four-rollers-belt are conducted. However the parameters related to length of each belt span in Section 2.1 need to be adjusted following the same length with multi-rollers-belt system. The updated values for each belt span are list in Table 2.3, with reference of multi-rollers-belt system. Notice both these two system are with tensioner.

Table 2.3: Updated length of each belt span in four-roller-belt system

span in FRB system	refer to span in multi system	length
l_1	$l_1 + l_2 + l_3$	0.9170 m
l_2	$l_4 + \cdots + l_{12}$	1.3510 m
l_3	$\frac{1}{2}(l_{13} + l_{14} + l_{15})$	0.2740 m
l_4	$\frac{1}{2}(l_{13} + l_{14} + l_{15})$	0.2740 m

The other system parameters can refer to Table 2.1 and Table 2.2. One more thing need to be emphasized here is that the parameters of belt length for four-roller-belt system are simply summed up value from multi-roller-belt system in Table 2.3. This could lead to big differences in system performance by effecting

K, and **C** in Eq. (2.9), since the series connection of several pieces of linear spring is not linear length summation. Therefore another adjusted four-roller-belt system is also structured with same length but a regulation in **K** which is timed by 0.591. The magnitude of frequency response from T_p on the systems are depicted in Fig. 2.8 (a), (b), (c), (d).

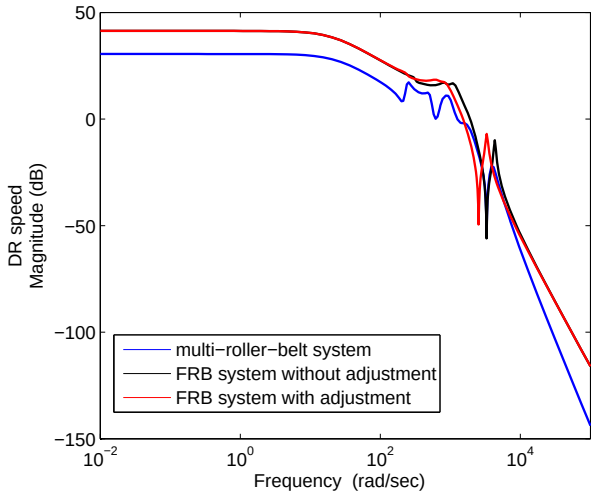

(a) speed of the roller connected with motor

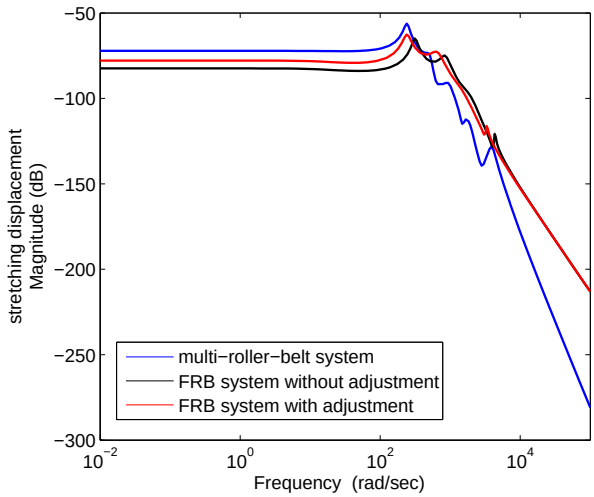

(b) stretching displacement

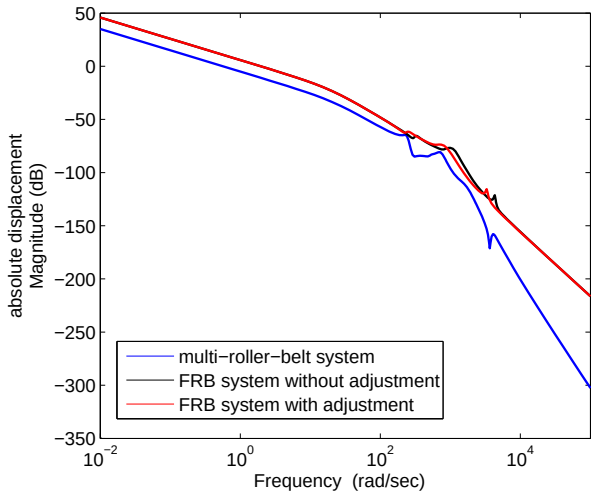

(c) absolute displacement

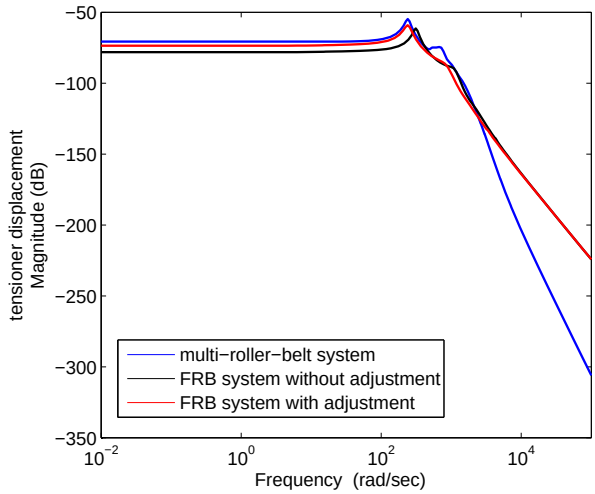

(d) tensioner displacement x_t

Figure 2.8: Magnitude of frequency responses from T_p to multi-rollers-belt model and four-rollers-belt model

The blue lines reflect the results of multi-rollers-belt system, the black lines are from unadjusted four-rollers-belt system, and the red lines are four-rollers-belt system with stiffness adjustment. Fig. 2.8 (a) is the influences from loading disturbance T_p on the speed of the roller which is connected with motor. Fig. 2.8

(b) is about the stretching displacement, and Fig. 2.8 (c) shows the absolute displacement. Additionally, Fig. 2.8 (d) graphs the results of tensioner displacement x_t. Four-rollers-belt system without adjustment shows big differences to multi-rollers-belt system, however the one with stiffness adjustment performs similar system characteristics with multi-rollers-belt system. It is understandable that the series connection of several pieces of linear spring requires stiffness adjustment. Moreover both in stretching displacement and absolute displacement, it is clear that the first peaks are caused by the variation in tensioner. The frequencies of the peaks are 225.2 rad/sec for the multi-rollers-belt model, and 523.5 rad/sec for the unadjusted four-rollers-belt one. That is the same with the results in Fig. 2.8 (d). Since the parameters for length of each belt span simulated in the multi-rollers-belt model is based on the real machine, it is reasonable to apply the four-rollers-belt system for the further investigation. And the differences between them can be modeled as system uncertainty.

2.4 Investigations of Effects from System Uncertainty on Passive Control Methods

2.4.1 System Uncertainty and Effects on Frequency Response

There are several origins leading to the uncertainty in a system, like parameters in the linear model that are only known approximately or simply in error. Also the real system does not always perform in the linear condition. The operating conditions could be one of the reasons that introduce nonlinearities to a linear system. Additionally, measurements containing imperfections may give rise to the uncertainty when involved with system identifications. So the relationships between the inputs and outputs through a real system could look like in Fig. 2.9 where the information of the block labeled system is known whereas the block with Δ [85].

In the process of modeling for the image transfer belt system, the assumption that no slip between roller and belt span is taken into consideration is made, that

may lead nonlinear uncertainty to the system. Also the coefficients in Rayleigh damping model are originated from experimental data which also one of the uncertain elements. Therefore it is quite necessary to investigate how far the uncertainties of system parameters can effect on the belt variations.

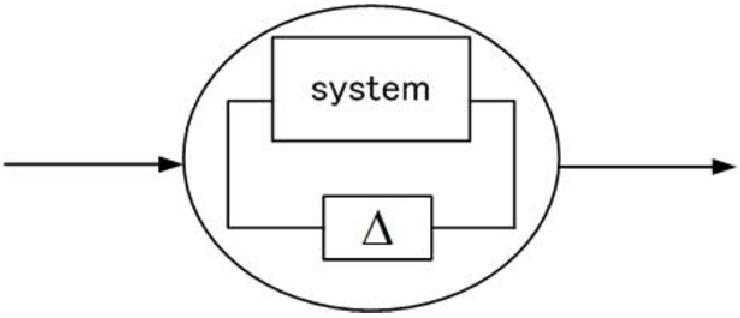

Figure 2.9: the Real System Containing Uncertainty

From this section, the four-rollers-belt system will be used for investigation, and the rollers are renamed as: burden roller (BR) where the paper is carried into the belt; tension roller (TR) that is connected to the tensioner; drive roller (DR) which is driven by the motor; assist roller (AR). The model is shown in Fig. 2.10, the notations are not changed, only the numbers to functional names.

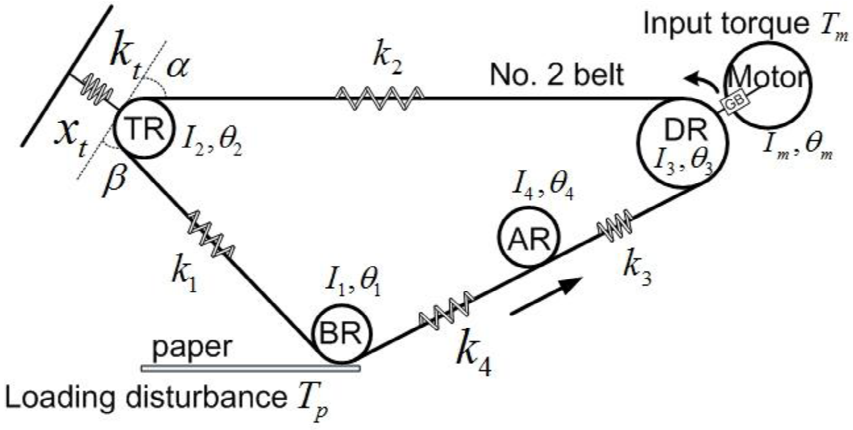

Figure 2.10: the Four-Rollers-Belt System with Functional Names

As explained in the previous, one of the uncertainties is led by the parametric uncertainty. It can be quantified by assuming that each uncertain parameter is bounded within some region. As in a real system, we assume the transfer

function of the nominal one which means containing no model uncertainty can be represented as $G_n(s)$, and the transfer function of the uncertainty part can be denoted as $G_p(s)$ that it is bounded as [86]:

$$G_p(s) = \Delta G_n(s) \tag{2.13}$$

where when $G(s)$ is scalar, the bound on Δ is that $\|\Delta\| \leqslant 1$, otherwise the bound is $\|\Delta\|_\infty \leqslant 1$. Therefore the real system can be expressed as:

$$G(s) = (\mathbf{1} + \Delta)G_n(s) \tag{2.14}$$

Notice that the $\mathbf{1}$ is a general symbol as 1 for scalar, and $\mathbf{I}$ for transfer function matrices in this section.

Consider a linear uncertainty in the equations of motion in Eq. (2.9) that bound in 5%, 10%, 20% of $\mathbf{M}$, and $\mathbf{K}$ separately. The effects on the DR speed, stretching displacement, and absolute displacement are graphed in Fig. 2. 11 (a), (b), and (c) respectively.

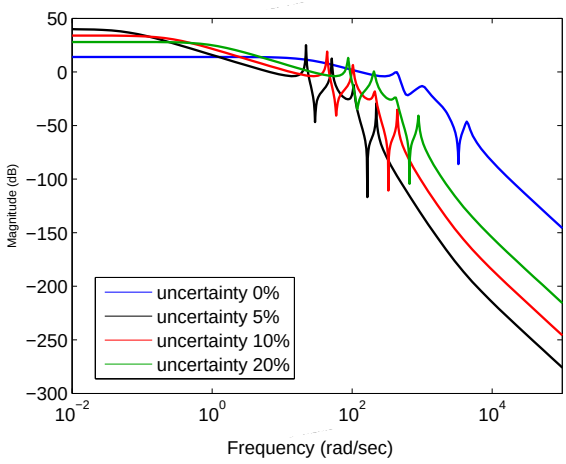

(a) DR speed

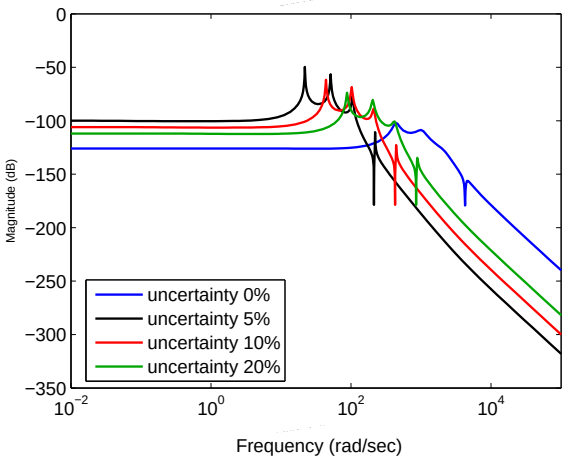

(b) stretching displacement

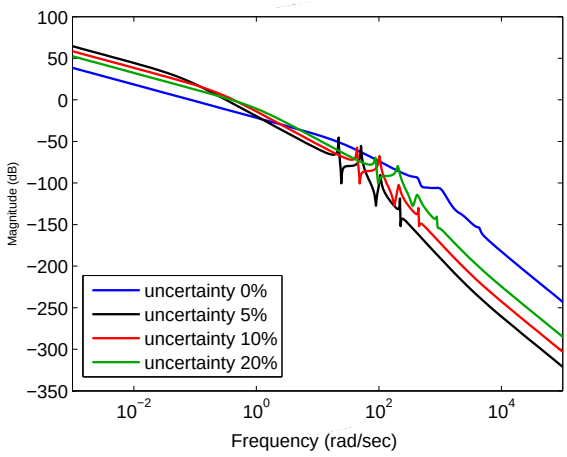

(c) absolute displacement

Figure 2.11: Effects of Different Uncertainty on the Magnitude of Frequency Response in Four-Rollers-Belt System

The longitudinal axis represents the magnitude of the frequency response from loading disturbance T_p to each outputs under different circumstance: system with no uncertainty in blue lines; system with 5% uncertainty in black line; system with 10% uncertainty in red line; system with 20% uncertainty in green line. It is clear that natural frequencies reflected in the peaks partly of the system vary with the system uncertainty. This could be explained by the fact that the uncertainty

model is purely based on linear variation of the system parameters. Although the nonlinear uncertainty is not included in this study, it is not hard to find out that even slight unknown part in the system could affect the system behavior largely. And the influences on the control design for the image transfer belt system from it will be studied next.

2.4.2 Effects on Passive Control Method by Flywheel

Generally speaking, a passive control method is the idea that change the system behavior by additional apparatus, like flywheel [87]. A flywheel is a rotating mechanical device that is used to store rotational energy [88]. It has a significant moment of inertia, and thus resist changes in rotational speed. In the previous research of the author, the various inertia of flywheel with different location were investigated. Since the four-rollers-belt system is unstable due to the tensioner part, the H_2 norm of the system is infinite. As a result, a finite integration of the magnitude of frequency response in the system is used instead of the H_2 norm, to evaluate the system performance, showing as:

$$J_i = \int_0^{\omega_{max}} |G_i(j\omega)|^2 \ , \tag{2.15}$$

where i refers the number of the outputs and G_i represents the transfer function from T_p on the $i-$th outputs. In order to reflect the comparison between system with and without the flywheel, the ratio of J_i between uncompensated system and compensated system is applied in the study. Cases of different inertia of flywheel combined with various adding location are investigated, and the results are shown in Fig. 2.12 (a), (b), (c), respectively.

The horizontal axle is the inertia ratio of the flywheel compared with the inertia of roller where it is added. That means the added flywheel becomes heavier along the horizontal axle. Various colors represents the different location: black line is on burden roller, blue line is on tension roller, red line is on drive roller, and green line is on assist roller. Fig. 2.12 (a) shows the effects on speed of drive roller. It is obviously that all these locations reduce the vibration on speed of drive roller, and the attenuation effect becomes stronger as the flywheel goes heavier. This is following the inertia principle. Fig. 2.12 (b) depicts the

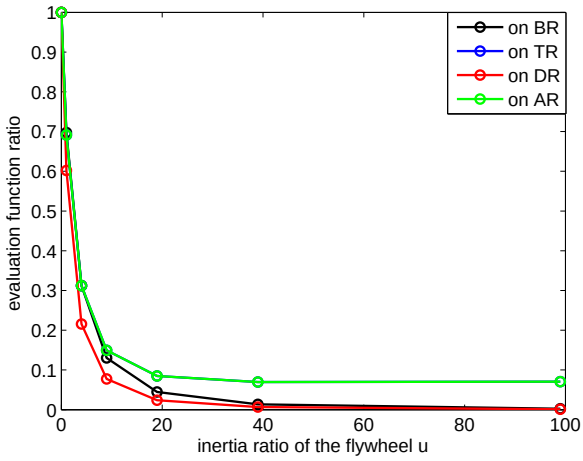

(a) DR speed

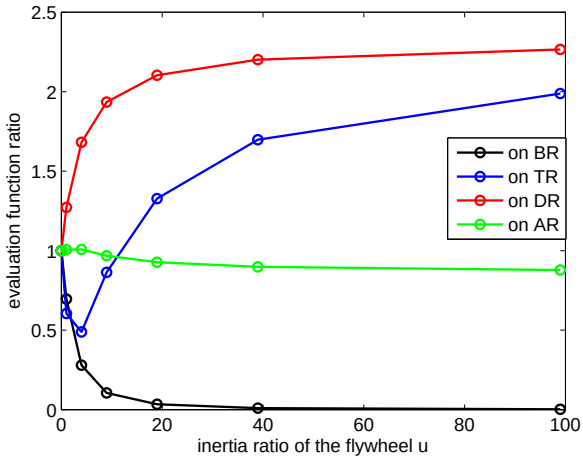

(b) stretching displacement

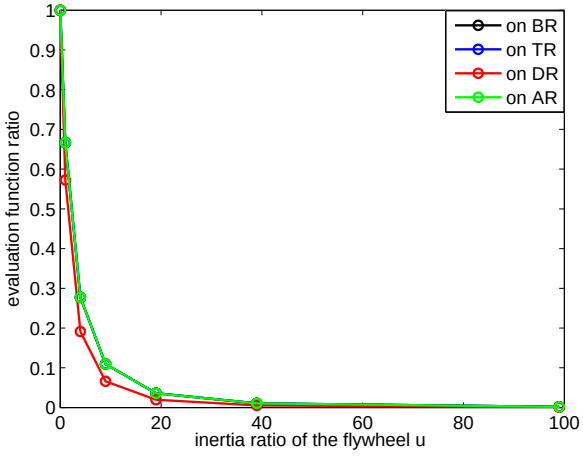

(c) absolute displacement

Figure 2.12: Ratio of evaluation function from T_p on outputs under different conditions

results of stretching displacement which differs a lot. Only by putting flywheel on burden roller can efficiently reduce the displacement on it, and other locations worsen the situation. The interesting part is when the location is tension roller, the suppressing effect first becomes better, then goes worse as the inertia becomes larger. Fig. 2.12 (c) is about the absolute displacement that almost shows the similar change as the speed of drive roller. Therefore as a result, the best location is burden roller, and the large inertia of flywheel is preferred.

As mentioned before, system uncertainty affect the system performance a lot. The investigation of its effect on passive control method with flywheel is conducted to show the shortage of this control method. Now consider compensating the system by adding flywheel on the best place, the burden roller. The results of system with uncertainty are shown as Fig. 2.13 (a), (b), (c), separately.

The blue line is the results from original system with no uncertainty, and the red line shows the results in the system with 5% uncertainty of $\mathbf{K}$. Also the horizontal and longitudinal axle represents the same meaning as in Fig. 2.12.

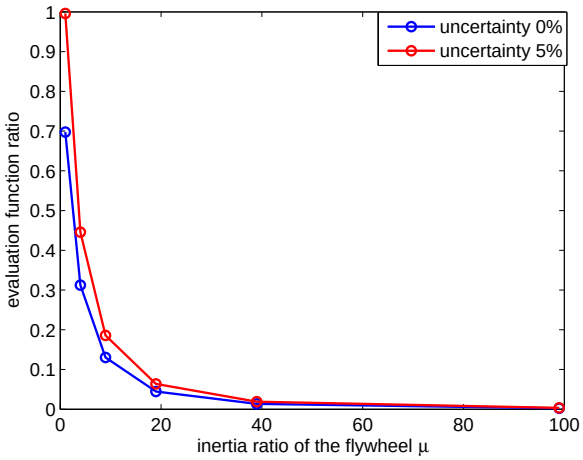

(a) DR speed

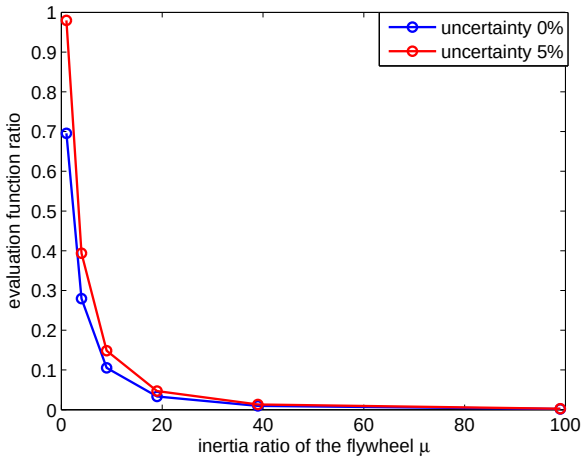

(b) stretching displacement

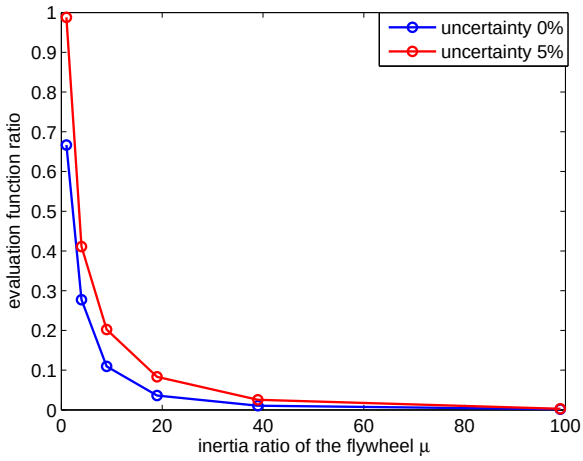

(c) absolute displacement

Figure 2.13: Ratio of evaluation function from T_p on outputs with and without system uncertainty with flywheel on burden roller

It is clearly that this time even the best location which is burden roller can not attenuate none of the outputs. And in order to resist the affect from system uncertainty, extremely large flywheel is needed. In all of these three figures, it is indicated if the inertia of the flywheel is big enough, the desired attenuating results can be achieved. However this is out of the industrial applicability and manufacture.

2.5 Summary

This chapter investigated the mathematical model for image transfer belt system. Based several assumptions, the four-rollers-belt system model with descriptions for belt variation is established. By comparing the model with and without tensioner part, it is ascertained that tensioner can not be ignored since it is one of the factors leading to belt vibration. Also multi-rollers-belt model is compared with the four-rollers-belt one to certify that the latter one is proper to be applied in control design as a simplification from real machinery. Additionally, affect from system uncertainty on passive control method by flywheel to attenuate belt vibration is investigated. Results indicate that active control emphasizing robustness is required.

Chapter 3

Optimal State Feedback Control for Image Transfer Belt System Based on H_2 Norm

3.1 Introduction

Feedback control has a long history which goes back to the steam engine invented by Watt in 1781. The reasons why the feedback control is needed in a system are many, like stabilizing the unstable open-loop system, dealing with the model uncertainty, and rejecting unknown disturbance. Though there are various types of feedback control designs, they all require the information fed to the controller from the system, either the state status of the system, or the errors of variables need to be controlled. Also according to the control purposes, the architecture and solution for a feedback control could go far apart from others.

It is very common applying motor speed control in a belt driven system. Nevertheless the purpose of this control design is to maintain the drive speed in a constant value which is not suitable for the image transfer belt system, since the belt variation is the foremost concern. As a result, to design a suitable controller for attenuating the belt vibration caused as the loading disturbance is quite necessary. An optimal control method based on the H_2 norm of the outputs via state feedback is developed in this chapter. Although the original purpose of

building a state feedback controller is mostly to reassign the poles in a system. This chapter applies the state feedback structure to optimize the outputs in a system.

A brief introduction of the H_2 norm and the motivation of H_2 norm based optimal control are exhibited in Section 3.2. The structure of this state feedback design and control objectives are explained in Section 3.3. Methods and proofs to generate the desired controller are explained in detail in Section 3.4, including stability proof, program to calculate parameters in controller through linear matrix inequalities (LMIs). Section 3.5 exhibits the obtained controller and its performance on the image transfer belt system with the loading disturbance. Summary is drawn in Section 3.6.

3.2 H_2 Norm and Motivation for H_2 Optimal Control

3.2.1 Definition of H_2 Norm

The H_2 norm is originated from the definition of the L_2 norm in signal norms [89]. For a scalar-valued signal $f(t)$, the L_2 norm is defined as:

$$\|f(t)\|_{L_2} = \sqrt{\int_0^\infty f(t)^2 dt} \ . \tag{3.1}$$

Its interpretation can be seen as the energy of the signal $f(t)$. When the representation changes to Laplace domain, the L_2 norm can be written as:

$$\|f(s)\|_{L_2} = \sqrt{\frac{1}{2\pi}\int_{-\infty}^\infty |f(j\omega)|^2 d\omega} \ . \tag{3.2}$$

These two equations are equal by *Parseval's* theorem which is not explained here.

For a vector signal $f(t) = [f_1(t), ..., f_n(t)]^{\mathrm{T}}$, the L_2 norm is the root square of

the sum of each L_2 norm for the scalar-valued signal [90]:

$$\|f(t)\|_{L_2} = \sqrt{\sum_{i=1}^{n} \|f_i(t)\|_{L_2}^2} = \sqrt{\int_0^\infty f(t)^{\mathrm{T}} f(t)} \ . \tag{3.3}$$

Similarly for the Laplace domain, it is expressed as:

$$\|f(s)\|_{L_2} = \sqrt{\frac{1}{2\pi} \int_{-\infty}^{\infty} f(j\omega)^{\mathrm{T}} f(j\omega) d\omega} \ . \tag{3.4}$$

Now go to a system, the H_2 norm is finite if and only if the system is stable, otherwise, it is infinite. For a stable single-input-single-output (SISO) system with a transfer function $G(s)$, the H_2 norm is defined as:

$$\|G\|_{H_2} = \sqrt{\frac{1}{2\pi} \int_{-\infty}^{\infty} |G(j\omega)|^2 d\omega} \ . \tag{3.5}$$

And for a multi-inputs-multi-outputs (MIMO) system with a transfer function matrix $G(s) = [G_{ik}(s)]$, the definition generalizes as [91]:

$$\begin{aligned} \|G\|_{H_2} &= \sqrt{\sum_{i,k} \|G_{ik}\|_{H_2}^2} \\ &= \sqrt{\frac{1}{2\pi} \int_{-\infty}^{\infty} \sum_{i,k} |G_{ik}(j\omega)|^2 d\omega} \\ &= \sqrt{\frac{1}{2\pi} \int_{-\infty}^{\infty} \mathrm{tr}[G(j\omega)^{\mathrm{T}} G(j\omega)] d\omega} \ . \end{aligned} \tag{3.6}$$

where the symbol tr means the trace of a square matrix that is the sum of the elements on the main diagonal from the upper left to the lower right.

By the definition, it is not difficult to find out that the evaluation function defined in Chapter 2 is part value of this H_2 norm due to the instability of the original system.

3.2.2 Motivation

The H_2 norm optimal control of a system could have several feedback types, like output feedback or state feedback. But the control objective is unique that is to minimize the H_2 norm of the system. Also the stabilization problem is included in the design.

For a system with the transfer function G, assume the input is Gaussian noise with signal variance S, then the output of this system is also a noise but with density:

$$S_{out}(j\omega) = G(j\omega)S(j\omega)G(j\omega)^{\mathrm{T}} \ . \tag{3.7}$$

Based on Eq. (3.7), the power of the output can be calculated. If the input signal is white noise which means $S(j\omega) = \mathrm{I}$, then the energy of the output is just the square of H_2 norm of this system $\|G\|_{H_2}^2$. Thus if the control design minimizes the H_2 norm of a system, it will minimize the variance of the system under the influence of colored noise.

3.3 Control Architecture

Now recall the image transfer belt system which is modeled as the four-rollers-belt system. According to the equations of motion, Eq. (2.5), the state vector of this system is picked as:

$$\begin{aligned} X &= \left[x, \dot{x}\right]^{\mathrm{T}} \\ &= \left[\theta_1, \theta_2, \theta_3, \theta_4, \theta_m, x_t, \dot{\theta}_1, \dot{\theta}_2, \dot{\theta}_3, \dot{\theta}_4, \dot{\theta}_m, \dot{x}_t\right]^{\mathrm{T}} \ . \end{aligned} \tag{3.8}$$

Based on Eq. (2.9), the state vector equation is established as:

$$\dot{X} = \mathbf{A}X + \mathbf{B}_1 T_p + \mathbf{B}_2 T_m \ , \tag{3.9}$$

where

$$\mathbf{A} = \begin{bmatrix} \mathbf{0} & \mathbf{I} \\ -\mathbf{M}^{-1}\mathbf{K} & -\mathbf{M}^{-1}\mathbf{C} \end{bmatrix} , \mathbf{B}_1 = \begin{bmatrix} \mathbf{0} \\ \mathbf{M}^{-1}\mathbf{P}_1 \end{bmatrix} , \mathbf{B}_2 = \begin{bmatrix} \mathbf{0} \\ \mathbf{M}^{-1}\mathbf{P}_2 \ . \end{bmatrix}$$

The outputs are selected for attenuating the belt variation and maintaining the rotation speed for the system, which are:

$$Y = \begin{bmatrix} \dot{\theta}_3 \\ \theta_3 r_3 - \theta_2 r_2 + x_t \sin\alpha \\ \frac{1}{2}(\theta_3 r_3 + \theta_2 r_2 + x_t \sin\alpha) \end{bmatrix} . \tag{3.10}$$

The last two items are stretching displacement and absolute displacement of the No. 2 belt in Fig. 2.10. Again the output vector equation is derived as:

$$Y = \mathbf{C}X + \mathbf{D}_1 T_p + \mathbf{D}_2 T_m \ , \tag{3.11}$$

where

$$\mathbf{C} = \begin{bmatrix} & \mathbf{0}_{1\times 6} & & 0 & 0 & 1 & 0 & 0 & 0 \\ 0 & -r_2 & r_3 & 0 & 0 & \sin\alpha & & \mathbf{0}_{1\times 6} & \\ 0 & \frac{r_2}{2} & \frac{r_3}{2} & 0 & 0 & \frac{\sin\alpha}{2} & & \mathbf{0}_{1\times 6} & \end{bmatrix} , \mathbf{D}_1 = \mathbf{0} \ , \mathbf{D}_2 = \mathbf{0} \ .$$

Notice that the outputs of the image transfer belt system can be adjusted for desired control results. For Eq. (3.9), and Eq. (3.11), the signal flow of the state space expression is depicted as:

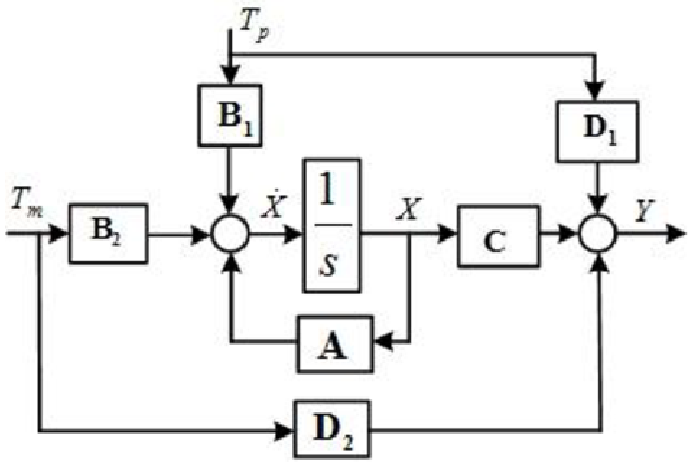

Figure 3.1: The signal flow in state space equations

To this system, there are two inputs: loading torque T_p that is disturbance

to the system, the motor torque T_m that is set as the control signal. In Fig. 3.1, the system is a open-loop one. The state feedback control K is added to make the closed-loop system shown as:

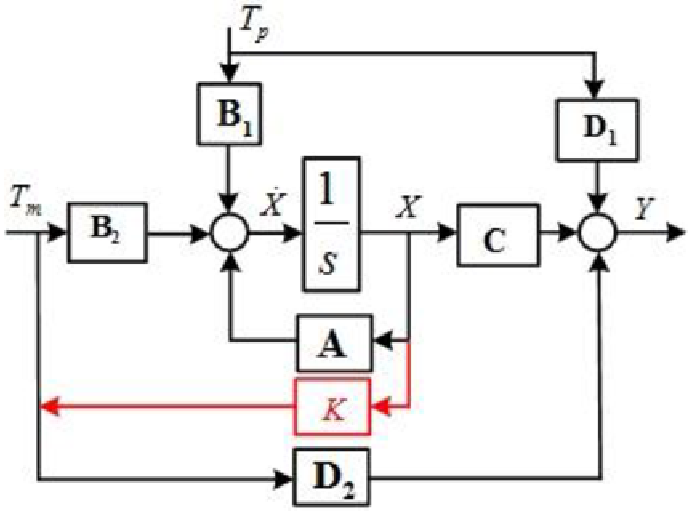

Figure 3.2: The signal flow in closed-loop system

The block K is the controller needed to be constructed. The request to this controller is:

- stabilize the image transfer belt system.
- reduce the affect from disturbance T_p on system outputs Y, that is minimize the H_2 norm of the transfer function from T_p to Y.

3.4 Optimal State Feedback Control in H_2 Norm

3.4.1 Solution for Stability Problem

The general concept of the stability also known as Lyapunov Theory is declared as:

Theorem 1 (Lyapunov)

Suppose there exists a continuously differentiable function V for which $V(0) = 0$ and $V(x) > 0$ for $x \neq 0$. Furthermore, suppose $\lim_{\|x\|\to\infty} V(x) = \infty$ and

$$\lim_{h\to 0^+} \frac{V(x(t+h)) - V(x(t))}{h} = \frac{d}{dt}V(x(t)) < 0$$

for any x such that $\dot{x}(t) = f(x(t))$. Then for any $x(0) \in \mathbb{R}$ the system of equations

$$\dot{x}(t) = f(x(t))$$

has a unique solution which is stable in the sense of Lyapunov [92].

Now consider a state vector equation $\dot{x}(t) = Ax(t)$, where A is a matrix. And if $x(t) \to 0$ as $t \to \infty$ which means stable, the following inequality is required.

Lemma 1 (Lyapunov Inequality)

A is stable if and only if there exists a $P > 0$ such that

$$A^{\mathrm{T}}P + PA < 0 \ . \tag{3.12}$$

Before the proof for this lemma, the definition of a positive definite matrix is given as:

Definition 1

A symmetric matrix $P = P^{\mathrm{T}}$ is positive definite, denoted as $P > 0$ if $x^{\mathrm{T}}Px > 0$ for all $x \neq 0$. This definition can also be applied for the negative definite matrix if $-P > 0$ [93].

Then the proof for **Lemma 1** is as following:

Suppose there exists a $P > 0$ such that $A^{\mathrm{T}}P + PA < 0$, the Lyapunov function is defined as $V(x(t)) = x(t)^{\mathrm{T}}Px(t)$. It is obvious that $V(x(t)) > 0$ for $x(t) \neq 0$ since $P > 0$, $V(0) = 0$. Furthermore,

$$\begin{aligned}\dot{V}(x(t)) &= \dot{x}(t)^{\mathrm{T}}Px(t) + x(t)^{\mathrm{T}}P\dot{x}(t) \\ &= x(t)^{\mathrm{T}}A^{\mathrm{T}}Px(t) + x(t)^{\mathrm{T}}PAx(t) \\ &= x(t)^{\mathrm{T}}(A^{\mathrm{T}}P + PA)x(t)\end{aligned}$$

Since $A^{\mathrm{T}}P + PA < 0$, therefore $\dot{V}(x(t)) < 0$ for all $x \neq 0$ which means the system is globally stable. This means A is stable.

For the other direction, assume A is stable, then let

$$P = \int_0^\infty e^{A^{\mathrm{T}}s} e^{As} ds$$

this P is convergent because A is stable. Also

$$\begin{aligned} PA &= \int_0^\infty e^{A^{\mathrm{T}}s} e^{As} A ds \\ &= \int_0^\infty e^{A^{\mathrm{T}}s} A e^{As} ds \\ &= \int_0^\infty e^{A^{\mathrm{T}}s} \frac{d}{ds}(e^{As}) ds \\ &= \left[e^{A^{\mathrm{T}}s} e^{As} \right]_0^\infty - \int_0^\infty \frac{d}{ds} e^{A^{\mathrm{T}}s} e^{As} \\ &= -I - \int_0^\infty A^{\mathrm{T}} e^{A^{\mathrm{T}}s} e^{As} \\ &- I - A^{\mathrm{T}} P \ , \end{aligned}$$

therefore $PA + A^{\mathrm{T}}P = -I < 0$.

For a system described as $\dot{x} = Ax + Bu$, where u is the input, then the Lyapunov Inequality can be formed as:

Lemma 2

(A, B) is controllable if and only if there exists a $P > 0$ such that

$$A^{\mathrm{T}}P + PA + BB^{\mathrm{T}} < 0 \tag{3.13}$$

The proof is not presented here [94].

3.4.2 Solution for Bound in H_2 Norm

Consider a system G with the following description:

$$\begin{aligned} \dot{x} &= Ax + Bu \\ y &= Cx \ . \end{aligned}$$

The transfer function $G(s)$ is derived as:

$$G(s) = C(sI - A)^{-1}B \tag{3.14}$$

The following theorem is declared as:

Theorem 2

The system described in Eq. (3.14), then the following are equivalent [95].

1. A is stable and $\|G(s)\|_{H_2}^2 < \gamma$
2. There exists some $P > 0$ such that

$$\begin{aligned} \mathrm{tr}CP^{\mathrm{T}}C &< \gamma \\ AP + PA^{\mathrm{T}} + BB^{\mathrm{T}} &< 0 \end{aligned}$$

The proof from 1 to 2 is as following:

The Laplace transform of e^{At} is conducted as:

$$\begin{aligned} e^{At}(s) &= \int_0^\infty e^{At} e^{-ts} dt \\ &= \int_0^\infty e^{-(sI-A)t} dt \\ &= -(sI-A)^{-1} e^{-(sI-A)t} dt|_{t=0}^{t=\infty} \\ &= (sI-A)^{-1} \end{aligned}$$

and this leads to the Laplace transform for $Ce^{At}B$ is:

$$Ce^{At}B(s) = C(sI-A)^{-1}B \tag{3.15}$$

Now recall the representation of the H_2 norm of $G(s)$ in Laplace domain:

$$\begin{aligned} \|G(s)\|_{H_2}^2 &= \|C(sI-A)^{-1}B\|_{H_2}^2 \\ &= \frac{1}{2\pi}\int_0^\infty \mathrm{tr}((C(j\omega I-A)^{-1}B)^{\mathrm{T}}(C(j\omega I-A)^{-1}B))d\omega \\ &= \frac{1}{2\pi}\int_0^\infty \mathrm{tr}((C(j\omega I-A)^{-1}B)(C(j\omega I-A)^{-1}B)^{\mathrm{T}})d\omega \end{aligned} \tag{3.16}$$

Eq. (3.15) shows that the inverse Laplace transform from $C(j\omega I-A)^{-1}B$ to $Ce^{At}B$. By substituting it into Eq. (3.16), the H_2 norm is rewritten as:

$$\|G(s)\|_{H_2}^2 = \mathrm{tr}\int_{-\infty}^{\infty} Ce^{At}BB^{\mathrm{T}}e^{A^{\mathrm{T}}t}C^{\mathrm{T}}dt \tag{3.17}$$

If A is stable, then the Controllability Grammian is defined as:

$$P = \int_0^\infty e^{At} B B^{\mathrm{T}} e^{A^{\mathrm{T}}} dt$$

By substituting it to Eq. (3.17)

$$\|G(s)\|_{H_2}^2 = \mathrm{tr} C P C^{\mathrm{T}} \tag{3.18}$$

Since $\|G(s)\|_{H_2}^2 < \gamma$, therefore $P > 0$ and $\mathrm{tr} C P C^{\mathrm{T}} < \gamma$. Also based on **Lemma 2**, A is stable then $AP + PA^{\mathrm{T}} + BB^{\mathrm{T}} < 0$. So it ascertains the statement 1 leads statement 2. The inverse part is not shown here but the idea is the same.

3.4.3 Calculation Procedure with Linear Matrix Inequalities (LMIs)

Now go back to the problem concerning to image transfer belt system. Recall Fig. 3.2, the open-loop system with the desired controller can be transformed to the general representation shown in Fig. 3.3:

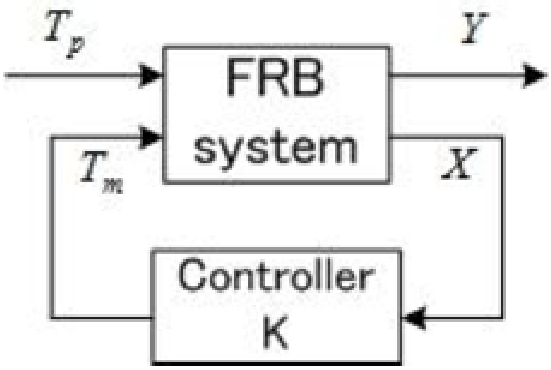

Figure 3.3: General plant for four-rollers-belt system with controller

For the general plant, T_p is the exogenous input, T_m is the actuator input obtained from controller K. X is the sensed outputs also knowns as feedback outputs, Y is the regulated outputs. The equations of these variables are listed

as:

$$\begin{aligned} \dot{X} &= \mathbf{A}X + \mathbf{B}_1 T_p + \mathbf{B}_2 T_m \\ Y &= \mathbf{C}X + \mathbf{D}_1 T_p + \mathbf{D}_2 T_m \\ T_m &= KX \ . \end{aligned} \tag{3.19}$$

Based on these equations, the general plant in closed-loop structure can be reformed as a open-loop system shown in Fig. 3.4:

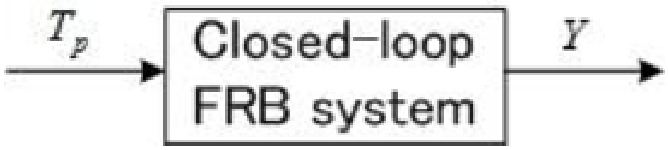

Figure 3.4: Reformed general plant for four-rollers-belt system containing controller

The actuator input T_m and the sensed outputs X are included in the closed-loop FRB system. And the system description for it can be derived based on Eq. (3.19) listed as:

$$\begin{aligned} \dot{X} &= (\mathbf{A} + \mathbf{B}_2 K)X + \mathbf{B}_1 T_p \\ Y &= (\mathbf{C} + \mathbf{D}_2)X + \mathbf{D}_1 T \ . \end{aligned} \tag{3.20}$$

Now the system with controller becomes the similar formation in **Theorem 2**. The transfer function from T_p on Y is denoted as $O(s)$, where:

$$O(s) = \frac{Y(s)}{T_p(s)} \ . \tag{3.21}$$

To minimize the H_2 norm of $P(s)$, the constraint is set as $\|O(s)\|_{H_2} < \gamma_2$. By minimizing γ_2, the objective is achieved.

Applying **Theorem 2** to the system described in Eq. (3.20), the problem becomes to search some $P > 0$ where

$$\begin{aligned} \mathbf{A}P + \mathbf{B}_2 KP + PK^{\mathrm{T}}\mathbf{B}_2^{\mathrm{T}} + P\mathbf{A}^{\mathrm{T}} + \mathbf{B}_1\mathbf{B}_1^{\mathrm{T}} < 0 \\ \mathrm{tr}(\mathbf{C}_1 + \mathbf{D}_2 K)P(K^{\mathrm{T}}\mathbf{D}_2^{\mathrm{T}} + \mathbf{C}_1) < \gamma_2 \ . \end{aligned} \tag{3.22}$$

Now assume there exist a matrix Z that $K = ZP^{-1}$, then Eq. (3.22) can be rewritten as:

$$\begin{aligned} \begin{bmatrix} \mathbf{A} & \mathbf{B}_2 \end{bmatrix} \begin{bmatrix} P \\ Z \end{bmatrix} + \begin{bmatrix} P & Z^{\mathrm{T}} \end{bmatrix} \begin{bmatrix} \mathbf{A}^{\mathrm{T}} \\ \mathbf{B}_2^{\mathrm{T}} \end{bmatrix} + \mathbf{B}_1 \mathbf{B}_1^{\mathrm{T}} < 0 \\ \mathrm{tr}(\mathbf{C}_1 P + \mathbf{D}_2 Z) P^{-1} (\mathbf{C}_1 P + \mathbf{D}_2 Z) < \gamma_2 \ . \end{aligned} \tag{3.23}$$

However nonlinearity item is involved in the second inequality. By using the Schur Complement, Eq. (3.23) is reformulated as:

$$\begin{aligned} \begin{bmatrix} \mathbf{A} & \mathbf{B_2} \end{bmatrix} \begin{bmatrix} P \\ Z \end{bmatrix} + \begin{bmatrix} P & Z^{\mathrm{T}} \end{bmatrix} \begin{bmatrix} \mathbf{A}^{\mathrm{T}} \\ \mathbf{B}_2^{\mathrm{T}} \end{bmatrix} + \mathbf{B}_1 \mathbf{B}_1^{\mathrm{T}} < 0 \\ \begin{bmatrix} P & (\mathbf{C}_1 P + \mathbf{D}_2 Z)^{\mathrm{T}} \\ \mathbf{C}_1 P + \mathbf{D}_2 Z & W \end{bmatrix} > 0 \\ \mathrm{tr}(W) < \gamma_2 \ . \end{aligned} \tag{3.24}$$

The Schur Complement and this procedure are explained in Appendix B.

Therefore the control problem is to find some Z, and $P > 0$ satisfying Eq. (3.24) and minimize γ_2. The desired controller K can be obtained from $K = ZP^{-1}$. The rough calculation process is shown in Fig. 3.5 briefly, and explained as [95]:

1. (Initialization step: $i = 1$): choose a $P^0 > 0$.

2. (Step i, first part): for fixed P^i, solve the following LMI relaxation of minimization problem of Eq. (3.24):

$$\gamma_{2,1}^i = \min_Z \mathrm{tr}(W) \text{ subject to Eq. (3.24)}$$

At the optimum, fix $Z^i = Z$

3. (Step i, second part): for fixed Z^i, solve the following LMI relaxation of minimization problem of Eq. (3.24):

$$\gamma_{2,2}^i = \min_P \mathrm{tr}(W) \text{ subject to Eq. (3.24)}$$

At the optimum, fix $P^i = P$.

4. (Termination step), if $\gamma_{2,1}^i < \gamma_{2,2}^i$, then stop, $K = Z^i (P^i)^{-1}$, otherwise change i to $i + 1$ and go to step 2.

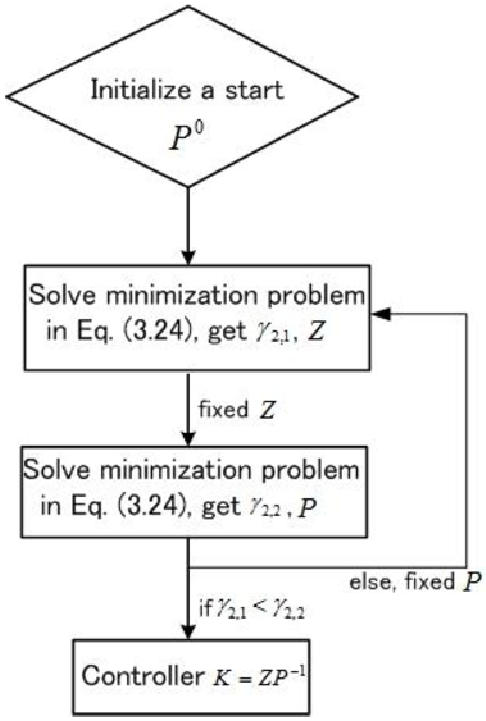

Figure 3.5: Calculation process for H_2 optimal state feedback control problem

3.5 Numerical Simulation

In this section, the proposed controller is put to the open-loop system and the control results are studied. The parameters used for four-rollers-belt system are in Table 2.1. As explained previously, the outputs which are also the minimizing objects are changeable in order to achieve the desired control performance. Three different methods are exhibited here.

First the effectiveness of this H_2 optimal state feedback controller is certified as following. The outputs Y are the same in Eq. (3.10), which are the speed of drive roller, stretching displacement, and absolute displacement. The obtained controller K is:

$$T_m = KX \ , \tag{3.25}$$

where

$$K = [6.38 \times 10^7 \quad -9.16 \times 10^{10} \quad -2.62 \times 10^{12} \quad -9.16 \times 10^{10}$$
$$-1.24 \times 10^{11} \quad 4.62 \times 10^{12} \quad -6.20 \times 10^4 \quad -2.75 \times 10^7$$
$$-4.00 \times 10^{14} \quad -2.75 \times 10^7 \quad -3.19 \times 10^5 \quad 1.38 \times 10^9]$$

And the achieved minimized H_2 norm γ_2 is 0.0047.

The comparisons of the frequency response from disturbance T_p on each outputs between the open-loop system and closed-loop system with controller in Eq. (3.25) are shown in Fig. 3.6 (a), (b), (c), respectively.

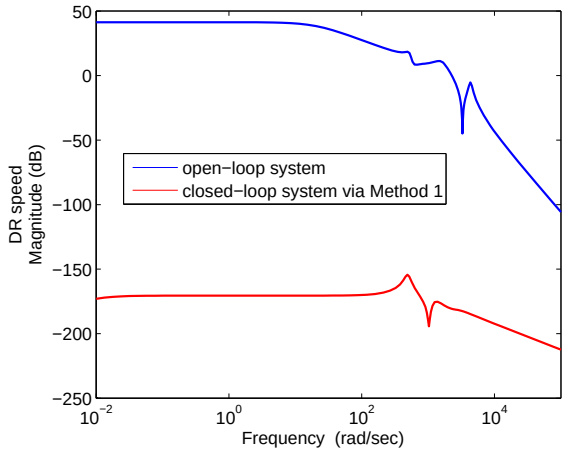

(a) DR speed

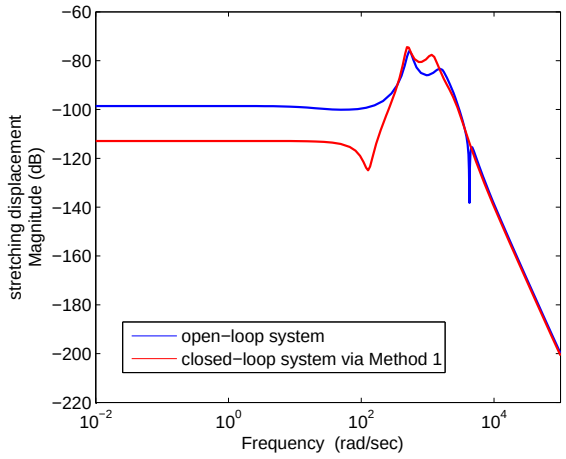

(b) stretching displacement

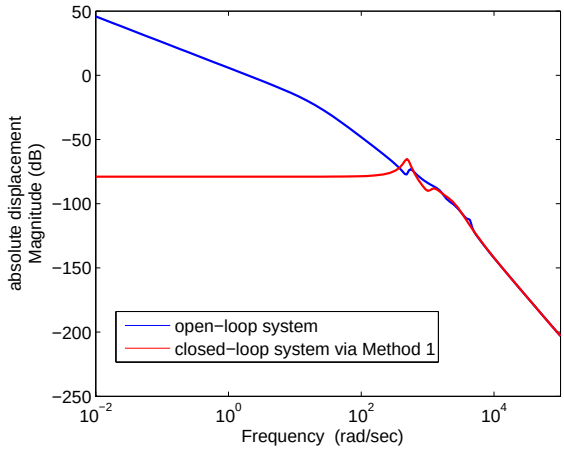

(c) absolute displacement

Figure 3.6: Magnitude of frequency response from T_p on outputs in open-loop and closed-loop system

Firstly, the controller K stabilizes the open-loop system, and it reduces the effect from T_p on the systems especially in lower frequency range concerning the stretching displacement and absolute displacement. Also the control performance on speed of drive roller is significant. The response to a impulse signal in the open-loop system and closed-loop system is shown in Fig. 3.7 (a), (b), (c),individually.

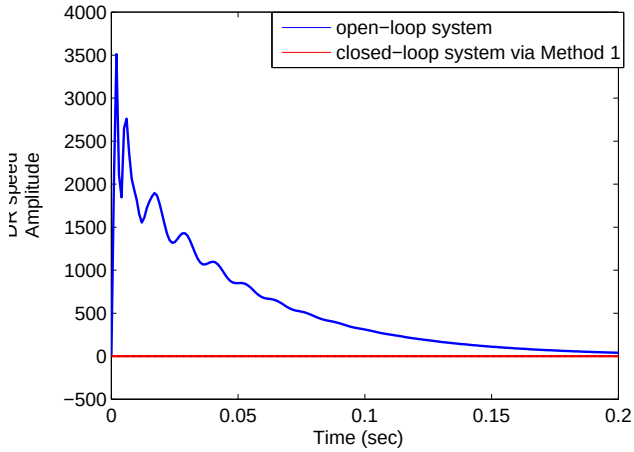

(a) DR speed

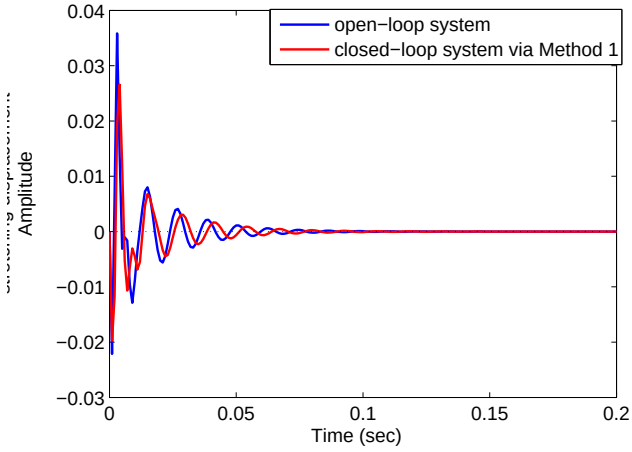

(b) stretching displacement

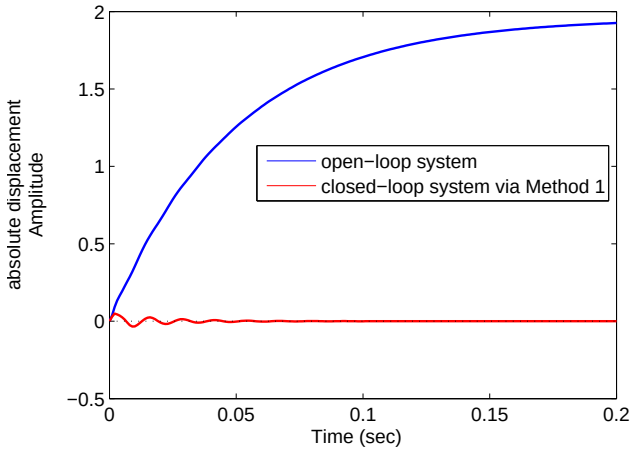

(c) absolute displacement

Figure 3.7: Response to impulse signal in open-loop system and closed-loop system

Response for speed of drive roller is graphed in Fig. 3.7 (a). It is shown that controller endows it a strong stability resisting to the disturbance with a maximum variation of 4.54×10^{-7}. And the variation decays within 0.15 seconds. Fig. 3.7 (b) is the results of stretching displacement. It oscillates as the impulse disturbance functioned on system with a maximum value of 0.036 and decays within 0.08 seconds. Although the decay time in closed-loop system is not improved so

much, the maximum variable is reduced to 0.025. Also the control effects on absolute displacement in Fig. 3.7 (c) proves its effectiveness by stabilizing the variation, and achieving a maximum value of 0.048.

This controller is named as Method 1, and the other two method are discussed to find out the best control performance by selecting different objectives. Notice that the main concerning is the belt variation so the stretching displacement and absolute displacement are the two assessment standards.

Method 2

In chapter 2, it is already ascertained that part of the reason is because of the variation from tensioner. Based on it, the tensioner displacement x_t, stretching displacement, absolute displacement are chosen as the outputs of the closed-loop system, that is:

$$Y_{m2} = \begin{bmatrix} x_t \\ \theta_3 r_3 - \theta_2 r_2 + x_t \sin\alpha \\ \dfrac{1}{2}(\theta_3 r_3 + \theta_2 r_2 + x_t \sin\alpha) \end{bmatrix} . \tag{3.26}$$

The value of matrix $\mathbf{C}$ also needs adjustment as:

$$\mathbf{C} = \begin{bmatrix} 0 & 0 & 0 & 0 & 0 & 1 & \mathbf{0}_{1\times 6} \\ 0 & -r_2 & r_3 & 0 & 0 & \sin\alpha & \mathbf{0}_{1\times 6} \\ 0 & \dfrac{r_2}{2} & \dfrac{r_3}{2} & 0 & 0 & \dfrac{\sin\alpha}{2} & \mathbf{0}_{1\times 6} \end{bmatrix} .$$

Based on the method in the previous section, the new controller is calculated as:

$$T_m = K_{m2} X \ , \tag{3.27}$$

where

$$\begin{aligned} K_{m2} = [& -3.00\times 10^7 \quad 2.02\times 10^7 \quad -2.22\times 10^8 \quad -2.04\times 10^7 \\ & -2.76\times 10^6 \quad 1.70\times 10^9 \quad -1.17\times 10^5 \quad -1.13\times 10^5 \\ & -3.42\times 10^4 \quad -6.20\times 10^4 \quad -86.33 \quad -1.15\times 10^7] \end{aligned}$$

And the achieved minimized H_2 norm γ_2 is 0.0058.

The comparisons of the frequency response from disturbance T_p on each outputs between method 1 in Eq. (3.25) and method 2 in Eq. (3.26) are shown in Fig. 3.8 (a), (b), respectively.

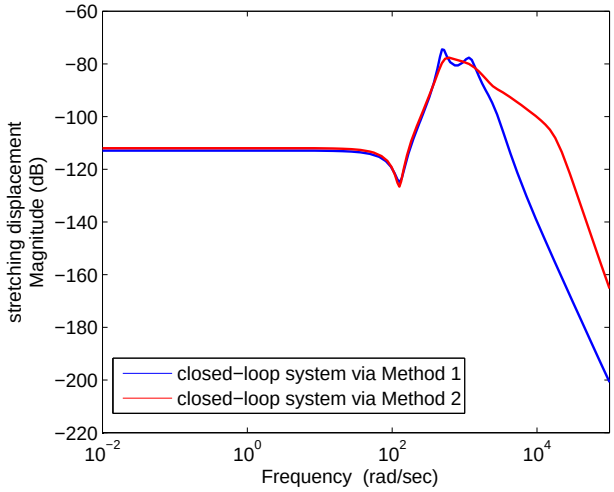

(a) stretching displacement

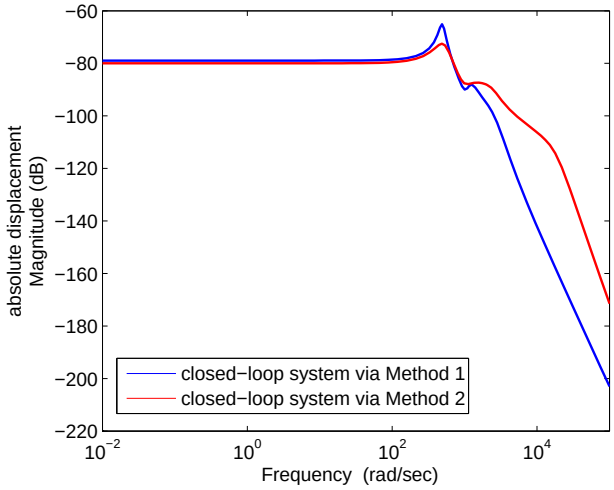

(b) absolute displacement

Figure 3.8: Magnitude of frequency response from T_p on outputs with method 1 and method 2

Since the first output of these two methods are different, its result is not shown

here. Both methods stabilizes the open-loop system, although the first achieves better effect than the second only judging from the magnitude of frequency response. To prove this, the response to impulse disturbance of the system using method 1 and 2 are obtained in Fig. 3.9 (a), and (b).

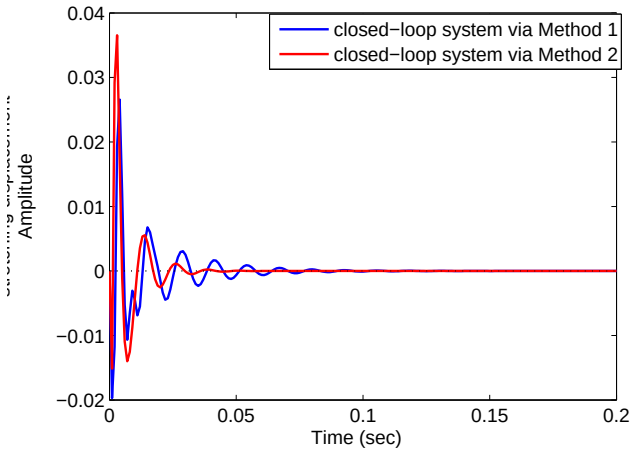

(a) stretching displacement

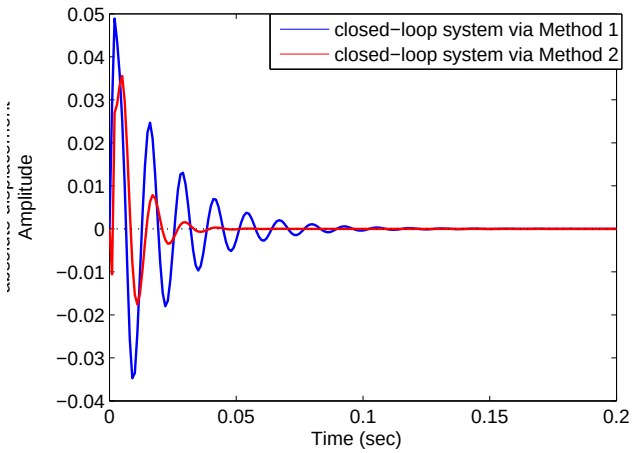

(b) absolute displacement

Figure 3.9: Response to impulse disturbance of system with method 1 and method 2

The blue line reflects control results by method 1, and the red line graphs the method 2. It is quite obviously both stretching displacement and absolute

displacement resist to the disturbance better with the first method, although the tensioner displacement is part of the factors causing them. The obtained γ_2 also certifies this conclusion.

Method 3

Recall the mathematical expressions of the belt variation. There are three items involved that are speed of drive roller, tensioner displacement, and speed of tension roller. Therefore it is reasonable to set speed of tension roller as one of the control objectives. The outputs of closed-loop system in method 3 are picked up:

$$Y_{m3} = \begin{bmatrix} \dot{\theta}_2 \\ \theta_3 r_3 - \theta_2 r_2 + x_t \sin\alpha \\ \dfrac{1}{2}(\theta_3 r_3 + \theta_2 r_2 + x_t \sin\alpha) \end{bmatrix} . \tag{3.28}$$

The value of matrix $\mathbf{C}$ is adjusted as:

$$\mathbf{C} = \begin{bmatrix} & \mathbf{0}_{1\times 6} & & 0 & 1 & 0 & 0 & 0 & 0 \\ 0 & -r_2 & r_3 & 0 & 0 & \sin\alpha & & \mathbf{0}_{1\times 6} & \\ 0 & \dfrac{r_2}{2} & \dfrac{r_3}{2} & 0 & 0 & \dfrac{\sin\alpha}{2} & & \mathbf{0}_{1\times 6} & \end{bmatrix} .$$

The desired controller in this method is expressed as:

$$T_m = K_{m3} X \ , \tag{3.29}$$

where

$$\begin{aligned} K_{m3} = [& -1.73\times 10^{11} \quad 3.52\times 10^{11} \quad -1.99\times 10^{11} \quad -3.59\times 10^{9} \\ & -2.03\times 10^{9} \quad -3.22\times 10^{10} \quad -5.57\times 10^{7} \quad -2.23\times 10^{9} \\ & -6.70\times 10^{7} \quad -1.11\times 10^{6} \quad -2.49\times 10^{4} \quad -9.97\times 10^{6}] \end{aligned}$$

And the minimized H_2 norm is $\gamma_2 = 1.0015$. It seems that this method does not improve the H_2 norm compared to method 1. However the results of belt variation exhibit some contrary situation. The responses of stretching displacement and absolute displacement to a impulse disturbance with method 1 and 3 are depicted

in Fig. 3.10 (a), (b) respectively.

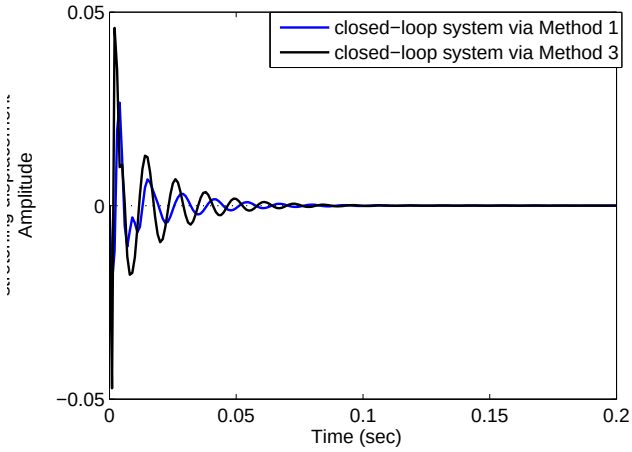

(a) stretching displacement

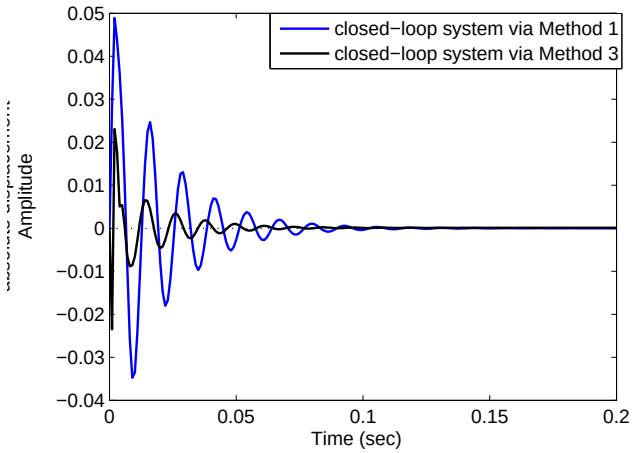

(b) absolute displacement

Figure 3.10: Response to impulse disturbance of system with method 1 and method 3

The blue line indicates results of method 1, and black line exhibits method 3. It is interesting that the stretching displacement performs better with method 1, whereas absolute displacement. With method 3, the peak value of absolute displacement is attenuated more than 100% compared with method 1. Recall that

there is another variables optimized along with belt variation. It is drive roller speed in method 1, and tension roller speed in method 3. Also the mathematical expressions of these two displacements reflect that part of them are contrary to each other. And that part is the displacement happening on tension roller. Therefore choosing which roller speed to be optimized is one of the reasons leading to this result. And it provides some reference to design the weighting on these two displacements.

The results of these three methods are concluded in Table 3.1

Table 3.1: Comparison results of these three method in H_2 optimal control

method	1	2	3
γ_2	0.0047	0.0058	1.0015
SD	best	worst	
AD		worst	best

3.6 Summary

This chapter developed an optimal state feedback control architecture for the obtained FRB model of image transfer belt system in the previous chapter. The procedure of system stabilization and minimization of H_2 norm problem is deducted and exhibited in detail to explain the reason choosing this controller. To achieve better control performance, several combinations of output to be regulated are made including drive roller speed, tensioner displacement, and tension roller speed. Numerical simulation results ascertained the effectiveness of this controller, and indicate that stretching displacement achieves best result controlled with drive roller speed, and performance of absolute displacement is more desirable when optimized along with tension roller speed.

Chapter 4

Output Feedback Control for Image Transfer Belt System via H_∞ Norm

4.1 Introduction

Although state feedback control ease the burden on controller, it is often difficult to access the full state of a system in real condition. Additionally, for multi-input-multi-output (MIMO) system with large scale state variables, it is time consuming for controller to calculate actuating command, and expensive for the measurement. Hence, proper choice of some outputs from a system as feedback information is more suitable and applicable. Another problem needed to pay attention in controller design is the influence of system uncertainty. As studied previously, passive control method is simply but lack of flexibility facing to uncertain system. These two principles are elementary in this chapter.

Based on these concerning, this chapter establishes an optimal H_∞ output feedback controller for the image transfer belt system. Tensioner displacement and motor speed are selected as the feedback signals to this controller due to their easiness to obtain. Like the former design, the belt variation and drive roller speed are the controlled variables. The controller minimizes the maximum energy of these outputs to maintain system in a stable and satisfying condition,

confronted with system parameter uncertainty. Several simulation results are presented to ensure the correctness.

The organization of this chapter is composed as: H_∞ norm and the motivation to conduct this approach are explained in Section 4.2. Detailed controller design including equation expressions and control objectives are shown in Section 4.3. Approaches to solve this problem are developed thoroughly in Section 4.4. Numerical simulations are conducted in Section 4.5 including comparisons between open-loop system and closed-loop system, conventional PID controller and proposed controller, controller performance with and without system uncertainty. Finally, this chapter is summarized in Section 4.6.

4.2 H_∞ Norm and Motivation for H_∞ Optimal Control

4.2.1 Definition of H_∞ Norm

The L_p norm of a signal $f(t)$ is first declared in general as:

$$\|f(t)\|_p = \left(\int_0^\infty |f(t)|^p dt \right)^{\frac{1}{p}}, \ p \geqslant 1 \tag{4.1}$$

As $p \to \infty$, the L_p norm tends to the so-called ∞ norm, which can be characterized as

$$\|f\|_\infty = \max_t |f(t)| \tag{4.2}$$

If the maximum in Eq. (4.2) does not exist, the modified way is to define the L_∞ norm as the least upper hound of the absolute value,

$$\|f\|_\infty = \sup_t |f(t)| \tag{4.3}$$

Now consider a stable single-input-single-output (SISO) system with transfer function $G(s)$. The H_∞ norm is defined as [96]:

$$\|G\|_{H_\infty} = \max_\omega |G(j\omega)|, \tag{4.4}$$

or

$$\|G\|_{H_\infty} = \sup_\omega |G(j\omega)| \tag{4.5}$$

Now the relationship between H_∞ norm and H_2 norm of a system is exhibit here. Consider an input $u(t)$ with $u(s)$ in Laplace domain, then H_2 norm of the output in system G is calculated as:

$$\begin{aligned}
\|Gu\|_{H_2} &= \sqrt{\frac{1}{2\pi}\int_{-\infty}^{\infty} |G(j\omega)u(j\omega)|^2 d\omega} \\
&= \sqrt{\frac{1}{2\pi}\int_{-\infty}^{\infty} |G(j\omega)|^2 |u(j\omega)|^2 d\omega} \\
&\leqslant \sup_\omega |G(j\omega)| \sqrt{\frac{1}{2\pi}\int_{-\infty}^{\infty} |u(j\omega)|^2 d\omega} \\
&= \|G\|_{H_\infty} \|u\|_{H_2}
\end{aligned}$$

Therefore $\|G\|_{H_\infty} \geqslant \dfrac{\|Gu\|_{H_2}}{\|u\|_{H_2}}$, all $u \neq 0$. So an alternative definition for H_{norm} is

$$\|G\|_{H_\infty} = \sup\left\{ \frac{\|Gu\|_{H_2}}{\|u\|_{H2}} : \ u \neq 0 \right\} \tag{4.6}$$

As for multi-input-multi-output (MIMO) system, it is often expressed as [97]:

$$\|G\|_{H_\infty} = \sup_\omega \sigma(G(j\omega)), \tag{4.7}$$

where $\sigma(G(j\omega))$ is the singular value of the matrix $G(j\omega)$.

4.2.2 Motivation

From Eq. (4.6), it is easy to understand that H_∞ norm of a system represents the maximum energy of the output. As explained before, the real system contains various uncertain elements, like dynamic uncertainty from system itself

and actuator, system parameter uncertainty, and so on. The objective of a H_∞ optimal controller is to minimize the H_∞ norm of a system, as:

$$\min \sup_{u} \frac{\|Gu\|_{H_2}}{\|u\|_{H_2}}$$

By this approach, the real system can maintain in a desired condition even with several unknown factors. In another word, the H_∞ optimal controller ascertain the system functioning properly in the worse case [98, 99].

4.3 Control Architecture

The state vector is not changed as in Eq. (3.8), while the outputs from the image transfer belt system are adjusted as two part: the measured outputs which are sent to controller, and the regulated outputs list as:

$$Y = \begin{bmatrix} \dot{\theta}_3 \\ \theta_3 r_3 - \theta_2 r_2 + x_t \sin\alpha \\ \frac{1}{2}(\theta_3 r_3 + \theta_2 r_2 + x_t \sin\alpha) \end{bmatrix}, \; Y_m = \begin{bmatrix} \dot{\theta_m} \\ x_t \end{bmatrix} \tag{4.8}$$

The reason to pick up speed of motor and tensioner displacement as measured outputs feedback to controller, is they are easy to access in the real xerographic printing machine. Also full measurements of the state vector of the system is not easy and lead heavy burden to the controller. And the output equations are established as:

$$\begin{aligned} Y &= \mathbf{C}_1 X + \mathbf{D}_{11} T_p + \mathbf{D}_{12} T_m \\ Y_m &= \mathbf{C}_m X + \mathbf{D}_{m1} T_p + \mathbf{D}_{m2} T_m, \end{aligned} \tag{4.9}$$

where

$$\mathbf{C}_1 = \begin{bmatrix} & \mathbf{0}_{1\times 6} & & & & & 0 & 0 & 1 & 0 & 0 & 0 \\ 0 & -r_2 & r_3 & 0 & 0 & \sin\alpha & & & \mathbf{0}_{1\times 6} & & & \\ 0 & \frac{r_2}{2} & \frac{r_3}{2} & 0 & 0 & \frac{\sin\alpha}{2} & & & \mathbf{0}_{1\times 6} & & & \end{bmatrix}, \mathbf{D}_{11} = \mathbf{0}_{3\times 1}, \mathbf{D}_{12} = \mathbf{0}_{3\times 1}$$

$$\mathbf{C}_m = \begin{bmatrix} \mathbf{0}_{1\times5} & 0 & 0 & 0 & 0 & 0 & 1 & 0 \\ \mathbf{0}_{1\times5} & 1 & 0 & 0 & 0 & 0 & 0 & 0 \end{bmatrix} , \mathbf{D}_{m1} = \mathbf{0}_{2\times1} , \mathbf{D}_{m2} = \mathbf{0}_{2\times1}$$

The signal flow of this open-loop system with controller K_∞ is pictured in Fig. 4.1.

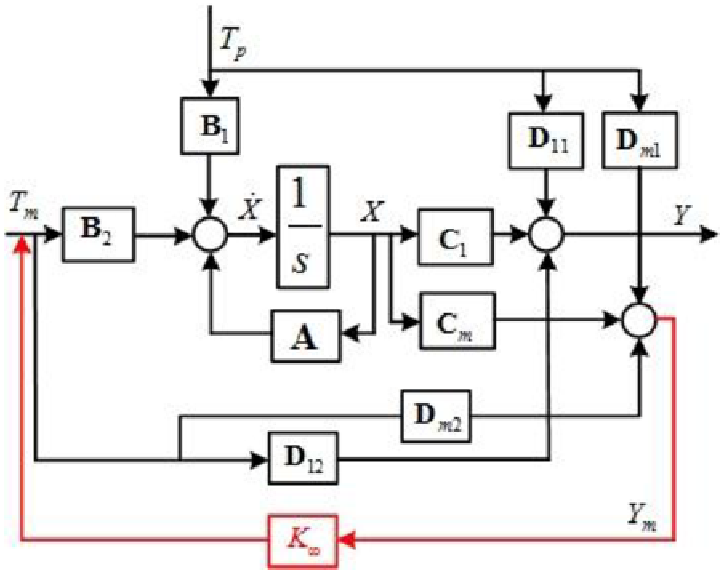

Figure 4.1: The signal flow of open-loop system with controller K_∞

The block K_∞ is the controller needed to be constructed. The request to this controller is:

- stabilize the image transfer belt system.
- reduce the affect from disturbance T_p on system outputs Y, that is minimize the H_∞ norm of the transfer function from T_p to Y based on feedback information Y_m.

4.4 Outputs Feedback Control in H_∞ Norm

4.4.1 Solution for Stability Problem

Like the explanation for stability of a system stated in chapter 3, to stabilize a system, the controller is designed to transform the open-loop system into a

closed-loop system that satisfies **Lemma 2** as:

There exists a $P > 0$ such that

$$A^{\mathrm{T}}P + PA + BB^{\mathrm{T}} < 0.$$

The proof procedure can be referred in chapter 3.

4.4.2 Solution for Bound in H_∞ Norm

Consider a system describe by the state space equation like:

$$\begin{aligned} \dot{x} &= Ax + Bu \\ y &= Cx + Du \ . \end{aligned} \tag{4.10}$$

The transfer function from input u to output y is denoted as $G(s)$. Then the following Lemma holds as:

Lemma 4 (KYP Lemma)

A system in Eq. (4.10). Then the following are equivalent [100]:

1. $\|G\|_{H_\infty} \leqslant \gamma$
2. There exists a $P > 0$ such that

$$\begin{bmatrix} A^{\mathrm{T}}P + PA & PB \\ B^{\mathrm{T}}P & -\gamma I \end{bmatrix} + \frac{1}{\gamma}\begin{bmatrix} C^{\mathrm{T}} \\ D^{\mathrm{T}} \end{bmatrix}\begin{bmatrix} C & D \end{bmatrix} < 0$$

The proof from 2 to is is conducted as following:

Suppose there is a matrix $P > 0$ that make 2 hold. Then $A^{\mathrm{T}}P + PA < 0$ indicates that A is stable. Also there exist some $\varepsilon < 0$ that

$$\begin{bmatrix} A^{\mathrm{T}}P + PA & PB \\ B^{\mathrm{T}}P & -\gamma I \end{bmatrix} + \frac{1}{\gamma}\begin{bmatrix} C^{\mathrm{T}} \\ D^{\mathrm{T}} \end{bmatrix}\begin{bmatrix} C & D \end{bmatrix} < \begin{bmatrix} 0 & 0 \\ 0 & -\varepsilon I \end{bmatrix} \ ,$$

that leads to

$$\begin{bmatrix} A^{\mathrm{T}}P + PA & PB \\ B^{\mathrm{T}}P & -(\gamma - \varepsilon) I \end{bmatrix} + \frac{1}{\gamma}\begin{bmatrix} C^{\mathrm{T}} \\ D^{\mathrm{T}} \end{bmatrix}\begin{bmatrix} C & D \end{bmatrix} < 0 \ . \tag{4.11}$$

Eq. (4.11) certifies the matrix in left side is negative definite, which leads to the

following:

$$\begin{aligned}
&\begin{bmatrix} x \\ u \end{bmatrix}^{\mathrm{T}} \left[\begin{bmatrix} A^{\mathrm{T}}P + PA & PB \\ B^{\mathrm{T}}P & -(\gamma-\varepsilon)I \end{bmatrix} + \frac{1}{\gamma} \begin{bmatrix} C^{\mathrm{T}} \\ D^{\mathrm{T}} \end{bmatrix} \begin{bmatrix} C & D \end{bmatrix} \right] \begin{bmatrix} x \\ u \end{bmatrix} < 0 \\
&\begin{bmatrix} x \\ u \end{bmatrix}^{\mathrm{T}} \begin{bmatrix} A^{\mathrm{T}}P + PA & PB \\ B^{\mathrm{T}}P & -(\gamma-\varepsilon)I \end{bmatrix} \begin{bmatrix} x \\ u \end{bmatrix} + \frac{1}{\gamma} \begin{bmatrix} x \\ u \end{bmatrix}^{\mathrm{T}} \begin{bmatrix} C^{\mathrm{T}} \\ D^{\mathrm{T}} \end{bmatrix} \begin{bmatrix} C & D \end{bmatrix} \begin{bmatrix} x \\ u \end{bmatrix} < 0 \ .
\end{aligned} \tag{4.12}$$

Recall the Eq. (4.10), that means:

$$\begin{aligned}
\dot{x}^{\mathrm{T}} &= x^{\mathrm{T}}A^{\mathrm{T}} + u^{\mathrm{T}}B^{\mathrm{T}} \\
y = \begin{bmatrix} C & D \end{bmatrix} \begin{bmatrix} x \\ u \end{bmatrix}&, \ y^{\mathrm{T}} = \begin{bmatrix} x \\ u \end{bmatrix}^{\mathrm{T}} \begin{bmatrix} C^{\mathrm{T}} \\ D^{\mathrm{T}} \end{bmatrix}
\end{aligned} \tag{4.13}$$

By substituting Eq. (4.13) to Eq. (4.12), the following formula holds:

$$\begin{aligned}
&\begin{bmatrix} x \\ u \end{bmatrix}^{\mathrm{T}} \begin{bmatrix} A^{\mathrm{T}}P + PA & PB \\ B^{\mathrm{T}}P & -(\gamma-\varepsilon)I \end{bmatrix} \begin{bmatrix} x \\ u \end{bmatrix} + \frac{1}{\gamma} \begin{bmatrix} x \\ u \end{bmatrix}^{\mathrm{T}} \begin{bmatrix} C^{\mathrm{T}} \\ D^{\mathrm{T}} \end{bmatrix} \begin{bmatrix} C & D \end{bmatrix} \begin{bmatrix} x \\ u \end{bmatrix} \\
=&\begin{bmatrix} x \\ u \end{bmatrix}^{\mathrm{T}} \begin{bmatrix} A^{\mathrm{T}}P + PA & PB \\ B^{\mathrm{T}}P & -(\gamma-\varepsilon)I \end{bmatrix} \begin{bmatrix} x \\ u \end{bmatrix} + \frac{1}{\gamma} y^{\mathrm{T}}y \\
=&x^{\mathrm{T}}(A^{\mathrm{T}}P + PA)x + x^{\mathrm{T}}PBu + u^{\mathrm{T}}B^{\mathrm{T}}Px - (\gamma-\varepsilon)u^{\mathrm{T}}u + \frac{1}{\gamma}y^{\mathrm{T}}y \\
=&\dot{x}^{\mathrm{T}}Px + x^{\mathrm{T}}P\dot{x} - (\gamma-\varepsilon)\|u\|^2 + \frac{1}{\gamma}\|y\|^2 < 0
\end{aligned} \tag{4.14}$$

Let $V(x) = x^{\mathrm{T}}Px$, then $\dot{V}(x) = \dot{x}^{\mathrm{T}}Px + x^{\mathrm{T}}P\dot{x}$. Then Eq. (4.14) becomes:

$$\dot{V}(x) - (\gamma-\varepsilon)\|u\|^2 + \frac{1}{\gamma}\|y\|^2 < 0 \ . \tag{4.15}$$

By integrating in time, the following inequality holds:

$$\begin{aligned}
&\int_0^\infty \left(\dot{V}(x(t)) - (\gamma - \varepsilon)\|u(t)\|^2 + \frac{1}{\gamma}\|y(t)\|^2 \right) dt \\
=&V(x(\infty)) - V(x(0)) - (\gamma - \varepsilon)\int_0^\infty \|u(t)\|^2 dt + \frac{1}{\gamma}\int_0^\infty \|y(t)\|^2 dt \\
=&V(x(\infty)) - V(x(0)) - (\gamma - \varepsilon)\|u\|_{H_2}^2 + \frac{1}{\gamma}\|y\|_{H_2}^2 < 0 \ .
\end{aligned} \tag{4.16}$$

Since A is stable, that means when $t \longrightarrow \infty$, $x(\infty) = 0$. Also the initial state status $x(0) = 0$. Due to property of positive definite matrix P, $V(0) = 0^{\mathrm{T}} P 0 = 0$. Therefore, Eq. (4.16) becomes:

$$\begin{aligned}
&0 - 0 - (\gamma - \varepsilon)\|u\|_{H_2}^2 + \frac{1}{\gamma}\|y\|_{H_2}^2 \\
=&-(\gamma - \varepsilon)\|u\|_{H_2}^2 + \frac{1}{\gamma}\|y\|_{H_2}^2 < 0
\end{aligned} \tag{4.17}$$

Thus $\|y\|_{H_2}^2 < (\gamma^2 - \varepsilon\gamma)\|u\|_{H_2}^2$. By definition of the H_∞ norm of G, this means $\|G\|_{H_\infty}^2 < (\gamma^2 - \varepsilon\gamma) < \gamma^2$, that is

$$\|G\|_{H_\infty} < \gamma \ .$$

And this proves statement 2 can lead statement 1. The inverse part is not shown here but the method is similar.

Next, recall the Schur Complement, then statement 2 in **Lemma 4** can be transformed as another formation shown as [101]:

$$\begin{bmatrix} A^{\mathrm{T}}P + PA & PB & C^{\mathrm{T}} \\ B^{\mathrm{T}}P & -\gamma I & D^{\mathrm{T}} \\ C & D & -\gamma I \end{bmatrix} < 0 \ . \tag{4.18}$$

4.4.3 Calculation Procedure with Linear Matrix Inequalities (LMIs)

The control problem stated in section 3.3 is considered in a general plant approach shown in Fig. 4.2:

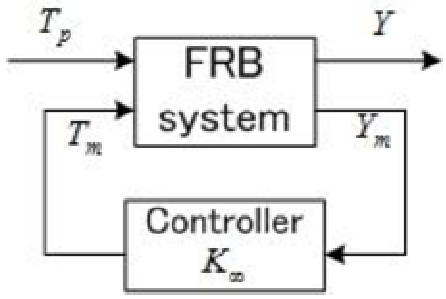

Figure 4.2: General plant for four-rollers-belt system with H_∞ Controller

As mentioned before, T_p is the exogenous input, T_m is the actuator input obtained from controller K_∞. Y_m is the sensed or measured outputs, and Y is the regulated outputs. The state space equations of the general plant are listed as: par

$$\begin{aligned} \dot{X} &= \mathbf{A}X + \mathbf{B}_1 T_p + \mathbf{B}_2 T_m \\ Y &= \mathbf{C}_1 X + \mathbf{D}_{11} T_p + \mathbf{D}_{12} T_m \\ Y_m &= \mathbf{C}_m X + \mathbf{D}_{m1} T_p + \mathbf{D}_{m2} T_m \end{aligned} \tag{4.19}$$

To controller, the input is Y_m, and the output is T_m. So assume the desired controller K_∞ could be described as:

$$\begin{aligned} \dot{x}_k &= A_k x_k + B_k Y_m \\ T_m &= C_k x_k + D_k Y_m \end{aligned} \tag{4.20}$$

By combining these two equations, the closed-loop system with controller in Fig. 4.2 could be transformed as a open-loop system with input T_p and output Y. And for this reformed system, the state space equations are obtained as:

$$\begin{aligned} \dot{x}_{cl} &= A_{cl} x_{cl} + B_{cl} T_p \\ Y &= C_{cl} x_{cl} + D_{cl} T_p \ , \end{aligned} \tag{4.21}$$

where

$$
\begin{aligned}
x_{cl} &= \begin{bmatrix} X & x_k \end{bmatrix}^{\mathrm{T}} \\
A_{cl} &= \begin{bmatrix} \mathbf{A} & \mathbf{0} \\ \mathbf{0} & A_k \end{bmatrix} + \begin{bmatrix} \mathbf{B}_2 & \mathbf{0} \\ \mathbf{0} & B_k \end{bmatrix} \begin{bmatrix} I & -D_k \\ -\mathbf{D}_{m2} & I \end{bmatrix}^{-1} \begin{bmatrix} \mathbf{0} & C_k \\ \mathbf{C}_m & \mathbf{0} \end{bmatrix} \\
&= \begin{bmatrix} \mathbf{A} & \mathbf{0} \\ \mathbf{0} & A_k \end{bmatrix} + \begin{bmatrix} \mathbf{B}_2 & \mathbf{0} \\ \mathbf{0} & B_k \end{bmatrix} \begin{bmatrix} I + D_k Q \mathbf{D}_{m2} & D_k Q \\ Q\mathbf{D}_{m2} & Q \end{bmatrix} \begin{bmatrix} \mathbf{0} & C_k \\ \mathbf{C}_m & \mathbf{0} \end{bmatrix} \\
&= \begin{bmatrix} \mathbf{A} + \mathbf{B}_2 D_k Q \mathbf{C}_m & \mathbf{B}_2 (I + D_k Q \mathbf{D}_{m2}) C_k \\ B_k Q \mathbf{C}_m & A_k + B_k Q \mathbf{D}_{m2} C_k \end{bmatrix} \\
B_{cl} &= \begin{bmatrix} \mathbf{B}_1 + \mathbf{B}_2 D_k Q \mathbf{D}_{m1} \\ B_k Q \mathbf{D}_{m1} \end{bmatrix} \\
C_{cl} &= \begin{bmatrix} \mathbf{C}_1 + \mathbf{D}_{12} D_k Q \mathbf{C}_m & \mathbf{D}_{12} (I + D_k Q \mathbf{D}_{m2}) C_k \end{bmatrix} \\
D_{cl} &= \mathbf{D}_{11} + \mathbf{D}_{12} D_k Q \mathbf{D}_{m1},\ Q = (I - \mathbf{D}_{m2} D_k)^{-1}
\end{aligned}
$$

To simplify the writing, the following transformation is conducted as:

$$
\begin{aligned}
A_{k2} &= A_k + B_k Q \mathbf{D}_{m2} C_k,\ B_{k2} = B_k Q \\
C_{k2} &= (I + D_k Q \mathbf{D}_{m2}) C_k,\ D_{k2} = D_k Q
\end{aligned}
\tag{4.22}
$$

Then the closed-loop system can be expressed in a large matrix as:

$$
\begin{bmatrix} A_{cl} & B_{cl} \\ C_{cl} & D_{cl} \end{bmatrix} = \begin{bmatrix} \mathbf{A} & \mathbf{0} & \mathbf{B}_1 \\ \mathbf{0} & \mathbf{0} & \mathbf{0} \\ \mathbf{C}_1 & \mathbf{0} & \mathbf{D}_{11} \end{bmatrix} + \begin{bmatrix} \mathbf{0} & \mathbf{B}_2 \\ I & \mathbf{0} \\ \mathbf{0} & \mathbf{D}_{12} \end{bmatrix} \begin{bmatrix} A_{k2} & B_{k2} \\ C_{k2} & D_{k2} \end{bmatrix} \begin{bmatrix} \mathbf{0} & I & \mathbf{0} \\ \mathbf{C}_m & \mathbf{0} & \mathbf{D}_{m1} \end{bmatrix} \tag{4.23}
$$

Like the transfer function $O(s)$ from T_p on Y defined in Eq. (3.21), in order to minimize the H_∞ norm of $O(s)$, the constraint is set as $\|O(s)\|_{H_\infty} < \gamma_\infty$. By minimizing γ_∞, the objective is achieved.

Lemma 6 is declared in order to solve this problem as [102]:
The following statements are equivalent.
1. There exists a controller K described as in Eq. (4.11) such that $\|O(s)\|_{H_\infty} < \gamma_\infty$.

2. There exists $P_1, S_1, A_n, B_n, C_n, D_n$ such that $\begin{bmatrix} P_1 & I \\ I & S_1 \end{bmatrix} > 0$, and

$$\begin{bmatrix} \mathbf{A}S_1 + S_1\mathbf{A}^{\mathrm{T}} + \mathbf{B}_2C_n + C_n^{\mathrm{T}}\mathbf{B}_2^{\mathrm{T}} & *^{\mathrm{T}} & *^{\mathrm{T}} & *^{\mathrm{T}} \\ \mathbf{A}^{\mathrm{T}} + A_n + \mathbf{C}_m^{\mathrm{T}}D_n^{\mathrm{T}}\mathbf{B}_2^{\mathrm{T}} & P_1\mathbf{A} + \mathbf{A}^{\mathrm{T}}P_1 + B_n\mathbf{C}_m + \mathbf{C}_m^{\mathrm{T}}B_n^{\mathrm{T}} & *^{\mathrm{T}} & *^{\mathrm{T}} \\ \mathbf{B}_1^{\mathrm{T}} + \mathbf{D}_{m1}^{\mathrm{T}}D_n^{\mathrm{T}}\mathbf{B}_2^{\mathrm{T}} & \mathbf{B}_1^{\mathrm{T}}P_1^{\mathrm{T}} + \mathbf{D}_{m1}^{\mathrm{T}}B_n^{\mathrm{T}} & -\gamma_\infty I & \\ \mathbf{C}_1S_1 + \mathbf{D}_{12}C_n & \mathbf{C}_1 + \mathbf{D}_{12}D_n\mathbf{C}_m & \mathbf{D}_{11} + \mathbf{D}_{12}D_n\mathbf{D}_{m1} & -\gamma_\infty I \end{bmatrix}$$

$$< 0$$

The proof from statement 2 to 1 is conducted as:

Statement 2 leads to the fact that there exist P_2, P_3, S_2, S_3 such that

$\begin{bmatrix} P_1 & P_2 \\ P_2^{\mathrm{T}} & P_3 \end{bmatrix} = \begin{bmatrix} S_1 & S_2 \\ S_2^{\mathrm{T}} & S_3 \end{bmatrix}^{-1} > 0$, and $S_{cl} = \begin{bmatrix} S_1 & I \\ S_2^{\mathrm{T}} & \mathbf{0} \end{bmatrix}$ has full row rank.

Now choose the transformed controller parameters as:

$$\begin{bmatrix} A_{k2} & B_{k2} \\ C_{k2} & D_{k2} \end{bmatrix} = \begin{bmatrix} P_2 & P_1\mathbf{B}_2 \\ \mathbf{0} & I \end{bmatrix}^{-1} \left(\begin{bmatrix} A_n & B_n \\ C_n & D_n \end{bmatrix} - \begin{bmatrix} P_1\mathbf{A}S_1 & \mathbf{0} \\ \mathbf{0} & \mathbf{0} \end{bmatrix} \right) \begin{bmatrix} S_2^{\mathrm{T}} & \mathbf{0} \\ \mathbf{C}_mS_1 & I \end{bmatrix}^{-1} \tag{4.24}$$

Then the constructed controller K are derived from:

$$\begin{aligned} &D_k = (I + D_{k2}\mathbf{D}_{m2})^{-1}D_{k2},\ B_k = B_{k2}(I - \mathbf{D}_{m2}D_k) \\ &C_k = (I - D_k\mathbf{D}_{m2})C_{k2},\ A_k = A_{k2} - B_k(I - \mathbf{D}_{m2}D_k)^{-1}\mathbf{D}_{m2}C_k\ . \end{aligned} \tag{4.25}$$

As discussed previously in Eq. (4.23), the closed-loop system now becomes as:

$$\begin{aligned} \begin{bmatrix} A_{cl} & B_{cl} \\ C_{cl} & D_{cl} \end{bmatrix} = &\begin{bmatrix} \mathbf{A} & \mathbf{0} & \mathbf{B}_1 \\ \mathbf{0} & \mathbf{0} & \mathbf{0} \\ \mathbf{C}_1 & \mathbf{0} & \mathbf{D}_{11} \end{bmatrix} + \begin{bmatrix} \mathbf{0} & \mathbf{B}_2 \\ I & \mathbf{0} \\ \mathbf{0} & \mathbf{D}_{12} \end{bmatrix} \begin{bmatrix} P_2 & P_1\mathbf{B}_2 \\ \mathbf{0} & I \end{bmatrix}^{-1} \\ &\left(\begin{bmatrix} A_n & B_n \\ C_n & D_n \end{bmatrix} - \begin{bmatrix} P_1\mathbf{A}S_1 & \mathbf{0} \\ \mathbf{0} & \mathbf{0} \end{bmatrix} \right) \begin{bmatrix} S_2^{\mathrm{T}} & \mathbf{0} \\ \mathbf{C}_mS_1 & I \end{bmatrix}^{-1} \begin{bmatrix} \mathbf{0} & I & \mathbf{0} \\ \mathbf{C}_m & \mathbf{0} & \mathbf{D}_{m1} \end{bmatrix} \end{aligned} \tag{4.26}$$

Based on Eq. (4.17), and the inequality in statement 2, the following formula

holds, that is:

$$\begin{bmatrix} S_{cl}^{\mathrm{T}} & \mathbf{0} & \mathbf{0} \\ \mathbf{0} & I & \mathbf{0} \\ \mathbf{0} & \mathbf{0} & I \end{bmatrix} \begin{bmatrix} A_{cl}^{\mathrm{T}}P + PA_{cl} & P_{cl}B & C_{cl}^{\mathrm{T}} \\ B_{cl}^{\mathrm{T}}P & -\gamma_\infty I & D_{cl}^{\mathrm{T}} \\ C_{cl} & D_{cl} & -\gamma_\infty I \end{bmatrix} \begin{bmatrix} S_{cl} & \mathbf{0} & \mathbf{0} \\ \mathbf{0} & I & \mathbf{0} \\ \mathbf{0} & \mathbf{0} & I \end{bmatrix} =$$

$$\begin{bmatrix} \mathbf{A}S_1 + S_1\mathbf{A}^{\mathrm{T}} + \mathbf{B}_2C_n + C_n^{\mathrm{T}}\mathbf{B}_2^{\mathrm{T}} & *^{\mathrm{T}} & *^{\mathrm{T}} & *^{\mathrm{T}} \\ \mathbf{A}^{\mathrm{T}} + A_n + \mathbf{C}_m^{\mathrm{T}}D_n^{\mathrm{T}}\mathbf{B}_2^{\mathrm{T}} & P_1\mathbf{A} + \mathbf{A}^{\mathrm{T}}P_1 + B_n\mathbf{C}_m + \mathbf{C}_m^{\mathrm{T}}B_n^{\mathrm{T}} & *^{\mathrm{T}} & *^{\mathrm{T}} \\ \mathbf{B}_1^{\mathrm{T}} + \mathbf{D}_{m1}^{\mathrm{T}}D_n^{\mathrm{T}}\mathbf{B}_2^{\mathrm{T}} & \mathbf{B}_1^{\mathrm{T}}P_1^{\mathrm{T}} + \mathbf{D}_{m1}^{\mathrm{T}}B_n^{\mathrm{T}} & -\gamma_\infty I & \\ \mathbf{C}_1S_1 + \mathbf{D}_{12}C_n & \mathbf{C}_1 + \mathbf{D}_{12}D_n\mathbf{C}_m & \mathbf{D}_{11} + \mathbf{D}_{12}D_n\mathbf{D}_{m1} & -\gamma_\infty I \end{bmatrix} < 0 \tag{4.27}$$

This indicates that $\begin{bmatrix} A_{cl}^{\mathrm{T}}P + PA_{cl} & P_{cl}B & C_{cl}^{\mathrm{T}} \\ B_{cl}^{\mathrm{T}}P & -\gamma_\infty I & D_{cl}^{\mathrm{T}} \\ C_{cl} & D_{cl} & -\gamma_\infty I \end{bmatrix} < 0$ which based on **Lemma 4**, that proves that there is controller K described as in Eq. (4.20) make $\|O(s)\|_{H_\infty} < \gamma_\infty$ holds.

And this leads to statement 1. The inverse part is not shown here.

Based on **Lemma 5**, the calculation to solve the H_∞ optimal outputs feedback problem stated in section 4.3 becomes as:

$\min(\gamma_\infty)$ subject to $\gamma_\infty, P_1, S_1, A_n, B_n, C_n, D_n$ such that:

$$\begin{bmatrix} P_1 & I \\ I & S_1 \end{bmatrix} > 0$$

$$\begin{bmatrix} \mathbf{A}S_1 + S_1\mathbf{A}^{\mathrm{T}} + \mathbf{B}_2C_n + C_n^{\mathrm{T}}\mathbf{B}_2^{\mathrm{T}} & *^{\mathrm{T}} & *^{\mathrm{T}} & *^{\mathrm{T}} \\ \mathbf{A}^{\mathrm{T}} + A_n + \mathbf{C}_m^{\mathrm{T}}D_n^{\mathrm{T}}\mathbf{B}_2^{\mathrm{T}} & P_1\mathbf{A} + \mathbf{A}^{\mathrm{T}}P_1 + B_n\mathbf{C}_m + \mathbf{C}_m^{\mathrm{T}}B_n^{\mathrm{T}} & *^{\mathrm{T}} & *^{\mathrm{T}} \\ \mathbf{B}_1^{\mathrm{T}} + \mathbf{D}_{m1}^{\mathrm{T}}D_n^{\mathrm{T}}\mathbf{B}_2^{\mathrm{T}} & \mathbf{B}_1^{\mathrm{T}}P_1^{\mathrm{T}} + \mathbf{D}_{m1}^{\mathrm{T}}B_n^{\mathrm{T}} & -\gamma_\infty I & \\ \mathbf{C}_1S_1 + \mathbf{D}_{12}C_n & \mathbf{C}_1 + \mathbf{D}_{12}D_n\mathbf{C}_m & \mathbf{D}_{11} + \mathbf{D}_{12}D_n\mathbf{D}_{m1} & -\gamma_\infty I \end{bmatrix} < 0 \tag{4.28}$$

The algorithm is similar to the one is Section 3.4 which is not explained again here.

4.5 Numerical Simulation

Numerical simulation results are presented in this section to exhibit the effectiveness of obtained K_∞ controller. Unlike the changeable outputs in Chapter 3, they are fixed in this control design due to consideration of the real condition in xerographic printing.

The proposed controller achieves the minimum value at $\gamma_\infty = 0.1518$, and has a structure shown as:

$$T_m = \begin{bmatrix} K_{\infty 1} \\ K_{\infty 2} \end{bmatrix} Y_m, \tag{4.29}$$

where:

$$\begin{aligned}
K_{\infty 1}(s) = & \frac{-6.264 \times 10^9 s^{11} - 1.004 \times 10^{14} s^{10} - 9.94 \times 10^{17} s^9}{s^{12} + 3.666 \times 10^5 s^{11} - 1.74 \times 10^{15} s^{10} - 2.784 \times 10^{19} s^9} \\
& \frac{-5.368 \times 10^{21} s^8 - 2.087 \times 10^{25} s^7 - 6.393 \times 10^{28} s^6 - 1.355 \times 10^{32} s^5}{-2.562 \times 10^{23} s^8 - 1.173 \times 10^{27} s^7 - 2.956 \times 10^{30} s^6 - 4.836 \times 10^{33} s^5} \\
& \frac{-1.975 \times 10^{35} s^4 - 2.111 \times 10^{38} s^3 - 7.533 \times 10^{40} s^2 - 5.159 \times 10^{43} s}{-5.255 \times 10^{36} s^4 - 1.894 \times 10^{39} s^3 - 1.315 \times 10^{42} s^2 + 5.73 \times 10^{42} s} \\
& \frac{-8.643 \times 10^{41}}{-5.321 \times 10^{36}} \\
K_{\infty 2}(s) = & \frac{-7.587 \times 10^5 s^{11} - 3.919 \times 10^{10} s^{10} - 1.039 \times 10^{15} s^9}{s^{12} + 3.666 \times 10^5 s^{11} - 1.74 \times 10^{15} s^{10} - 2.784 \times 10^{19} s^9} \\
& \frac{-1.688 \times 10^{19} s^8 - 1.646 \times 10^{23} s^7 - 7.927 \times 10^{26} s^6 - 2.031 \times 10^{30} s^5}{-2.562 \times 10^{23} s^8 - 1.173 \times 10^{27} s^7 - 2.956 \times 10^{30} s^6 - 4.836 \times 10^{33} s^5} \\
& \frac{-3.376 \times 10^{33} s^4 - 3.728 \times 10^{36} s^3 - 1.349 \times 10^{39} s^2 - 9.42 \times 10^{41} s}{-5.255 \times 10^{36} s^4 - 1.894 \times 10^{39} s^3 - 1.315 \times 10^{42} s^2 + 5.73 \times 10^{42} s} \\
& \frac{+7.252 \times 10^{35}}{-5.321 \times 10^{36}}
\end{aligned}$$

With this controller, the frequency response from T_p on each regulated output compared with open-loop system is depicted in Fig. 4.3 (a), (b), (c), respectively. The parameters of the system here can refer to Table 2.1.

The blue line depicts response from open-loop system, and red line shows from closed-loop system with the optimal H_∞ controller. It is indicated that system is stabilized by proposed controller, and magnitude of frequency response

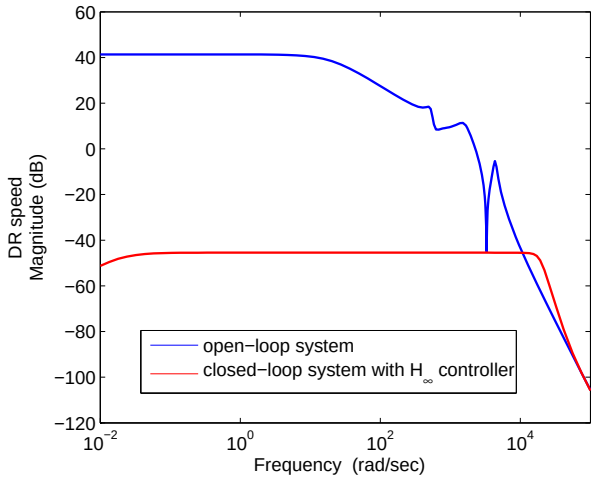

(a) DR speed

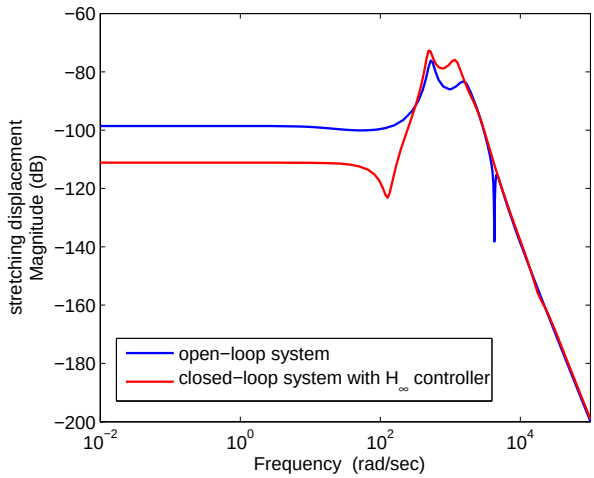

(b) stretching displacement

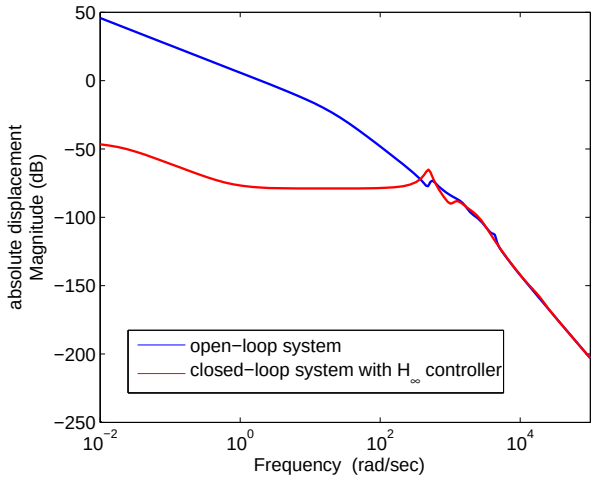

(c) absolute displacement

Figure 4.3: Magnitude of frequency response from T_p of open-loop system and closed-loop system with K_∞ controller

from disturbance on each output is attenuated efficiently especially around lower frequency range. Next responses to a impulse disturbance are graphed in Fig. 4.4 (a), (b), and (c).

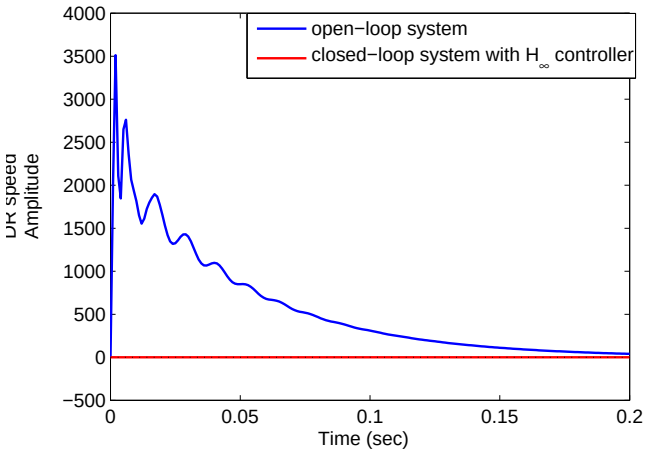

(a) DR speed

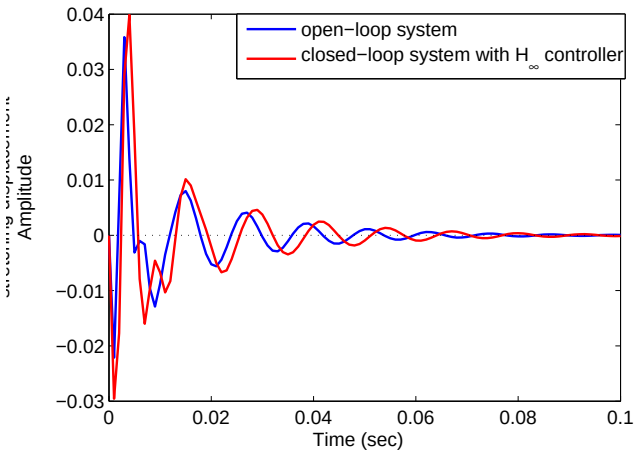

(b) stretching displacement

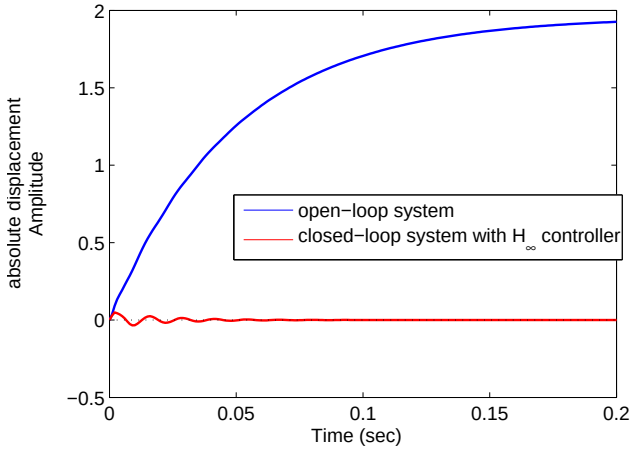

(c) absolute displacement

Figure 4.4: Response to impulse T_p of open-loop system and closed-loop system with K_∞ controller

Again blue line is for open-loop system, and red line for the one with controller K_∞. Each output performs strong resistance to the impulse disturbance with K_∞ unsurprisingly. There are barely no variation in drive roller speed K_∞, and the slight peak in absolute displacement is only 0.016 m, and decays within 0.08 second. The other hand, absolute displacement in open-loop system rises continuously due to instability. However, the stretching displacement is sacrificed for system robustness.

In real xerographic printing, the loading disturbance from paper could be modeled as a half sinusoid function. Now consider a machine with a printing speed of 120 pieces of paper per minute (120ppm), then the mathematical expression of this disturbance in one cycle of xerographic printing can be written as: par

$$T_p(t) = -0.5\sin(100\pi t)\ ,\ 1\text{s} \leq t \leq 1.01\text{s} \tag{4.30}$$

The constrain on time t is simply to show that this disturbance starts at 1 second, and last for 0.01 second. However, it will affect the system twice every second. Fig. 4.5 depicts this disturbance in one cycle starting at 1 second.

It is not difficult to imagine that the open-loop system will function badly under this disturbance. So to make the comparisons more convincing, a conven-

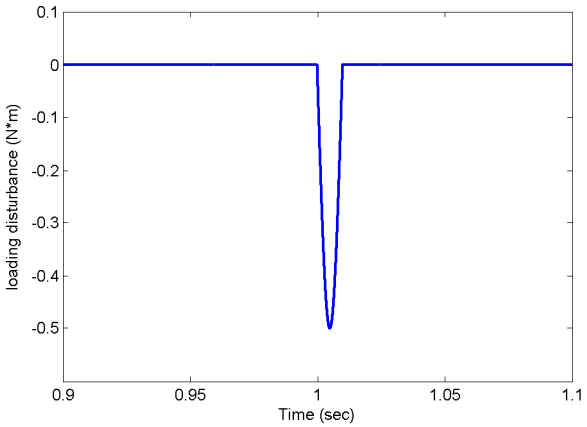

Figure 4.5: Loading disturbance T_p in one cycle of xerographic printing

tional PID controller is also applied to the open-loop system. The feedback signal is motor speed $\dot{\theta}_m$, and the function function of this PID controller is expressed as:

$$K_{\text{PID}}(s) = \frac{K_d s^2 + K_p s + K_i}{s}, \tag{4.31}$$

where $K_p = 0.0127,\ K_i = 17.71,\ K_d = 2.28 \times 10^{-6}$ according to Ziegler-Nichols method. The tuning procedure is not explained here [103, 104].

Responses to the disturbance in Eq. (4.30) without controller, with PID controller and with optimal H_∞ controller are shown in Fig. 4.6 (a),(b),(c).

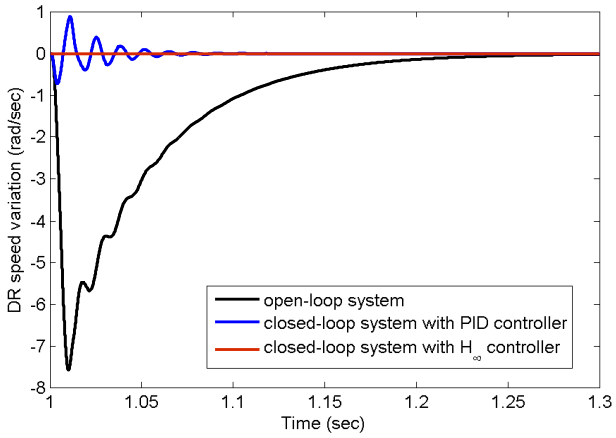

(a) DR speed

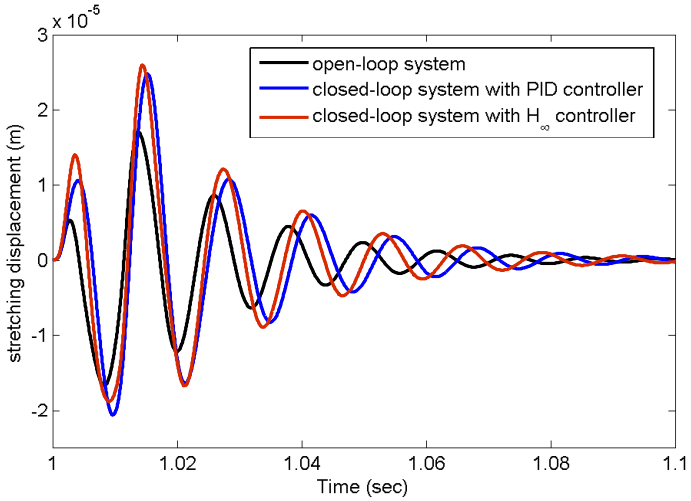

(b) stretching displacement

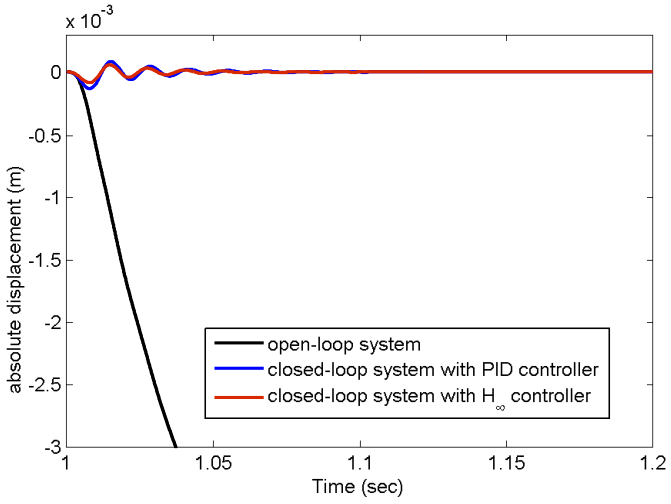

(c) absolute displacement

Figure 4.6: Response to the half sinusoid disturbance in open-loop system, with PID, and with H_∞ controller

The black line is results in open-loop system, the blue line is with PID controller, and the red line is with optimal H_∞ controller. Fig. 4.6 (a) shows the DR speed variation when the loading disturbance is put into the system. It is obviously indicated that the proposed controller endow DR speed a strong stability against the disturbance with a largest variation only about 1.17×10^{-4} rad/s, comparing to the 7.59 rad/s of the open-loop system and the 3.039 rad/s of the

closed-loop system with PID controller.

Fig. 4.6 (c) is the compared performance of the absolute displacement in the belt. When paper is carried through BR, the absolute displacement will continuously decrease due to the speed variations of DR, TR, and tensioner displacement. This means that the centre point of the belt where the latent image is developed is misaligned, which leads to the low quality in the final image. Nevertheless, it performed well in the closed-loop system modified by the proposed controller K_∞ with an average absolute value of 2.78×10^{-6} m which is only 1/4 of the results in PID control. Therefore, with the proposed controller the misalignment will be reduced high effectively. The stretching displacement did not display much improvement shown in Fig. 4.6 (b) with the proposed method due to the compromise made for the optimization of the other two variables. Also this is contrary to the results when the disturbance is an impulse one.

One of the objectives in the proposed K_∞ controller is to keep the control effectiveness under system uncertainty. Since one of the system uncertainty is the lacking knowledge of damping parameters in image transfer belt system, the performance of proposed controller K_∞ is investigated under damping parameter uncertainty. The uncertainty percentage is set at 5% varied from the nominal system damping factor, and response to an impulse disturbance of the uncertain system output with controller K_∞ is shown in Fig. 4.7 (a),(b),(c), respectively.

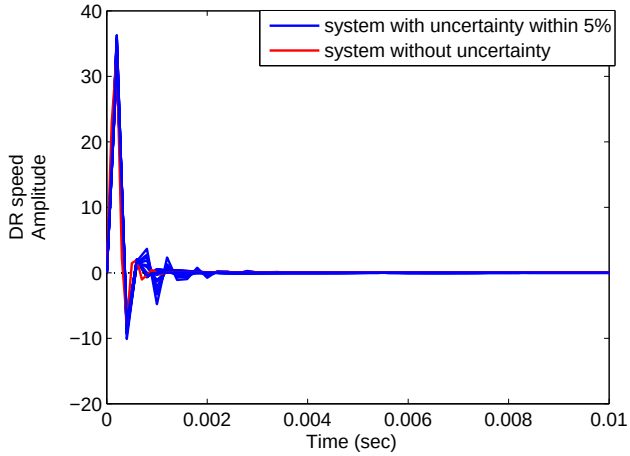

(a) DR speed

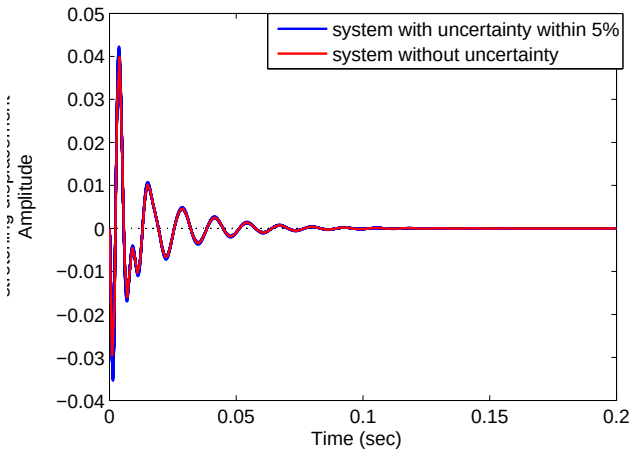

(b) stretching displacement

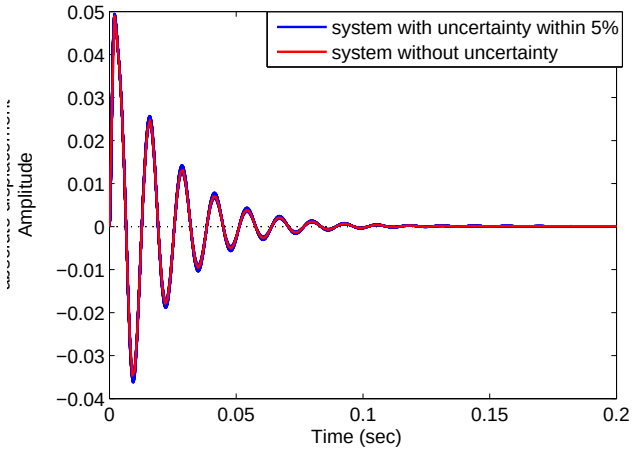

(c) absolute displacement

Figure 4.7: Response to impulse disturbance with 5% system uncertainty by H_∞ controller

The multiple blue lines simulates the results from system containing uncertainty in different level bounded in 5% from the nominal system, and red line reflects the nominal system. Fig. 4.7 (a) shows performance of drive roller speed. Although uncertainty worsens the control result, the speed keeps in a stable and acceptable condition that the variation in worst case is less than 0.015 rad/sec. Fig. 4.7 (b), and (c) are response of stretching displacement and absolute dis-

placement to the disturbance in detailed. It is indicated that control effectiveness on belt variation varies little from the nominal system that refers to a strong robustness with this optimal K_∞ controller.

Comparison between proposed controller K_∞ and PID controller in Eq. (4.31) with system uncertainty are also made here to strengthen the importance of robustness. Due to instability caused by PID controller under large uncertainty element, 5% uncertainty from damping model is again set in the following simulation. And results of response to the disturbance in Eq. (4.30) are graphed in Fig. 4.8 (a), (b), (c), separately.

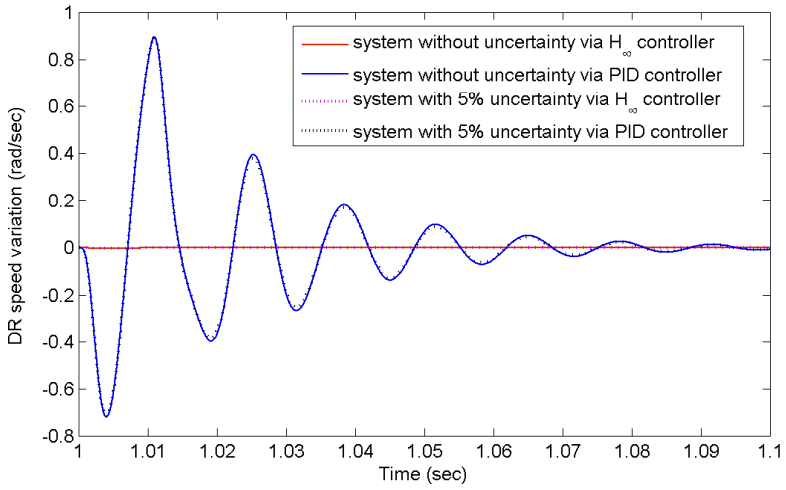

(a) DR speed

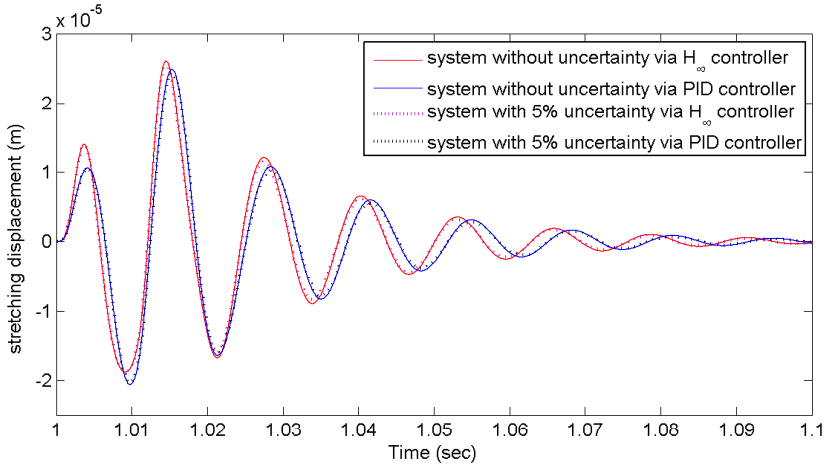

(b) stretching displacement

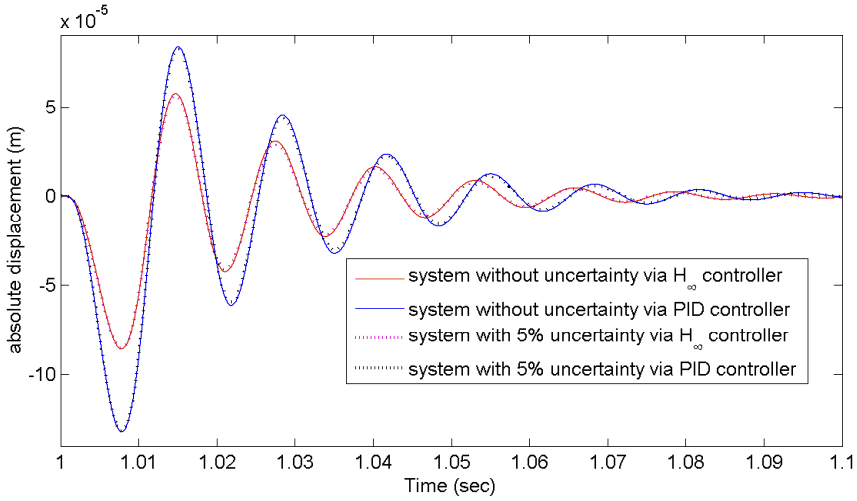

(c) absolute displacement

Figure 4.8: Response to half sinusoid disturbance without, with 5% system uncertainty by PID controller, and H_∞ controller

Solid lines are for system without uncertainty, and dot lines are with 5% uncertainty. Both of these two controller maintain system in stable status. Peak value of drive roller speed with H_∞ controller varies from 8.55×10^{-6} rad/sec in system without uncertainty to 2.2×10^{-5} rad/sec in system with uncertainty. It varies from 0.895 rad/sec in system without uncertainty to 0.898 rad/sec in system with uncertainty by PID controller. Results concerning to stretching displacement and absolute displacement can refer to Table 4.1.

Table 4.1: Peak value of response to half sinusoid disturbance without, with 5% system uncertainty by PID controller and optimal H_∞ controller

	H_∞ without rad/sec	H_∞ with rad/sec	PID without m	PID with m
DR speed	8.55×10^{-6}	2.2×10^{-5}	0.895	0.898
SD	2.60×10^{-5}	2.67×10^{-5}	2.48×10^{-5}	2.54×10^{-5}
AD	5.70×10^{-5}	5.83×10^{-5}	8.33×10^{-5}	8.49×10^{-5}

It reflects that with or without system uncertainty, drive roller speed and absolute displacement behave better with the propose optimal H_∞ controller than conventional PID controller. The results is reversed in stretching displacement,

but the difference is slight enough to ignore, and declare that they obtain the same control performance on stretching displacement. As a result, the effectiveness of this optimal H_∞ controller is ascertained in both nominal system and uncertain system.

4.6 Summary

To maintain system robustness against to parameter uncertainty, an optimal H_∞ output feedback controller is proposed in this chapter. Detailed establishment and proofs are expressed along with motivation for this controller. To certify the effectiveness, a real loading disturbance modelled as half sinusoid function is input to the open-loop system, and results regulated by optimal H_∞ controller are compared with conventional PID speed control. Also the controller is functioning under different system uncertainty to indicate validity on system robustness. Simulation results proved that this proposed controller achieved better performance than previous control both in output response and system robustness.

Chapter 5

Mixed H_2/H_∞ Output Feedback Control for Image Transfer Belt System

5.1 Introduction

According to mathematical definition of H_2 norm and H_∞ norm, both of controllers that optimizing one of them focus on different system characteristics separately. Optimal H_2 controller is to attenuate the overall energy of system output [105], and optimal H_∞ controller is to reduce the maximum energy of system output [106]. One is for the general, and another is for the worst case. So it is reasonable to combine these two control design ideas together to obtain both advantages from them. This kind of control design is called mixed H_2/H_∞ control, and it was studied thoroughly in 1990s [107]. Although approaches to solve this control problem have been developed into several branches, linear matrix inequalities (LMIs) is the fundamental one. The difficulty in solving mixed H_2/H_∞ by LMIs is that the optimization sometimes returns null due to improper constrains and objectives. Hence, it will be emphasized in the control design part of this chapter.

A mixed optimal H_2/H_∞ controller is designed for image transfer belt system in this chapter. Due to reality concern, output feedback instead of full state

feedback is chosen in control design. The main concerned variables are still belt variation. Also compared to the other two controller designed in the previous two chapter, the controller here consists of two actuator due to the difficulty to obtain the optimal solution. A linear actuator is added on the tensioner part, since the tensioner also need actuating force adjusting tensile force applied on belt. The decision of which variable is bounded in H_2 norm or H_∞ norm is studied in detail with numerical simulations to get the optimal design.

The structure of this chapter is organized as following: Section 5.2 explains the control architecture for the closed-loop system, and the objectives for the controller. Interpretation of how to solve this problem by LMIs approach is in Section 5.3. Numerical simulations related to different constraints choice are conducted in Section 5.4. Section 5.5 summarizes and ends this chapter.

5.2 Control Architecture

The state vector is not adjusted as in Eq. (3.8), while the outputs are separated into three parts, one for H_2 norm optimization, one for H_∞ norm optimization, and last for measurement fed back to proposed controller. Generally, outputs needed to be regulated are drive roller speed, stretching displacement, and absolute displacement. For now, which is for H_2 or H_∞ constraints has not be restraint yet. The selection decision that leading different results will be discussed in the numerical simulation section. Also in order to achieve the optimal solution, dual actuators structure is considered instead of the single actuator one. Since the tensioner part also needs actuating force to adjust the tension applied on belt, it is applicable to choose tensioner actuator as the second one. Therefore in general, the output equations are described as:

$$\begin{aligned} Y_\infty &= \mathbf{C}_\infty X + \mathbf{D}_{\infty 1} T_p + \mathbf{D}_{\infty 2} u \\ Y_2 &= \mathbf{C}_2 X + \mathbf{D}_{21} T_p + \mathbf{D}_{22} u \\ Y_m &= \mathbf{C}_m X + \mathbf{D}_{m1} T_p + \mathbf{D}_{m2} u, \end{aligned} \tag{5.1}$$

where

$$\mathbf{C}_m = \begin{bmatrix} \mathbf{0}_{1\times 5} & 0 & 0 & 0 & 0 & 0 & 1 & 0 \\ \mathbf{0}_{1\times 5} & 1 & 0 & 0 & 0 & 0 & 0 & 0 \end{bmatrix} , \mathbf{D}_{m1} = \mathbf{0}_{2\times 1} , \mathbf{D}_{m2} = \mathbf{0}_{2\times 1}$$

Notice that the actuated signal is now changed into u, which contains:

$$u = \begin{bmatrix} T_m \\ f \end{bmatrix}, \tag{5.2}$$

where f is the linear actuator located along with the tensioner. The signal flow of the designed system is pictured in Fig. 5.1.

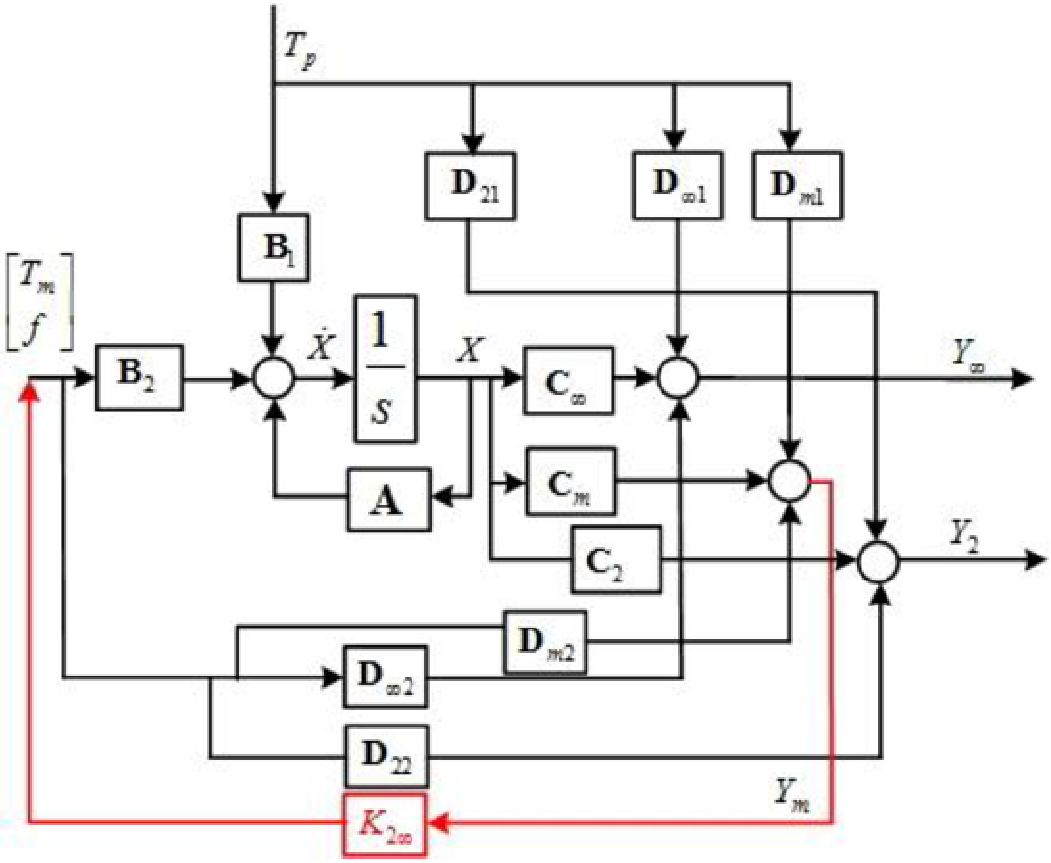

Figure 5.1: The signal flow of open-loop system with controller $K_{2\infty}$

The block $K_{2\infty}$ is the controller needed to be constructed. The objectives are set as:

- stabilize the image transfer belt system.
- restrain the H_∞ norm of transfer function from T_p on Y_∞ within γ_∞, that is $\|\frac{Y_\infty}{T_p}\|_{H_\infty} < \gamma_\infty$.

- restrain the H_2 norm of transfer function from T_p on Y_2 within γ_2, that is $\|\frac{Y_2}{T_p}\|_{H_2} < \gamma_2$.
- minimize the value $\mu_1\|\frac{Y_\infty}{T_p}\|_{H_\infty} + \mu_2\|\frac{Y_2}{T_p}\|_{H_2}$.

5.3 Calculation Procedure with Linear Matrix Inequalities (LMIs)

To solve the problem in section 5.2, first the state space description of the closed-loop system is developed. Assume the desired controller has the following state space equations:

$$\begin{aligned} \dot{x}_k &= A_k x_k + B_k u \\ u &= C_k x_k + D_k Y_m, \end{aligned} \tag{5.3}$$

and the closed-loop system with this controller can be expressed as:

$$\begin{aligned} \dot{x}_{cl} &= A_{cl} x_{cl} + B_{cl} u \\ Y_\infty &= C_{cl1} x_{cl} + D_{cl1} u \\ Y_2 &= C_{cl2} x_{cl} D_{cl2} u, \end{aligned} \tag{5.4}$$

where

$$\begin{aligned} x_{cl} &= \begin{bmatrix} X & x_k \end{bmatrix}^{\mathrm{T}} \\ A_{cl} &= \begin{bmatrix} \mathbf{A} + \mathbf{B}_2 D_k Q \mathbf{C}_m & \mathbf{B}_2 (I + D_k Q \mathbf{D}_{m2}) C_k \\ B_k Q \mathbf{C}_m & A_k + B_k Q \mathbf{D}_{m2} C_k \end{bmatrix} \\ B_{cl} &= \begin{bmatrix} \mathbf{B}_1 + \mathbf{B}_2 D_k Q \mathbf{D}_{m1} \\ B_k Q \mathbf{D}_{m1} \end{bmatrix} \\ C_{cl1} &= \begin{bmatrix} \mathbf{C}_\infty + \mathbf{D}_{\infty 2} D_k Q \mathbf{C}_m & \mathbf{D}_{\infty 2} (I + D_k Q \mathbf{D}_{m2}) C_k \end{bmatrix} \\ D_{cl1} &= \mathbf{D}_{\infty 1} + \mathbf{D}_{\infty 2} D_k Q \mathbf{D}_{m1} \\ C_{cl2} &= \begin{bmatrix} \mathbf{C}_2 + \mathbf{D}_{22} D_k Q \mathbf{C}_m & \mathbf{D}_{22} (I + D_k Q \mathbf{D}_{m2}) C_k \end{bmatrix} \\ D_{cl2} &= \mathbf{D}_{21} + \mathbf{D}_{22} D_k Q \mathbf{D}_{m1}, \; Q = (I - \mathbf{D}_{m2} D_k)^{-1} \end{aligned}$$

Based on **Lemma 2**, the stabilization problem can be reformed as:
find a $P > 0$ such that

$$A_{cl}^{\mathrm{T}} P + P A_{cl} + B_{cl} B_{cl}^{\mathrm{T}}. \tag{5.5}$$

Based on **Lemma 4** and **Lemma 5**, the bound problem on H_∞ norm can be transfered into:
find some $P_1, S_1, A_n, B_n, C_n, D_n$ such that:

$$\begin{bmatrix} P_1 & I \\ I & S_1 \end{bmatrix} > 0$$

$$\begin{bmatrix} \mathbf{A}S_1 + S_1\mathbf{A}^{\mathrm{T}} + \mathbf{B}_2 C_n + C_n^{\mathrm{T}}\mathbf{B}_2^{\mathrm{T}} & *^{\mathrm{T}} & *^{\mathrm{T}} & *^{\mathrm{T}} \\ \mathbf{A}^{\mathrm{T}} + A_n + \mathbf{C}_m^{\mathrm{T}} D_n^{\mathrm{T}} \mathbf{B}_2^{\mathrm{T}} & P_1\mathbf{A} + \mathbf{A}^{\mathrm{T}} P_1 + B_n \mathbf{C}_m + \mathbf{C}_m^{\mathrm{T}} B_n^{\mathrm{T}} & *^{\mathrm{T}} & *^{\mathrm{T}} \\ \mathbf{B}_1^{\mathrm{T}} + \mathbf{D}_{m1}^{\mathrm{T}} D_n^{\mathrm{T}} \mathbf{B}_2^{\mathrm{T}} & \mathbf{B}_1^{\mathrm{T}} P_1^{\mathrm{T}} + \mathbf{D}_{m1}^{\mathrm{T}} B_n^{\mathrm{T}} & -\gamma_\infty I & \\ \mathbf{C}_\infty S_1 + \mathbf{D}_{\infty 2} C_n & \mathbf{C}_\infty + \mathbf{D}_{\infty 2} D_n \mathbf{C}_m & \mathbf{D}_{\infty 1} + \mathbf{D}_{\infty 2} D_n \mathbf{D}_{m1} & -\gamma_\infty I \end{bmatrix} < 0 \tag{5.6}$$

To solve the third statement in the control objective, there are one more additional request on the original system, that is $D_{cl} = 0$. This could be satisfied by picking up proper outputs. And based on **Theorem 2**, this problem is restated as:
find two matrices P and Z such that [108]:

$$\begin{aligned} \begin{bmatrix} A_{cl}P + P A_{cl}^{\mathrm{T}} & B_{cl} \\ B_{cl}^{\mathrm{T}} & -I \end{bmatrix} &< 0 \\ \begin{bmatrix} Z & C_{cl2} P \\ P C_{cl2}^{\mathrm{T}} & P \end{bmatrix} &> 0 \\ \mathrm{tr}(Z) &< \gamma_2^2 \end{aligned} \tag{5.7}$$

The proofs are not explained again here.
Therefore the problem is changed into:
find the following matrices $P, Z, P_1, S_1, A_n, B_n, C_n, D_n$ to minimize:

$$\mu_1 \| \frac{Y_\infty}{T_p} \|_{H_\infty} + \mu_2 \| \frac{Y_2}{T_p} \|_{H_2}$$

and satisfies Eq. (5.5), (5.6), (5.7) simultaneously. Algorithm is similar to the one in chapter 3 which will not be explained again here.

5.4 Numerical Simulation

Several choices for regulated outputs on H_∞ norm and H_2 norm are investigated in this section to find out the proper one. The system parameters used in the simulation can be found in Table 2.1

Method 1

Stretching displacement and absolute displacement are the main concerning in this method. And the outputs to be regulated are expressed as:

$$\begin{aligned} Y_\infty &= \theta_3 r_3 - \theta_2 r_2 + x_t \sin\alpha \\ Y_2 &= \frac{1}{2}(\theta_3 r_3 + \theta_2 r_2 + x_t \sin\alpha). \end{aligned} \tag{5.8}$$

Parameters involved in the control objective stated in section 5.2 are:

$$\gamma_\infty = 100,\ \gamma_2 = 20,\ \mu_1 = 1,\ \mu_2 = 1. \tag{5.9}$$

The obtained controller based on the method in section 5.3 is expressed as:

$$\begin{bmatrix} T_m \\ f \end{bmatrix} = \begin{bmatrix} K^{11}_{2\infty 1} & K^{12}_{2\infty 1} \\ K^{21}_{2\infty 1} & K^{22}_{2\infty 1} \end{bmatrix} \begin{bmatrix} \dot{\theta}_m \\ x_t \end{bmatrix}, \tag{5.10}$$

where:

$$K^{11}_{2\infty 1}(s) = \frac{-2.23\times10^5 s^{11} - 2.256\times10^{10} s^{10} - 4.202\times10^{14} s^9}{s^{12} + 1.59\times10^6 s^{11} + 1.164\times10^{11} s^{10} - 6.199\times10^{14} s^9}$$
$$\frac{-3.137\times10^{18} s^8 - 1.439\times10^{22} s^7 - 5.635\times10^{25} s^6 - 1.396\times10^{29} s^5}{-2.247\times10^{19} s^8 - 8.373\times10^{22} s^7 - 4.449\times10^{26} s^6 - 6.963\times10^{29} s^5}$$
$$\frac{-2.348\times10^{32} s^4 - 2.719\times10^{35} s^3 - 1.244\times10^{38} s^2 - 1.234\times10^{40} s}{-1.901\times10^{33} s^4 - 1.349\times10^{36} s^3 - 2.412\times10^{39} s^2 - 3.462\times10^{41} s}$$
$$\frac{-3.771\times10^{40}}{-4.004\times10^{39}}$$

$$K_{2\infty1}^{12}(s) = \frac{5.163\times10^{6}s^{11} + 7.923\times10^{12}s^{10} + 6.918\times10^{17}s^{9}}{s^{12} + 1.59\times10^{6}s^{11} + 1.164\times10^{11}s^{10} - 6.199\times10^{14}s^{9}}$$
$$\frac{+7.822\times10^{21}s^{8} + 1.387\times10^{25}s^{7} - 4.083\times10^{27}s^{6} - 5.702\times10^{31}s^{5}}{-2.247\times10^{19}s^{8} - 8.373\times10^{22}s^{7} - 4.449\times10^{26}s^{6} - 6.963\times10^{29}s^{5}}$$
$$\frac{-3.441\times10^{35}s^{4} - 3.232\times10^{38}s^{3} - 6.806\times10^{41}s^{2} - 2.499\times10^{42}s}{-1.901\times10^{33}s^{4} - 1.349\times10^{36}s^{3} - 2.412\times10^{39}s^{2} - 3.462\times10^{41}s}$$
$$\frac{+9.809\times10^{39}}{-4.004\times10^{39}}$$

$$K_{2\infty1}^{21}(s) = \frac{1.391\times10^{11}s^{11} + 2.303\times10^{15}s^{10} + 1.15\times10^{19}s^{9}}{s^{12} + 1.59\times10^{6}s^{11} + 1.164\times10^{11}s^{10} - 6.199\times10^{14}s^{9}}$$
$$\frac{5.335\times10^{22}s^{8} + 1.411\times10^{26}s^{7} + 3.217\times10^{29}s^{6} + 5.08\times10^{32}s^{5}}{-2.247\times10^{19}s^{8} - 8.373\times10^{22}s^{7} - 4.449\times10^{26}s^{6} - 6.963\times10^{29}s^{5}}$$
$$\frac{+5.794\times10^{35}s^{4} + 4.971\times10^{38}s^{3} + 8.949\times10^{40}s^{2} + 4.47\times10^{42}s}{-1.901\times10^{33}s^{4} - 1.349\times10^{36}s^{3} - 2.412\times10^{39}s^{2} - 3.462\times10^{41}s}$$
$$\frac{+1.451\times10^{43}}{-4.004\times10^{39}}$$

$$K_{2\infty1}^{22}(s) = \frac{-4.9\times10^{12}s^{11} - 7.181\times10^{18}s^{10} + 9.82\times10^{21}s^{9}}{s^{12} + 1.59\times10^{6}s^{11} + 1.164\times10^{11}s^{10} - 6.199\times10^{14}s^{9}}$$
$$\frac{-3.303\times10^{25}s^{8} + 4.447\times10^{29}s^{7} + 2.71\times10^{32}s^{6} + 2.365\times10^{36}s^{5}}{-2.247\times10^{19}s^{8} - 8.373\times10^{22}s^{7} - 4.449\times10^{26}s^{6} - 6.963\times10^{29}s^{5}}$$
$$\frac{+6.301\times10^{38}s^{4} + 3.398\times10^{42}s^{3} - 4.264\times10^{44}s^{2} - 1.092\times10^{47}s}{-1.901\times10^{33}s^{4} - 1.349\times10^{36}s^{3} - 2.412\times10^{39}s^{2} - 3.462\times10^{41}s}$$
$$\frac{-1.278\times10^{45}}{-4.004\times10^{39}}$$

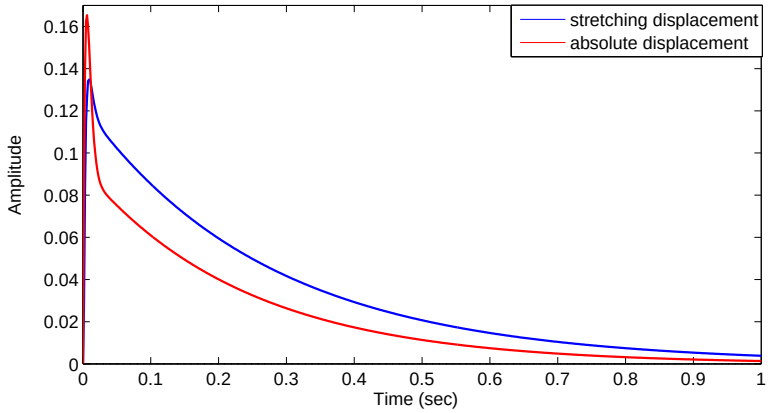

Figure 5.2: Response to an impulse disturbance of closed-loop system with controller $K_{2\infty1}$

The minimized H_∞ norm and H_2 norm are 0.6384, and 0.7221 respectively. Response to an impulse disturbance of closed-loop system with this controller is shown in Fig. 5.2. The blue line represents result of stretching displacement with a peak value of 0.1349 m, and the red line shows result of absolute displacement with a peak value of 0.1654 m. Both of the settling time of these two variables are around 1 second which is not satisfying.

Method 2

The regulated outputs are set as:

$$\begin{aligned} Y_\infty &= \frac{1}{2}(\theta_3 r_3 + \theta_2 r_2 + x_t \sin\alpha) \\ Y_2 &= \theta_3 r_3 - \theta_2 r_2 + x_t \sin\alpha. \end{aligned} \tag{5.11}$$

Parameters involved in the control objective stated in section 5.2 are:

$$\gamma_\infty = 250,\ \gamma_2 = 100,\ \mu_1 = 1,\ \mu_2 = 1. \tag{5.12}$$

The obtained controller based on the method in section 5.3 is expressed as:

$$\begin{bmatrix} T_m \\ f \end{bmatrix} = \begin{bmatrix} K^{11}_{2\infty 2} & K^{12}_{2\infty 2} \\ K^{21}_{2\infty 2} & K^{22}_{2\infty 2} \end{bmatrix} \begin{bmatrix} \dot{\theta}_m \\ x_t \end{bmatrix}, \tag{5.13}$$

where:

$$\begin{aligned} K^{11}_{2\infty 2}(s) = {} & \frac{-2.029\times 10^6 s^{11} - 1.206\times 10^{11} s^{10} - 1.503\times 10^{15} s^9}{s^{12} + 1.471\times 10^7 s^{11} + 5.745\times 10^{11} s^{10} - 1.133\times 10^{16} s^9} \\ & \frac{-7.266\times 10^{18} s^8 - 4.534\times 10^{22} s^7 - 2.118\times 10^{26} s^6 - 5.387\times 10^{29} s^5}{-1.156\times 10^{20} s^8 - 5.561\times 10^{23} s^7 - 1.909\times 10^{27} s^6 - 3.795\times 10^{30} s^5} \\ & \frac{-9.347\times 10^{32} s^4 - 9.971\times 10^{35} s^3 - 3.645\times 10^{38} s^2 - 3.057\times 10^{40} s}{-6.815\times 10^{33} s^4 - 7.406\times 10^{36} s^3 - 7.498\times 10^{39} s^2 - 5.601\times 10^{42} s} \\ & \frac{-1.494\times 10^{41}}{+3.414\times 10^{38}} \\ K^{12}_{2\infty 2}(s) = {} & \frac{4.638\times 10^6 s^{11} + 1.592\times 10^{13} s^{10} + 7.983\times 10^{17} s^9}{s^{12} + 1.471\times 10^7 s^{11} + 5.745\times 10^{11} s^{10} - 1.133\times 10^{16} s^9} \\ & \frac{-1.885\times 10^{21} s^8 - 2.175\times 10^{26} s^7 - 1.452\times 10^{30} s^6 - 3.963\times 10^{33} s^5}{-1.156\times 10^{20} s^8 - 5.561\times 10^{23} s^7 - 1.909\times 10^{27} s^6 - 3.795\times 10^{30} s^5} \end{aligned}$$

$$
\begin{aligned}
&\frac{-6.583\times10^{36}s^4-6.768\times10^{39}s^3-3.486\times10^{41}s^2+4.998\times10^{43}s}{-6.815\times10^{33}s^4-7.406\times10^{36}s^3-7.498\times10^{39}s^2-5.601\times10^{42}s}\\
&\frac{-5.501\times10^{39}}{+3.414\times10^{38}}\\
K^{21}_{2\infty2}(s) = &\frac{2.156\times10^{12}s^{11}+1.32\times10^{16}s^{10}+7.037\times10^{19}s^9}{s^{12}+1.471\times10^{7}s^{11}+5.745\times10^{11}s^{10}-1.133\times10^{16}s^9}\\
&\frac{2.29\times10^{23}s^8+5.657\times10^{26}s^7+1.064\times10^{30}s^6+1.439\times10^{33}s^5}{-1.156\times10^{20}s^8-5.561\times10^{23}s^7-1.909\times10^{27}s^6-3.795\times10^{30}s^5}\\
&\frac{+1.497\times10^{36}s^4+9.446\times10^{38}s^3+2.724\times10^{41}s^2+2.075\times10^{43}s}{-6.815\times10^{33}s^4-7.406\times10^{36}s^3-7.498\times10^{39}s^2-5.601\times10^{42}s}\\
&\frac{+1.664\times10^{44}}{+3.414\times10^{38}}\\
K^{22}_{2\infty2}(s) = &\frac{-4.296\times10^{12}s^{11}-7.377\times10^{18}s^{10}+4.834\times10^{22}s^9}{s^{12}+1.471\times10^{7}s^{11}+5.745\times10^{11}s^{10}-1.133\times10^{16}s^9}\\
&\frac{+3.547\times10^{26}s^8+1.517\times10^{30}s^7+3.346\times10^{33}s^6+5.091\times10^{36}s^5}{-1.156\times10^{20}s^8-5.561\times10^{23}s^7-1.909\times10^{27}s^6-3.795\times10^{30}s^5}\\
&\frac{+4.472\times10^{39}s^4+8.344\times10^{41}s^3-4.098\times10^{44}s^2-1.727\times10^{48}s}{-6.815\times10^{33}s^4-7.406\times10^{36}s^3-7.498\times10^{39}s^2-5.601\times10^{42}s}\\
&\frac{+1.08\times10^{44}}{+3.414\times10^{38}}
\end{aligned}
$$

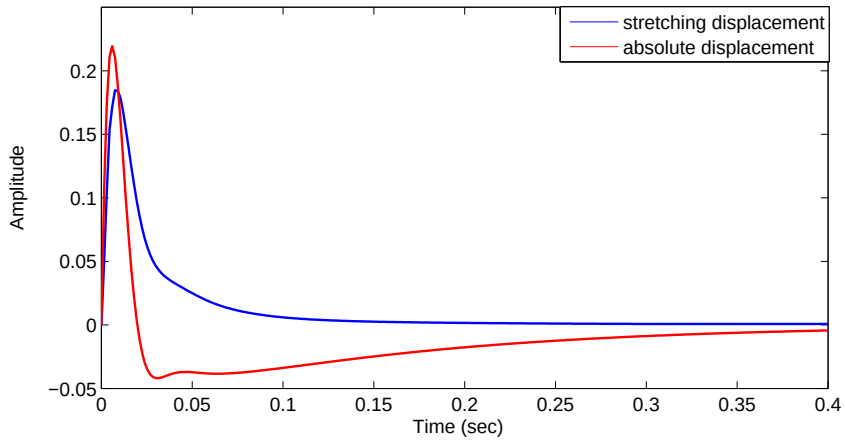

Figure 5.3: Response to an impulse disturbance of closed-loop system with controller $K_{2\infty2}$

The minimized H_∞ norm and H_2 norm are 21.3174, and 45.5384 respectively.

Response to an impulse disturbance of closed-loop system with this controller is shown in Fig. 5.3. The blue line represents result of stretching displacement with a peak value of 0.1847 m, and the red line shows result of absolute displacement with a peak value of 0.2195 m. Both of their settling time become shorter than the first one, which is 0.1 second for stretching displacement, and 0.4 second for absolute displacement.

Method 3

To strengthen the stability of the system, drive roller speed is additionally selected as one of the regulated outputs. Hence the expressions are adjusted as:

$$\begin{aligned} Y_\infty &= \dot{\theta}_3 \\ Y_2 &= \begin{bmatrix} \theta_3 r_3 - \theta_2 r_2 + x_t \sin\alpha \\ \dfrac{1}{2}(\theta_3 r_3 + \theta_2 r_2 + x_t \sin\alpha) \end{bmatrix}. \end{aligned} \tag{5.14}$$

Parameters involved in the control objective stated in section 5.2 are:

$$\gamma_\infty = 20,\ \gamma_2 = 300,\ \mu_1 = 0,\ \mu_2 = 1. \tag{5.15}$$

Simply speaking, the objective here is to bound the H_∞ norm on drive roller speed, and minimize the H_2 norm of stretching and absolute displacement. The obtained controller is expressed as:

$$\begin{bmatrix} T_m \\ f \end{bmatrix} = \begin{bmatrix} K^{11}_{2\infty 3} & K^{12}_{2\infty 3} \\ K^{21}_{2\infty 3} & K^{22}_{2\infty 3} \end{bmatrix} \begin{bmatrix} \dot{\theta}_m \\ x_t \end{bmatrix}, \tag{5.16}$$

where:

$$\begin{aligned} K^{11}_{2\infty 3}(s) = {} & \frac{1.03\times 10^6 s^{11} + 2.979\times 10^{11} s^{10} - 1.468\times 10^{15} s^9}{s^{12} + 1.076\times 10^7 s^{11} + 9.275\times 10^{12} s^{10} + 2.626\times 10^{17} s^9} \\ & \frac{-2.535\times 10^{19} s^8 - 1.283\times 10^{23} s^7 - 7.469\times 10^{26} s^6 - 2.219\times 10^{30} s^5}{+2.127\times 10^{21} s^8 + 1.159\times 10^{25} s^7 + 6.078\times 10^{28} s^6 + 2.363\times 10^{32} s^5} \\ & \frac{-4.113\times 10^{33} s^4 - 4.916\times 10^{36} s^3 - 1.909\times 10^{39} s^2 + 1.684\times 10^{42} s}{+5.589\times 10^{35} s^4 + 1\times 10^{39} s^3 + 1.018\times 10^{42} s^2 + 6.646\times 10^{44} s} \\ & \frac{-6.203\times 10^{42}}{+6.879\times 10^{38}} \\ K^{12}_{2\infty 3}(s) = {} & \frac{-6.135\times 10^6 s^{11} - 3.667\times 10^{13} s^{10} - 1.295\times 10^{19} s^9}{s^{12} + 1.076\times 10^7 s^{11} + 9.275\times 10^{12} s^{10} + 2.626\times 10^{17} s^9} \end{aligned}$$

$$
\begin{array}{l}
+3.576\times10^{22}s^8-1.754\times10^{26}s^7-6.622\times10^{30}s^6-3.96\times10^{34}s^5 \\
\hline
+2.127\times10^{21}s^8+1.159\times10^{25}s^7+6.078\times10^{28}s^6+2.363\times10^{32}s^5 \\
-1.115\times10^{38}s^4-1.771\times10^{41}s^3-1.926\times10^{44}s^2-7.41\times10^{45}s \\
\hline
+5.589\times10^{35}s^4+1\times10^{39}s^3+1.018\times10^{42}s^2+6.646\times10^{44}s \\
-5.557\times10^{39} \\
\hline
+6.879\times10^{38}
\end{array}
$$

$$
K^{21}_{2\infty3}(s)=\frac{6.983\times10^{12}s^{11}+7.675\times10^{16}s^{10}+4.739\times10^{20}s^9}{s^{12}+1.076\times10^{7}s^{11}+9.275\times10^{12}s^{10}+2.626\times10^{17}s^9}
$$

$$
\begin{array}{l}
1.868\times10^{24}s^8+5.1\times10^{27}s^7+1.052\times10^{31}s^6+1.539\times10^{34}s^5 \\
\hline
+2.127\times10^{21}s^8+1.159\times10^{25}s^7+6.078\times10^{28}s^6+2.363\times10^{32}s^5 \\
+1.656\times10^{37}s^4+1.14\times10^{40}s^3+3.529\times10^{42}s^2+1.122\times10^{45}s \\
\hline
+5.589\times10^{35}s^4+1\times10^{39}s^3+1.018\times10^{42}s^2+6.646\times10^{44}s \\
-9.94\times10^{44} \\
\hline
+6.879\times10^{38}
\end{array}
$$

$$
K^{22}_{2\infty3}(s)=\frac{-3.799\times10^{13}s^{11}-1.994\times10^{20}s^{10}+7.557\times10^{23}s^9}{s^{12}+1.076\times10^{7}s^{11}+9.275\times10^{12}s^{10}+2.626\times10^{17}s^9}
$$

$$
\begin{array}{l}
+2.501\times10^{28}s^8+1.482\times10^{32}s^7+4.218\times10^{35}s^6+8.902\times10^{38}s^5 \\
\hline
+2.127\times10^{21}s^8+1.159\times10^{25}s^7+6.078\times10^{28}s^6+2.363\times10^{32}s^5 \\
+1.081\times10^{42}s^4+1.014\times10^{45}s^3+3.712\times10^{47}s^2+2.111\times10^{50}s \\
\hline
+5.589\times10^{35}s^4+1\times10^{39}s^3+1.018\times10^{42}s^2+6.646\times10^{44}s \\
+2.189\times10^{44} \\
\hline
+6.879\times10^{38}
\end{array}
$$

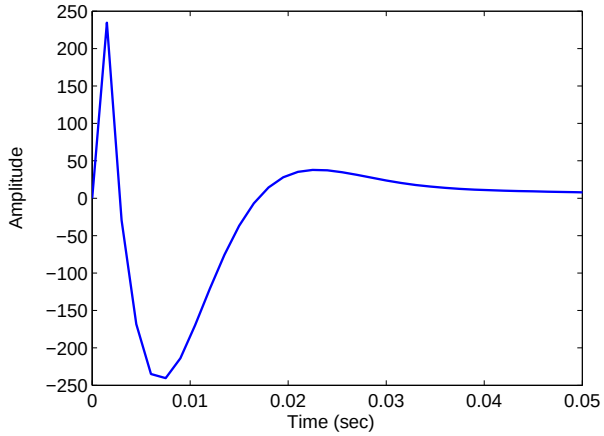

(a) DR speed

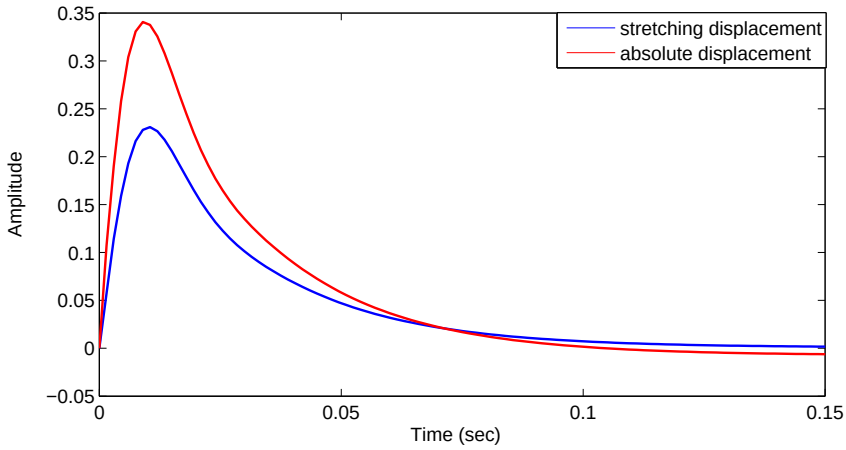

(b) belt displacement

Figure 5.4: Response to an impulse disturbance of closed-loop system with controller $K_{2\infty 3}$

The minimized H_∞ norm and H_2 norm are 20, and 6.7573 respectively. Responses to impulse disturbance are graphed in Fig. 5.4 (a), (b), separately. The maximum variation in stretching displacement is around 0.2308 m, and 0.3405 m in absolute displacement. However both of them can settle down within 0.14 second.

Method 4

In this method, the outputs are not changed but the objectives become as:

$$\mu_1 = 1, \ \mu_2 = 1. \tag{5.17}$$

It minimizes the linear combination of the H_∞ and H_2 norm of the outputs. The calculated controller has the following structure:

$$\begin{bmatrix} T_m \\ f \end{bmatrix} = \begin{bmatrix} K^{11}_{2\infty 4} & K^{12}_{2\infty 4} \\ K^{21}_{2\infty 4} & K^{22}_{2\infty 4} \end{bmatrix} \begin{bmatrix} \dot{\theta}_m \\ x_t \end{bmatrix}, \tag{5.18}$$

where:

$$K_{2\infty 4}^{11}(s) = \frac{1.03\times10^{6}s^{11} + 2.979\times10^{11}s^{10} - 1.468\times10^{15}s^{9}}{s^{12} + 1.194\times10^{7}s^{11} + 6.955\times10^{12}s^{10} + 9.74\times10^{16}s^{9}}$$
$$\frac{-2.535\times10^{19}s^{8} - 1.283\times10^{23}s^{7} - 7.469\times10^{26}s^{6} - 2.219\times10^{30}s^{5}}{+6.458\times10^{20}s^{8} + 6.832\times10^{24}s^{7} + 4.576\times10^{28}s^{6} + 1.999\times10^{32}s^{5}}$$
$$\frac{-4.113\times10^{33}s^{4} - 4.916\times10^{36}s^{3} - 1.909\times10^{39}s^{2} + 1.684\times10^{42}s}{+5.043\times10^{35}s^{4} + 9.317\times10^{38}s^{3} + 9.991\times10^{41}s^{2} + 6.912\times10^{44}s}$$
$$\frac{-6.203\times10^{42}}{+4.98\times10^{38}}$$

$$K_{2\infty 4}^{12}(s) = \frac{-6.135\times10^{6}s^{11} - 3.667\times10^{13}s^{10} - 1.295\times10^{19}s^{9}}{s^{12} + 1.194\times10^{7}s^{11} + 6.955\times10^{12}s^{10} + 9.74\times10^{16}s^{9}}$$
$$\frac{+3.576\times10^{22}s^{8} - 1.754\times10^{26}s^{7} - 6.622\times10^{30}s^{6} - 3.96\times10^{34}s^{5}}{+6.458\times10^{20}s^{8} + 6.832\times10^{24}s^{7} + 4.576\times10^{28}s^{6} + 1.999\times10^{32}s^{5}}$$
$$\frac{-1.115\times10^{38}s^{4} - 1.771\times10^{41}s^{3} - 1.926\times10^{44}s^{2} - 7.41\times10^{45}s}{+5.043\times10^{35}s^{4} + 9.317\times10^{38}s^{3} + 9.991\times10^{41}s^{2} + 6.912\times10^{44}s}$$
$$\frac{-5.557\times10^{39}}{+4.98\times10^{38}}$$

$$K_{2\infty 4}^{21}(s) = \frac{6.983\times10^{12}s^{11} + 7.675\times10^{16}s^{10} + 4.739\times10^{20}s^{9}}{s^{12} + 1.194\times10^{7}s^{11} + 6.955\times10^{12}s^{10} + 9.74\times10^{16}s^{9}}$$
$$\frac{1.868\times10^{24}s^{8} + 5.1\times10^{27}s^{7} + 1.052\times10^{31}s^{6} + 1.539\times10^{34}s^{5}}{+6.458\times10^{20}s^{8} + 6.832\times10^{24}s^{7} + 4.576\times10^{28}s^{6} + 1.999\times10^{32}s^{5}}$$
$$\frac{+1.656\times10^{37}s^{4} + 1.14\times10^{40}s^{3} + 3.529\times10^{42}s^{2} + 1.122\times10^{45}s}{+5.043\times10^{35}s^{4} + 9.317\times10^{38}s^{3} + 9.991\times10^{41}s^{2} + 6.912\times10^{44}s}$$
$$\frac{-9.94\times10^{44}}{+4.98\times10^{38}}$$

$$K_{2\infty 4}^{22}(s) = \frac{-3.799\times10^{13}s^{11} - 1.994\times10^{20}s^{10} + 7.557\times10^{23}s^{9}}{s^{12} + 1.194\times10^{7}s^{11} + 6.955\times10^{12}s^{10} + 9.74\times10^{16}s^{9}}$$
$$\frac{+2.501\times10^{28}s^{8} + 1.482\times10^{32}s^{7} + 4.218\times10^{35}s^{6} + 8.902\times10^{38}s^{5}}{+6.458\times10^{20}s^{8} + 6.832\times10^{24}s^{7} + 4.576\times10^{28}s^{6} + 1.999\times10^{32}s^{5}}$$
$$\frac{+1.081\times10^{42}s^{4} + 1.014\times10^{45}s^{3} + 3.712\times10^{47}s^{2} + 2.111\times10^{50}s}{+5.043\times10^{35}s^{4} + 9.317\times10^{38}s^{3} + 9.991\times10^{41}s^{2} + 6.912\times10^{44}s}$$
$$\frac{+2.189\times10^{44}}{+4.98\times10^{38}}.$$

The obtained optimal value on H_∞ norm is 87.5659, and 27.0396 on H_2 norm. Responses to impulse disturbance are also depicted as following:

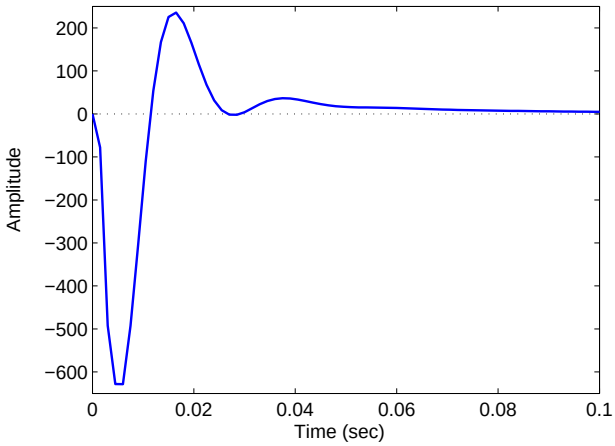

(a) DR speed

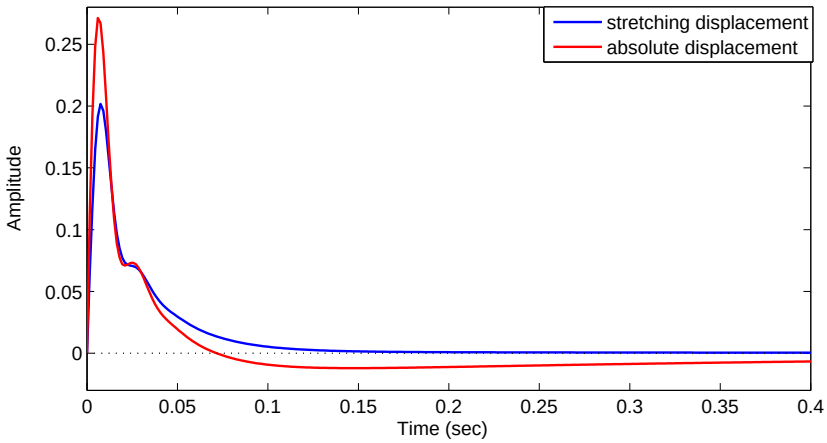

(b) belt displacement

Figure 5.5: Response to an impulse disturbance of closed-loop system with controller $K_{2\infty 4}$

Peak values become to 0.2018 m in stretching displacement, and 0.2712 m in absolute displacement. The settling time becomes longer in order to compensate the minimization problem set on H_∞ norm of drive roller speed.

Method 5

The outputs do not change, but decision about which one to be bounded in

H_∞ or H_2 norm is adjusted as:

$$\begin{aligned} Y_\infty &= \theta_3 r_3 - \theta_2 r_2 + x_t \sin\alpha \\ Y_2 &= \begin{bmatrix} \dot{\theta}_3 \\ \dfrac{1}{2}(\theta_3 r_3 + \theta_2 r_2 + x_t \sin\alpha) \end{bmatrix}. \end{aligned} \tag{5.19}$$

Parameters in objective are:

$$\gamma_\infty = 100,\ \gamma_2 = 10,\ \mu_1 = 1,\ \mu_2 = 1. \tag{5.20}$$

The obtained controller is expressed as:

$$\begin{bmatrix} T_m \\ f \end{bmatrix} = \begin{bmatrix} K^{11}_{2\infty5} & K^{12}_{2\infty5} \\ K^{21}_{2\infty5} & K^{22}_{2\infty5} \end{bmatrix} \begin{bmatrix} \dot{\theta}_m \\ x_t \end{bmatrix}, \tag{5.21}$$

where:

$$\begin{aligned} K^{11}_{2\infty5}(s) = {} & \frac{-6.959\times10^{7}s^{11} - 8.382\times10^{13}s^{10} - 8.039\times10^{17}s^{9}}{s^{12} + 1.541\times10^{7}s^{11} - 2.112\times10^{12}s^{10} - 1.982\times10^{19}s^{9}} \\ & \frac{-6.124\times10^{21}s^{8} - 3.287\times10^{25}s^{7} - 1.261\times10^{29}s^{6} - 3.964\times10^{32}s^{5}}{-1.774\times10^{23}s^{8} - 1.163\times10^{27}s^{7} - 5.4\times10^{30}s^{6} - 1.443\times10^{34}s^{5}} \\ & \frac{-8.922\times10^{35}s^{4} - 1.464\times10^{39}s^{3} - 1.611\times10^{42}s^{2} - 9.868\times10^{44}s}{-2.567\times10^{37}s^{4} - 2.713\times10^{40}s^{3} - 1.192\times10^{43}s^{2} + 8.773\times10^{45}s} \\ & \frac{-1.153\times10^{44}}{+2.342\times10^{40}} \\ K^{12}_{2\infty5}(s) = {} & \frac{3.249\times10^{8}s^{11} + 2.208\times10^{15}s^{10} + 2.185\times10^{21}s^{9}}{s^{12} + 1.541\times10^{7}s^{11} - 2.112\times10^{12}s^{10} - 1.982\times10^{19}s^{9}} \\ & \frac{+2.016\times10^{25}s^{8} + 8.502\times10^{28}s^{7} + 1.681\times10^{32}s^{6} - 3.7\times10^{34}s^{5}}{-1.774\times10^{23}s^{8} - 1.163\times10^{27}s^{7} - 5.4\times10^{30}s^{6} - 1.443\times10^{34}s^{5}} \\ & \frac{-7.747\times10^{38}s^{4} - 1.775\times10^{42}s^{3} - 2.199\times10^{45}s^{2} - 1.024\times10^{47}s}{-2.567\times10^{37}s^{4} - 2.713\times10^{40}s^{3} - 1.192\times10^{43}s^{2} + 8.773\times10^{45}s} \\ & \frac{-3.529\times10^{41}}{+2.342\times10^{40}} \\ K^{21}_{2\infty5}(s) = {} & \frac{4.216\times10^{14}s^{11} + 4.655\times10^{18}s^{10} + 3.221\times10^{20}s^{9}}{s^{12} + 1.541\times10^{7}s^{11} - 2.112\times10^{12}s^{10} - 1.982\times10^{19}s^{9}} \\ & \frac{1.436\times10^{26}s^{8} + 4.496\times10^{29}s^{7} + 1.029\times10^{33}s^{6} + 1.77\times10^{36}s^{5}}{-1.774\times10^{23}s^{8} - 1.163\times10^{27}s^{7} - 5.4\times10^{30}s^{6} - 1.443\times10^{34}s^{5}} \end{aligned}$$

$$K^{22}_{2\infty 5}(s) = \frac{\begin{array}{l}+2.154\times 10^{39}s^4 + 1.874\times 10^{42}s^3 + 8.345\times 10^{44}s^2 + 5.783\times 10^{46}s\\ \hline -2.567\times 10^{37}s^4 - 2.713\times 10^{40}s^3 - 1.192\times 10^{43}s^2 + 8.773\times 10^{45}s\\ -1.151\times 10^{46}\\ \hline +2.342\times 10^{40}\end{array}}{\begin{array}{l}-1.955\times 10^{15}s^{11} - 1.084\times 10^{22}s^{10} - 3.351\times 10^{26}s^9\\ \hline s^{12} + 1.541\times 10^{7}s^{11} - 2.112\times 10^{12}s^{10} - 1.982\times 10^{19}s^9\\ -2.423\times 10^{30}s^8 - 7.831\times 10^{33}s^7 - 1.646\times 10^{37}s^6 - 2.084\times 10^{40}s^5\\ \hline -1.774\times 10^{23}s^8 - 1.163\times 10^{27}s^7 - 5.4\times 10^{30}s^6 - 1.443\times 10^{34}s^5\\ -1.623\times 10^{43}s^4 - 9.754\times 10^{44}s^3 - 3.237\times 10^{48}s^2 + 2.781\times 10^{51}s\\ \hline -2.567\times 10^{37}s^4 - 2.713\times 10^{40}s^3 - 1.192\times 10^{43}s^2 + 8.773\times 10^{45}s\\ +7.416\times 10^{45}\\ \hline +2.342\times 10^{40}\end{array}}$$

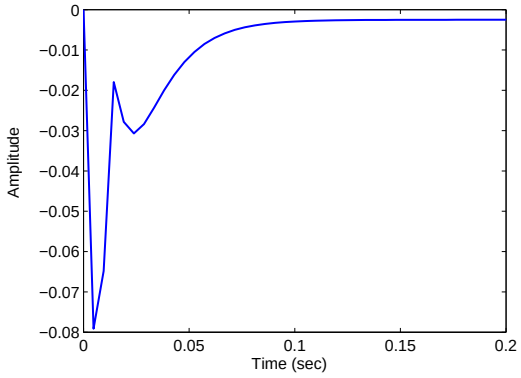

(a) DR speed

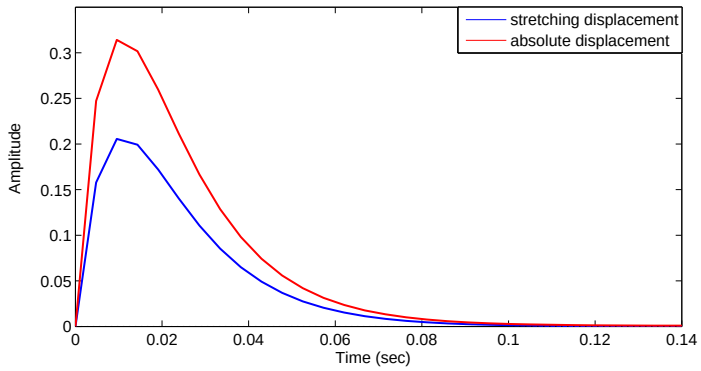

(b) belt displacement

Figure 5.6: Response to an impulse disturbance of closed-loop system with controller $K_{2\infty 5}$

The optimized H_∞ norm is 22.4092, and H_2 norm is 9.2096. Again responses to impulse disturbance are shown in Fig. 5.6 (a) and (b). Stretching displacement contains a peak value 0.2056 m, and absolute displacement has a peak value 0.3141 m. Both of the settling time are maintained within 0.1 second.

Method 6

Again change the combination as:

$$\begin{aligned} Y_\infty &= \frac{1}{2}(\theta_3 r_3 + \theta_2 r_2 + x_t \sin\alpha) \\ Y_2 &= \begin{bmatrix} \dot{\theta}_3 \\ \theta_3 r_3 - \theta_2 r_2 + x_t \sin\alpha \end{bmatrix}. \end{aligned} \tag{5.22}$$

Parameters in objective are:

$$\gamma_\infty = 50,\ \gamma_2 = 10,\ \mu_1 = 1,\ \mu_2 = 1. \tag{5.23}$$

The obtained controller is expressed as:

$$\begin{bmatrix} T_m \\ f \end{bmatrix} = \begin{bmatrix} K^{11}_{2\infty 6} & K^{12}_{2\infty 6} \\ K^{21}_{2\infty 6} & K^{22}_{2\infty 6} \end{bmatrix} \begin{bmatrix} \dot{\theta}_m \\ x_t \end{bmatrix}, \tag{5.24}$$

where:

$$\begin{aligned} K^{11}_{2\infty 6}(s) = & \frac{-8.284\times10^7 s^{11} - 9.329\times10^{13} s^{10} - 9.432\times10^{17} s^9}{s^{12} + 1.785\times10^7 s^{11} - 3.02\times10^{12} s^{10} - 2.173\times10^{19} s^9} \\ & \frac{-7.106\times10^{21} s^8 - 3.898\times10^{25} s^7 - 1.498\times10^{29} s^6 - 4.749\times10^{32} s^5}{-2.061\times10^{23} s^8 - 1.311\times10^{27} s^7 - 6.146\times10^{30} s^6 - 1.603\times10^{34} s^5} \\ & \frac{-1.071\times10^{36} s^4 - 1.737\times10^{39} s^3 - 1.911\times10^{42} s^2 - 1.097\times10^{45} s}{-2.731\times10^{37} s^4 - 2.665\times10^{40} s^3 - 6.543\times10^{42} s^2 + 1.459\times10^{46} s} \\ & \frac{-1.52\times10^{44}}{+3.979\times10^{40}} \\ K^{12}_{2\infty 6}(s) = & \frac{3.536\times10^8 s^{11} + 2.637\times10^{15} s^{10} + 2.516\times10^{21} s^9}{s^{12} + 1.785\times10^7 s^{11} - 3.02\times10^{12} s^{10} - 2.173\times10^{19} s^9} \\ & \frac{+1.964\times10^{25} s^8 + 7.177\times10^{28} s^7 + 6.74\times10^{31} s^6 - 5.053\times10^{35} s^5}{-2.061\times10^{23} s^8 - 1.311\times10^{27} s^7 - 6.146\times10^{30} s^6 - 1.603\times10^{34} s^5} \\ & \frac{-1.886\times10^{39} s^4 - 3.501\times10^{42} s^3 - 3.843\times10^{45} s^2 - 1.843\times10^{47} s}{-2.731\times10^{37} s^4 - 2.665\times10^{40} s^3 - 6.543\times10^{42} s^2 + 1.459\times10^{46} s} \\ & \frac{-6.208\times10^{41}}{+3.979\times10^{40}} \end{aligned}$$

$$K^{21}_{2\infty 6}(s) = \frac{5.112\times10^{14}s^{11} + 5.76\times10^{18}s^{10} + 4.093\times10^{22}s^{9}}{s^{12} + 1.785\times10^{7}s^{11} - 3.02\times10^{12}s^{10} - 2.173\times10^{19}s^{9}}$$
$$\frac{1.867\times10^{26}s^{8} + 6.028\times10^{29}s^{7} + 1.418\times10^{33}s^{6} + 2.524\times10^{36}s^{5}}{-2.061\times10^{23}s^{8} - 1.311\times10^{27}s^{7} - 6.146\times10^{30}s^{6} - 1.603\times10^{34}s^{5}}$$
$$\frac{+3.213\times10^{39}s^{4} + 2.939\times10^{42}s^{3} + 1.526\times10^{45}s^{2} + 2.013\times10^{47}s}{-2.731\times10^{37}s^{4} - 2.665\times10^{40}s^{3} - 6.543\times10^{42}s^{2} + 1.459\times10^{46}s}$$
$$\frac{-1.223\times10^{46}}{+3.979\times10^{40}}$$

$$K^{22}_{2\infty 6}(s) = \frac{-2.172\times10^{15}s^{11} - 1.367\times10^{22}s^{10} - 3.249\times10^{26}s^{9}}{s^{12} + 1.785\times10^{7}s^{11} - 3.02\times10^{12}s^{10} - 2.173\times10^{19}s^{9}}$$
$$\frac{-2.492\times10^{30}s^{8} - 7.507\times10^{33}s^{7} - 1.474\times10^{37}s^{6} - 1.614\times10^{40}s^{5}}{-2.061\times10^{23}s^{8} - 1.311\times10^{27}s^{7} - 6.146\times10^{30}s^{6} - 1.603\times10^{34}s^{5}}$$
$$\frac{-8.147\times10^{42}s^{4} + 5.723\times10^{45}s^{3} - 1.174\times10^{48}s^{2} + 4.621\times10^{51}s}{-2.731\times10^{37}s^{4} - 2.665\times10^{40}s^{3} - 6.543\times10^{42}s^{2} + 1.459\times10^{46}s}$$
$$\frac{+1.259\times10^{46}}{+3.979\times10^{40}}$$

Optimized norm are 13.4907 in H_∞ and 9.183 in H_2 norm. The responses to impulse disturbance are exhibited in Fig. 5.7 (a) and (b).

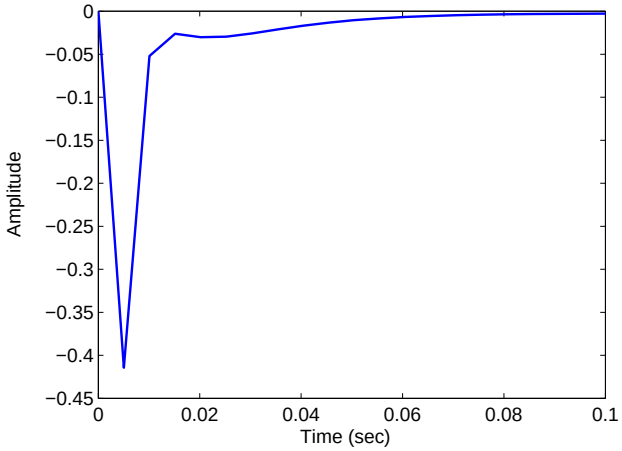

(a) DR speed

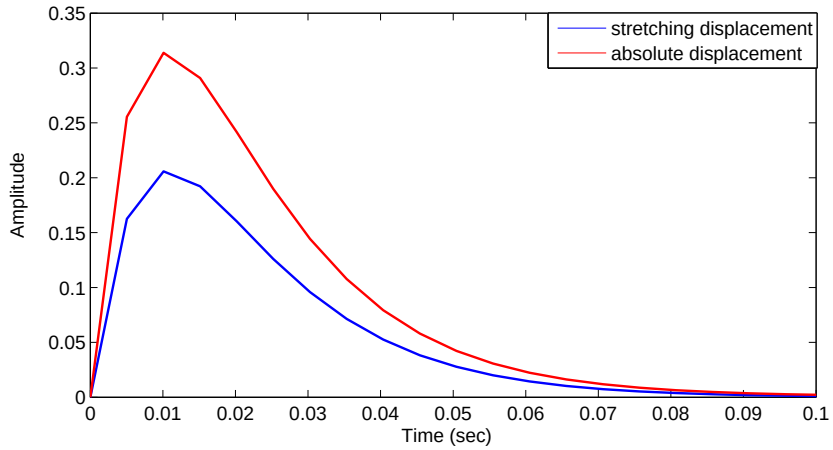

(b) belt displacement

Figure 5.7: Response to an impulse disturbance of closed-loop system with controller $K_{2\infty 6}$

Stretching displacement contains a peak value 0.2058 m, and absolute displacement has a peak value 0.3139 m. Both of the settling time are maintained within 0.1 second.

Method 7

Regulated outputs are changed to:

$$Y_\infty = \begin{bmatrix} \theta_3 r_3 - \theta_2 r_2 + x_t \sin\alpha \\ \frac{1}{2}(\theta_3 r_3 + \theta_2 r_2 + x_t \sin\alpha) \end{bmatrix} \tag{5.25}$$
$$Y_2 = \dot{\theta}_3.$$

Parameters in objective are:

$$\mu_1 = 1,\ \mu_2 = 1. \tag{5.26}$$

The obtained controller is expressed as:

$$\begin{bmatrix} T_m \\ f \end{bmatrix} = \begin{bmatrix} K_{2\infty 7}^{11} & K_{2\infty 7}^{12} \\ K_{2\infty 7}^{21} & K_{2\infty 7}^{22} \end{bmatrix} \begin{bmatrix} \dot{\theta}_m \\ x_t \end{bmatrix}, \tag{5.27}$$

where:

$$K^{11}_{2\infty 7}(s) = \frac{-3.956\times10^{6}s^{11} - 4.237\times10^{11}s^{10} - 3.972\times10^{15}s^{9}}{s^{12} + 1.058\times10^{7}s^{11} + 1.315\times10^{11}s^{10} - 9.485\times10^{16}s^{9}}$$
$$\frac{-1.969\times10^{19}s^{8} - 1.06\times10^{23}s^{7} - 2.975\times10^{26}s^{6} - 8.07\times10^{29}s^{5}}{-7.592\times10^{20}s^{8} - 2.246\times10^{24}s^{7} - 5.675\times10^{27}s^{6} + 5.416\times10^{30}s^{5}}$$
$$\frac{-8.584\times10^{32}s^{4} - 9.503\times10^{35}s^{3} + 6.449\times10^{38}s^{2} + 7.022\times10^{41}s}{+1.361\times10^{34}s^{4} + 7.909\times10^{37}s^{3} + 5.723\times10^{40}s^{2} + 9.873\times10^{43}s}$$
$$\frac{+2.353\times10^{40}}{+4.199\times10^{38}}$$

$$K^{12}_{2\infty 7}(s) = \frac{-1.348\times10^{6}s^{11} - 6.288\times10^{13}s^{10} - 7.191\times10^{18}s^{9}}{s^{12} + 1.058\times10^{7}s^{11} + 1.315\times10^{11}s^{10} - 9.485\times10^{16}s^{9}}$$
$$\frac{-1.268\times10^{23}s^{8} - 2.486\times10^{27}s^{7} - 1.377\times10^{31}s^{6} - 4.629\times10^{34}s^{5}}{-7.592\times10^{20}s^{8} - 2.246\times10^{24}s^{7} - 5.675\times10^{27}s^{6} + 5.416\times10^{30}s^{5}}$$
$$\frac{-1.102\times10^{38}s^{4} - 1.433\times10^{41}s^{3} - 1.556\times10^{44}s^{2} - 5.066\times10^{45}s}{+1.361\times10^{34}s^{4} + 7.909\times10^{37}s^{3} + 5.723\times10^{40}s^{2} + 9.873\times10^{43}s}$$
$$\frac{-2.157\times10^{40}}{+4.199\times10^{38}}$$

$$K^{21}_{2\infty 7}(s) = \frac{1.294\times10^{12}s^{11} + 8.349\times10^{15}s^{10} + 4.578\times10^{19}s^{9}}{s^{12} + 1.058\times10^{7}s^{11} + 1.315\times10^{11}s^{10} - 9.485\times10^{16}s^{9}}$$
$$\frac{1.3\times10^{23}s^{8} + 3.185\times10^{26}s^{7} + 4.819\times10^{29}s^{6} + 6.487\times10^{32}s^{5}}{-7.592\times10^{20}s^{8} - 2.246\times10^{24}s^{7} - 5.675\times10^{27}s^{6} + 5.416\times10^{30}s^{5}}$$
$$\frac{+4.699\times10^{35}s^{4} + 3.968\times10^{38}s^{3} + 5.51\times10^{40}s^{2} + 1.907\times10^{44}s}{+1.361\times10^{34}s^{4} + 7.909\times10^{37}s^{3} + 5.723\times10^{40}s^{2} + 9.873\times10^{43}s}$$
$$\frac{+2.259\times10^{44}}{+4.199\times10^{38}}$$

$$K^{22}_{2\infty 7}(s) = \frac{-5.696\times10^{11}s^{11} + 9.945\times10^{18}s^{10} + 1.293\times10^{24}s^{9}}{s^{12} + 1.058\times10^{7}s^{11} + 1.315\times10^{11}s^{10} - 9.485\times10^{16}s^{9}}$$
$$\frac{+4.796\times10^{27}s^{8} + 2.406\times10^{31}s^{7} + 3.995\times10^{34}s^{6} + 9.503\times10^{37}s^{5}}{-7.592\times10^{20}s^{8} - 2.246\times10^{24}s^{7} - 5.675\times10^{27}s^{6} + 5.416\times10^{30}s^{5}}$$
$$\frac{+6.41\times10^{40}s^{4} + 1.016\times10^{44}s^{3} - 1.067\times10^{44}s^{2} + 3.055\times10^{49}s}{+1.361\times10^{34}s^{4} + 7.909\times10^{37}s^{3} + 5.723\times10^{40}s^{2} + 9.873\times10^{43}s}$$
$$\frac{+1.298\times10^{44}}{+4.199\times10^{38}}$$

Optimized norms are actually very big that are 867.9870 for H_∞ and 1356.5 for H_2. Responses to impulse disturbance are calculated to show whether this method is effective or not.

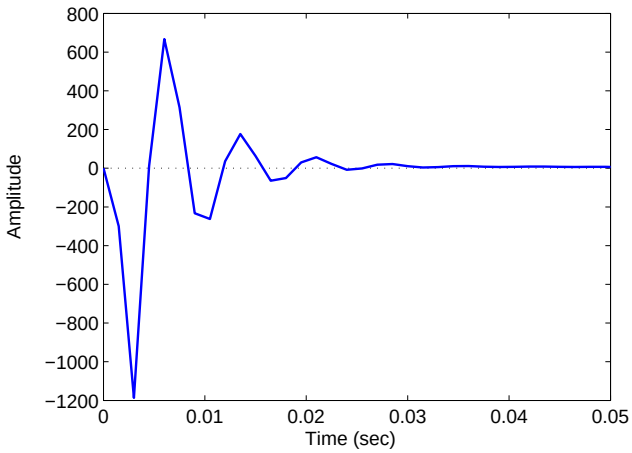

(a) DR speed

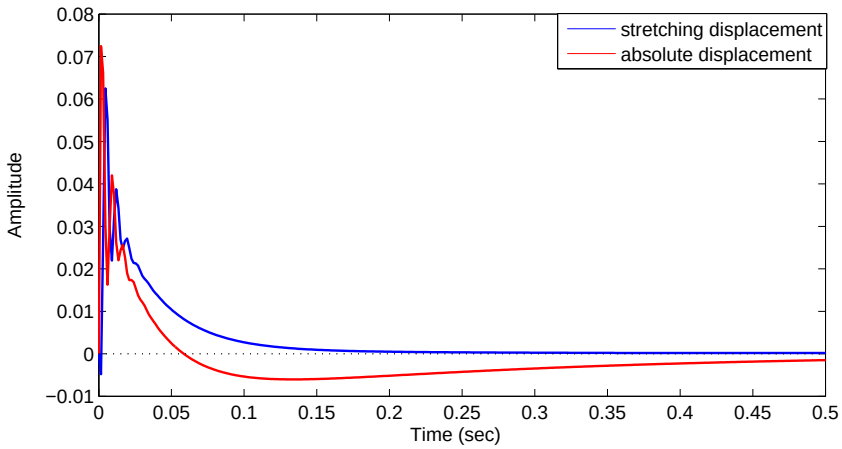

(b) belt displacement

Figure 5.8: Response to an impulse disturbance of closed-loop system with controller $K_{2\infty 7}$

The settling times are sacrificed for the much smaller peak, which are 0.0625 m for stretching displacement and 0.07243 m for absolute displacement.The curves trend to oscillate at the first beginning but converge within 0.5 second. This method achieves best performance resisting to impulse disturbance so far.

Method 8

Last combination is shown as:

$$Y_\infty = \begin{bmatrix} \dot{\theta}_3 \\ \frac{1}{2}(\theta_3 r_3 + \theta_2 r_2 + x_t \sin\alpha) \end{bmatrix} \tag{5.28}$$
$$Y_2 = \theta_3 r_3 - \theta_2 r_2 + x_t \sin\alpha.$$

Parameters in objective are:

$$\gamma_\infty = 600,\ \gamma_2 = \infty, \mu_1 = 0,\ \mu_2 = 1. \tag{5.29}$$

The ∞ on H_2 is to cooperate with the minimization problem. The obtained controller is expressed as:

$$\begin{bmatrix} T_m \\ f \end{bmatrix} = \begin{bmatrix} K^{11}_{2\infty 8} & K^{12}_{2\infty 8} \\ K^{21}_{2\infty 8} & K^{22}_{2\infty 8} \end{bmatrix} \begin{bmatrix} \dot{\theta}_m \\ x_t \end{bmatrix}, \tag{5.30}$$

where:

$$K^{11}_{2\infty 8}(s) = \frac{-1.371\times10^6 s^{11} - 2.67\times10^{11}s^{10} - 3.37\times10^{15}s^9}{s^{12} + 1.184\times10^7 s^{11} + 1.496\times10^{12}s^{10} - 3.794\times10^{16}s^9}$$
$$\frac{-1.946\times10^{19}s^8 - 1.053\times10^{23}s^7 - 4.091\times10^{26}s^6 - 1.144\times10^{30}s^5}{-4.442\times10^{20}s^8 - 1.689\times10^{24}s^7 - 5.637\times10^{27}s^6 - 2.832\times10^{30}s^5}$$
$$\frac{-2.013\times10^{33}s^4 - 2.58\times10^{36}s^3 - 1.531\times10^{39}s^2 - 2.538\times10^{41}s}{-3.435\times10^{33}s^4 + 3.075\times10^{37}s^3 + 2.142\times10^{40}s^2 + 4.277\times10^{43}s}$$
$$\frac{-1.578\times10^{42}}{+1.857\times10^{38}}$$

$$K^{12}_{2\infty 8}(s) = \frac{4.974\times10^6 s^{11} + 1.938\times10^{13}s^{10} + 3.576\times10^{18}s^9}{s^{12} + 1.184\times10^7 s^{11} + 1.496\times10^{12}s^{10} - 3.794\times10^{16}s^9}$$
$$\frac{-7.584\times10^{21}s^8 - 8.916\times10^{26}s^7 - 5.675\times10^{30}s^6 - 1.822\times10^{34}s^5}{-4.442\times10^{20}s^8 - 1.689\times10^{24}s^7 - 5.637\times10^{27}s^6 - 2.832\times10^{30}s^5}$$
$$\frac{-3.937\times10^{37}s^4 - 4.898\times10^{40}s^3 - 4.207\times10^{43}s^2 - 1.235\times10^{45}s}{-3.435\times10^{33}s^4 + 3.075\times10^{37}s^3 + 2.142\times10^{40}s^2 + 4.277\times10^{43}s}$$
$$\frac{-3.763\times10^{40}}{+1.857\times10^{38}}$$

$$K^{21}_{2\infty 8}(s) = \frac{2.58\times10^{12}s^{11} + 2.154\times10^{16}s^{10} + 1.242\times10^{20}s^9}{s^{12} + 1.184\times10^7 s^{11} + 1.496\times10^{12}s^{10} - 3.794\times10^{16}s^9}$$
$$\frac{4.628\times10^{23}s^8 + 1.266\times10^{27}s^7 + 2.594\times10^{30}s^6 + 3.886\times10^{33}s^5}{-4.442\times10^{20}s^8 - 1.689\times10^{24}s^7 - 5.637\times10^{27}s^6 - 2.832\times10^{30}s^5}$$

$$K^{22}_{2\infty 8}(s) = \frac{\begin{array}{l}+4.234\times10^{36}s^4+2.984\times10^{39}s^3+9.792\times10^{41}s^2+1.555\times10^{44}s\\ \hline -3.435\times10^{33}s^4+3.075\times10^{37}s^3+2.142\times10^{40}s^2+4.277\times10^{43}s\\ +5.305\times10^{44}\\ \hline +1.857\times10^{38}\end{array}}{\begin{array}{l}-1.028\times10^{13}s^{11}-4.546\times10^{19}s^{10}+6.199\times10^{23}s^9\\ \hline s^{12}+1.184\times10^{7}s^{11}+1.496\times10^{12}s^{10}-3.794\times10^{16}s^9\\ +3.186\times10^{27}s^8+1.919\times10^{31}s^7+4.019\times10^{34}s^6+9.229\times10^{37}s^5\\ \hline -4.442\times10^{20}s^8-1.689\times10^{24}s^7-5.637\times10^{27}s^6-2.832\times10^{30}s^5\\ +8.62\times10^{40}s^4+9.734\times10^{43}s^3+1.611\times10^{46}s^2+1.362\times10^{49}s\\ \hline -3.435\times10^{33}s^4+3.075\times10^{37}s^3+2.142\times10^{40}s^2+4.277\times10^{43}s\\ +5.859\times10^{44}\\ \hline +1.857\times10^{38}\end{array}}$$

The bound for each norm are 600 on H_∞, and 229.7114 on H_2. Responses to

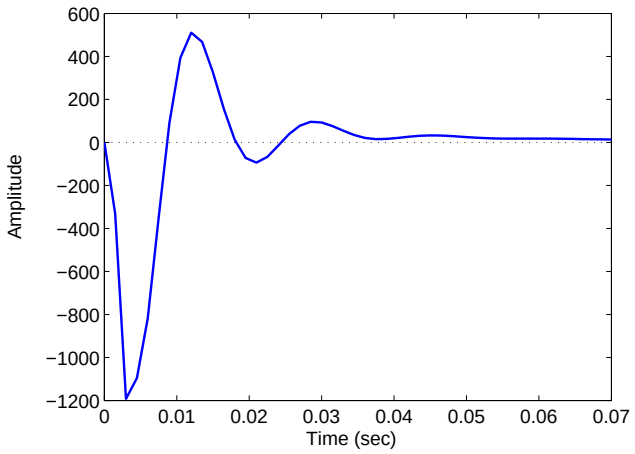

(a) DR speed

impulse disturbance are also shown in Fig. 5.9 (a) and (b). The results are not so promising, both of the displacements reflect some oscillation and peak values are much bigger than the best one, which are 0.1648 m for stretching displacement and 0.2031 m for absolute displacement.

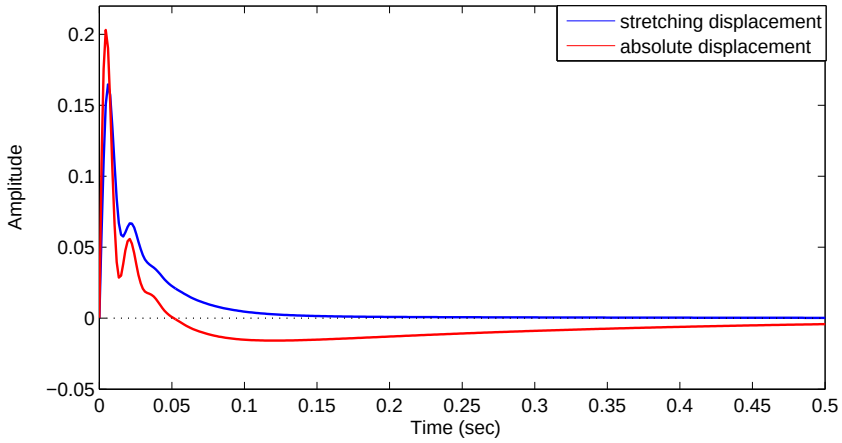

(b) belt displacement

Figure 5.9: Response to an impulse disturbance of closed-loop system with controller $K_{2\infty 8}$

Results from these eight methods are summarized in Table 5.1. S.t. is abbreviation for settling time.

Table 5.1: Comparison results of these eight methods in H_2/H_∞ optimal control

method	stretching displacement		absolute displacement	
	peak (amplitude)	s.t. (sec)	peak (amplitude)	s.t. (sec)
1	0.1349	1	0.1654	1
2	0.1847	0.1	0.2195	0.4
3	0.2308	0.14	0.3405	0.14
4	0.2018	0.1	0.2712	0.4
5	0.2056	0.1	0.3141	0.1
6	0.2058	0.09	0.3139	0.09
7	0.0625	0.15	0.07243	0.5
8	0.1648	0.13	0.2031	0.6

It is obviously that method 7 is most effective one, though the settling time from absolute displacement is somehow slow.

5.5 Summary

An optimal mixed H_2/H_∞ output feedback controller is constructed in this chapter to minimize the effect from loading disturbance and system uncertainty. Due to problem complexity, several combinations between outputs to be regulated and constraints are studied for existence of the desired controller. Numerical simulation results of impulse response in closed-loop system testified the validity of this control design. Also they reflect that stretching displacement and absolute displacement have some contrary due to their mathematical components. It is indicated that by constraining these two displacements under H_∞ norm, and drive roller speed under H_2 norm, the controller achieve best capability. Other combinations also show improved results by sacrificing settling time or one of the displacements performance.

Chapter 6

Conclusion

In this study, in order to attenuate belt vibration of image transfer belt system caused by loading disturbance, three novel control methods based on the ideas of optimal H_2 state feedback, optimal H_∞ output feedback, and optimal mixed H_2/H_∞ output feedback are proposed and their control performances are investigated. In order to conduct the control structure design, mathematical model of image transfer belt is studied in conditions of system with and without tensioner. The necessity of taking system uncertainty and tensioner into modelling consideration are studied by several simulations. Validity of these three control methods are ascertained by numerical simulation results. The procedure of the study is divided into the following four stages.

i) It proposed a mechanical model for image transfer belt system in xerographic printing process, called four-rollers-belt (FRB) system. Two mathematical expressions concerning to belt variation which is related to image printing quality are established. This model is simulated numerically with and without the tensioner part to reflect the effect from it on belt variation. It is also compared with a multi-rollers-belt system that is similar to the real equipment to certify its applicability. Additionally, uncertainty originated from system parameters are introduced to this model under passive control method by flywheel in order to show the importance of active control.

ii) It proposed an optimal state feedback controller based on minimizing the H_2 norm of transfer function from loading disturbance on system outputs.

The stabilization problem and optimization problem in this control design are investigated. Numerical simulations are conducted under different selections of the regulated output to find out best performance that can be achieved by this controller. Also its effectiveness is clarified during the comparisons.

iii) Due to calculation redundancy of state feedback controller, an optimal output feedback controller based on H_∞ norm to solve system uncertainty problem was designed. Criterion on H_∞ norm of transfer function from loading disturbance on system outputs are derived along with the obtaining procedure for controller. Numerical simulations are conducted with a simulated real loading disturbance signal to open-loop system without controller, with conventional PID speed controller, and the proposed one, in order to clarity its validity. Control performances with system uncertainty by the optimal H_∞ controller are investigated to proof its efficiency.

iv) A mixed H_2/H_∞ optimal output feedback controller was designed following the previous two steps in order to combine the advantages in both of these control objectives. Due to the strict constrain on existence of this controller, multiple combinations of outputs with different objectives are studied through numerical simulations. The improvement on system made by this controller is proven along with simulations.

■ Brief Conclusions

The conclusions obtained in the above mentioned study are briefly summarized as follows.

- Mechanical modeling study for image transfer belt system

  - Effect from tensioner part on belt variation can not be ignored based on simulation results. Moreover it one of the main reasons leading to belt vibration when loading disturbance entering the system.

  - The proposed mechanical model for image transfer belt system is applicable in control design compared to the complicated one that is similar to real equipment based on numerical comparison results.

- Passive control method by flywheel is ascertained its effectiveness on the proposed model. However it can not maintain the desired capability with system uncertainty, which leads to requirement of active control related to system robustness.

- Optimal H_2 state feedback control design

  - Effectiveness of this control method is ascertained compared to open-loop system response to impulse loading disturbance.

  - It is shown that different additional regulated output led various control performances on belt displacements. Attenuation along with drive roller speed leads to better result on stretching displacement, while constrain on tension roller speed obtains much more improvement on absolute displacement.

  - This kind of state feedback requires large amount of calculations for controller.

- Optimal H_∞ output feedback control design

  - Validity of this proposed controller is proven by simulation results of response to a simulated real loading disturbance signal, along with performance of open-loop system, and closed-loop system with conventional PID speed controller.

  - Robustness of the closed-loop system endowed by proposed controller is certified by calculating results reacted to loading disturbance along with system uncertainty

- Optimal mixed H_2/H_∞ output feedback control design

  - Usefulness of this mixed objectives controller is clarified by impulse response of closed-loop system numerically.

  - Various control performances according to different selections of regulated outputs and constrains are uncovered. And bounds of belt displacement on H_∞ norm with bounds of drive roller speed on H_2 norm achieves the most satisfying control results.

■ Future Outlook

As shown in the present thesis, the optimal control methods for attenuating belt vibration raised by loading disturbance in image transfer belt system of xerographic printing process was concentrated in this study. The proposed model and control methods are supported by many examples in numerical simulations and comparisons. However, it is worth mentioning that the arguments discussed in this thesis remains to be improved in the future studies. Like,

- High order controllers are obtained by proposed control designs which are not easy to apply in the real machinery. Reduced order controller with similar capability are desirable.
- The designs are based on feedback control architecture, however feedforward control is also worth of applying in loading disturbance rejection. Moreover, feedback control combined with feedforward control could achieve better performance according to other design examples.

It is expected that the proposed control methods can be applied to the real xerographic printing process along with the upper layer control architectures to achieve high quality printing.

Appendix A

system without tensioner described in Eq. (2.7):

select the motion vector as:

$$x_b = \begin{bmatrix} \theta_1 & \theta_2 & \theta_3 & \theta_4 \end{bmatrix}^{\mathrm{T}}, \tag{1}$$

and Eq. (2.7) is reformed as: par

$$\begin{bmatrix} \mathbf{M}_b & \mathbf{0}_{4\times1} \\ \mathbf{0}_{1\times4} & \mathbf{M}_m \end{bmatrix} \begin{bmatrix} \ddot{x}_b \\ \ddot{\theta}_m \end{bmatrix} + \begin{bmatrix} \mathbf{0}_{4\times4} & \mathbf{0}_{4\times1} \\ \mathbf{0}_{1\times4} & \mathbf{C}_m \end{bmatrix} \begin{bmatrix} \dot{x}_b \\ \dot{\theta}_m \end{bmatrix} + \begin{bmatrix} \mathbf{K}_b & \mathbf{0}_{4\times1} \\ \mathbf{0}_{1\times4} & \mathbf{K}_m \end{bmatrix} \begin{bmatrix} x_b \\ \theta_m \end{bmatrix} = \mathbf{P}_1 T_p + \mathbf{P}_2 T_m. \tag{2}$$

The Rayleigh damping model is calculated as:

$$\mathbf{C}_b = \lambda \mathbf{M}_b + \mu \mathbf{K}_b \ , \tag{3}$$

where $\lambda = 25$, and $\mu = 3 \times 10^{-4}$ according to the experimental identification. By substituting Eq. (3) into (2), the matrix form for equation of motions of system without tensioner is derived as Eq. (2.9).

system with tensioner described in Eq. (2.5):

Again select the same motion vector in Eq. (1), and Eq. (2.5) is rewritten as:

$$\begin{bmatrix} \mathbf{M_b} & \mathbf{0}_{4\times1} & \mathbf{0}_{4\times1} \\ \mathbf{0}_{1\times4} & \mathbf{M_m} & 0 \\ \mathbf{0}_{1\times4} & 0 & \mathbf{M_t} \end{bmatrix} \begin{bmatrix} \ddot{x}_b \\ \ddot{\theta}_m \\ \ddot{x}_t \end{bmatrix} + \begin{bmatrix} \mathbf{0}_{4\times4} & \mathbf{0}_{4\times1} & \mathbf{0}_{4\times1} \\ \mathbf{0}_{1\times4} & \mathbf{C_m} & 0 \\ \mathbf{0}_{1\times4} & 0 & 0 \end{bmatrix} \begin{bmatrix} \dot{x}_b \\ \dot{\theta}_m \\ \dot{x}_t \end{bmatrix} + \begin{bmatrix} \mathbf{K_b} & \mathbf{0}_{4\times1} & \mathbf{0}_{4\times1} \\ \mathbf{0}_{1\times4} & \mathbf{K_m} & 0 \\ \mathbf{0}_{1\times4} & 0 & \mathbf{K_t} \end{bmatrix} \begin{bmatrix} x_b \\ \theta_m \\ x_t \end{bmatrix} = \mathbf{P_1} T_p + \mathbf{P_2} T_m. \tag{4}$$

The Rayleigh damping model is modified as:

$$\mathbf{C}_b = \lambda \begin{bmatrix} \mathbf{M}_b \\ \mathbf{M}_t \end{bmatrix} + \mu \begin{bmatrix} \mathbf{K}_b \\ \mathbf{K}_t \end{bmatrix}, \tag{5}$$

where the coefficient are the same as $\lambda = 25$, and $\mu = 3 \times 10^{-4}$. The matrices involved in equations above are expressed as:

$$\mathbf{M}_b = \begin{bmatrix} I_1 & 0 & 0 & 0 \\ 0 & I_2 & 0 & 0 \\ 0 & 0 & I_3 & 0 \\ 0 & 0 & 0 & I_4 \end{bmatrix}, \ \mathbf{M_m} = I_m, \ \mathbf{M}_t = m_2$$

$$\mathbf{K_b} = \begin{bmatrix} (k_1+k_4)r_1^2 & -k_1 r_1 r_2 & 0 & -k_4 r_1 r_4 \\ -k_1 r_1 r_2 & (k_1+k_2)r_2^2 & -k_2 r_2 r_3 & 0 \\ 0 & -k_2 r_2 r_3 & (k_2+k_3)r_3^2 & -k_3 r_3 r_4 \\ -k_4 r_1 r_4 & 0 & -k_3 r_3 r_4 & (k_3+k_4)r_4^2 \end{bmatrix}$$

$$\mathbf{K}_m = \frac{k_m}{m}, \mathbf{K}_t = k_1 \sin^2\beta + k_2 \sin^2\alpha + k_t$$

$$\mathbf{C}_m = \frac{b_m}{m}.$$

Appendix B

Schur Complement is stated as the following block matrix:

$$\begin{bmatrix} Q & S \\ S^{\mathrm{T}} & R \end{bmatrix} \text{ is positive definite,} \tag{6}$$

if and only if,

$$Q > 0 \text{ and } R - S^{\mathrm{T}} R^{-1} S > 0, \tag{7}$$

or if and only if,

$$R > 0 \text{ and } Q - S R^{-1} S^{\mathrm{T}} > 0, \tag{8}$$

Proof from Eq. (1) to (2) is shown as following:

select the nonzero matrix x that:

$$x = \begin{bmatrix} I & -Q^{-1}S \\ 0 & I \end{bmatrix}, \tag{9}$$

then

$$x^{\mathrm{T}} = \begin{bmatrix} I & 0 \\ -S^{\mathrm{T}}Q^{-1} & I \end{bmatrix} \tag{10}$$

Based on Eq. (1), (4), and (5), the following equations hold:

$$
\begin{aligned}
x^{\mathrm{T}} \begin{bmatrix} Q & S \\ S^{\mathrm{T}} & R \end{bmatrix} x &= \begin{bmatrix} I & 0 \\ -S^{\mathrm{T}}Q^{-1} & I \end{bmatrix} \begin{bmatrix} Q & S \\ S^{\mathrm{T}} & R \end{bmatrix} \begin{bmatrix} I & -Q^{-1}S \\ 0 & I \end{bmatrix} \\
&= \begin{bmatrix} Q & 0 \\ 0 & R - S^{\mathrm{T}}R^{-1}S \end{bmatrix} > 0
\end{aligned}
\tag{11}
$$

And it leads to:

$$
\begin{aligned}
Q &> 0 \\
R - S^{\mathrm{T}}Q^{-1}S &> 0
\end{aligned}
\tag{12}
$$

which proved Eq. (2). The procedure from Eq. (1) to (3) and the reverse are similar which are not list here.

Appendix C

Transformation Lemma has the following statement:

Suppose that:

$$\begin{bmatrix} S_1 & I \\ I & P_1 \end{bmatrix} > 0 \tag{13}$$

Then there exist P_2, P_3, S_2, S_3 such that

$$\begin{aligned} P &= \begin{bmatrix} P_1 & P_2 \\ P_2^{\mathrm{T}} & P_3 \end{bmatrix} \\ &= \begin{bmatrix} S_1 & S_2 \\ S_2^{\mathrm{T}} & S_3 \end{bmatrix}^{-1} = S^{-1} > 0, \end{aligned} \tag{14}$$

where $S_{cl} = \begin{bmatrix} S_1 & I \\ S_2^{\mathrm{T}} & 0 \end{bmatrix}$ has full rank.

The proof from Eq. (1) to Eq. (2) is explained as following:

Since Eq. (1) holds, by Schur complement then

$$\begin{aligned} P_1 &> 0 \\ P_1^{-1} - S_1 &> 0 \end{aligned} \tag{15}$$

Since $I - P_1 S_1 = P_1(P_1^{-1} - S_1)$, then $I - P_1 S_1$ is invertible.

Now pick up two square invertible matrices P_2 and S_2 such that

$$P_2 S_2^{\mathrm{T}} = I - P_1 S_1. \tag{16}$$

Since P_2 and S_2 are non-singular,

$$S_{cl}^{\mathrm{T}} = \begin{bmatrix} S_1 & S_2 \\ I & 0 \end{bmatrix} \text{ and } P_{cl} = \begin{bmatrix} I & 0 \\ P_1 & P_2 \end{bmatrix} \tag{17}$$

are also non-singular.

Next define P and S as

$$\begin{aligned} P &= S_{cl}^{\mathrm{T}} P_{cl} \\ S &= P_{cl}^{-1} S_{cl}^{\mathrm{T}}, \end{aligned} \tag{18}$$

then

$$PS = S_{cl}^{-1} P_{cl} P_{cl}^{-1} S_{cl} = I$$

Therefore $S = P^{-1}$ that indicate Eq. (2)

References

[1] Michael Twyman. *The British Library Guide to Printing*. University of Toronto Press, London, first edition, 1998. 1

[2] Colin Clair. *A History of European Printing*. Academic Press, London, first edition, 1976. 1

[3] Douglas Crawford McMurtrie. *The Book; the Story of Printing and Bookmarking*. Oxford University Press, New York, London, third edition, 1943. 2

[4] Thomas Francis Carter. *The Invention of Printing in China and its Spread Westward*. The Ronald Press, New York, second edition, 1955. 2

[5] Elizabeth L. Eisenstein. *The Printing Revolution in Early Modern Europe*. Cambridge University Press, U.S.A, second edition, 2005. 2

[6] Eldred Robert A. Kusko Bruce H. Wick Daniel L. Schwab Richard N., Cahill Thomas A. "new evidence on the printing of the gutenberg bible: the inks in the doheny copy". *Papers of the Bibliographical Society of America*, vol. 79:pp. 375–410, 1985. 2

[7] Lucien Febvre. *The Coming of the Book: The Impact of Printing 1450-1800*. Verso Press, New York, London, second edition edition, 1997. 2

[8] Alexander Andrews. *The History of British Journalism: from the foundation of the newpaper press in England, to the repeal of the Stamp act in 1855*. London, first edition edition, 1959. 2

[9] C. F. Carlson. Electrophotography, October 6 1942. US Patent 2,297,691. 3

[10] Jimmy Hai Carlo Paventi Hod Lipson, Francis C. Moon. "3-d printing the history of mechanisms". *Journal of Mechanical Design*, vol. 5:pp. 1029–1033, 2004. 3

[11] C. D. Oughton R. M. Schaffert. "xerography: A new principe of photography and graphic reproduction". *Journal of the Optical Society of America*, vol. 38:pp. 991–998, 1948. 5

[12] Bode D. E. Neyhart J. H. Potok E. R. Blakney, R. M. Xerographic process, June 26 1962. US Patent 3,041,167. 5

[13] Paul M. Borsenberger. *Organic Photoreceptors for Xerography*. CRC Press, New York, first edition edition, 1998. 6

[14] T. L. Theis S. E. Powers A. Ahmadi, B. H. Williamson. "life-cycle inventory of toner produced for xerographic processes". *Journal of Cleaner Production*, vol. 11:pp. 573–582, 2002. 6

[15] C. Snelling. Reflex xerographic process, August 8 1967. US Patent 3,335,003. 6

[16] Langdon M. J. Draugelis V. C., Hartman W. R. Multicolor xerographic process, January 23 1979. US Patent 4,135,927. 6

[17] Gundlach R. W. Method for two-color development of a xerographic charge pattern, March 14 1978. US Patent 4,078,929. 6

[18] A. Akman. Transparency for multi-color electrostatic copying, December1974 1974. US Patent 3,854,942. 6

[19] Clemens C. F. Decalcomania, polymeric plasticizing material, January 3 1978. US Patent 4,066,802. 6

[20] Snelling C. Electronic color printing system, September 13 1983. US Patent 4,403,848. 6

[21] Klassen R. V. Dalal E. N., Balasubramanian T. System for printing color images with extra colorants in addition to primary colorants, April 6 1999. US Patent 5,892,891. 6

[22] Tracy Thieret Charles B. Duke, Jaan Noolandi. "the surface science of xerography". *Journal of Surface Science*, vol. 500:pp. 1005–1023, 2002. 6

[23] Eschbach Reiner Balasubramanian Raja. "reducting multi-separationg color moire by a variable undercolor removal and gray component replacement strategy". *Journal of Imaging Science and Technology*, vol. 2:pp. 152–160, 2001. 6

[24] Vackier L. Van den Bogaert J. Electrostatographic multi-color printer for duplex printing on a web-type toner receptor material, June 9 1998. US Patent 5,765,081. 6

[25] Martin D. W. Roetker M. S. Santana F. J. Darcy J. J., Griffin S. J. Welded polyimide intermediate transfer belt and process for making the belt, November 21 2006. US Patent 7,139,519. 7

[26] T. L. Theis S. E. Powers A. Ahmadi, B. H. Williamson. "life-cycle inventory of toner produced for xerographic processes". *Journal of Cleaner Production*, vol. 11:pp. 573–582, 2002. 7

[27] James E. Fay Ashok V. Kumar, Anirban Dutta. "electrophotographic printing of part and binder powders". *Journal of Rapid Prototyping*, vol. 10:pp. 7–13, 1995. 7

[28] Terada H. Nakamura M., Yamamoto H. Color electrophotographic apparatus having an intermediate transfer belt variable in speed, December 24 1996. US Patent 5,587,783. 7

[29] Radulski C. A. Till H. R., Warner F. A. Intermediate transfer apparatus, August 4 1987. US Patent 4,684,238. 7

[30] Yamaguchi N. Kanekura K. Color image forming apparatus including mechanism which provides tension to an intermediate transfer belt, November 5 2002. US Patent 6,477,349. 8

[31] Kawaishi Y. Multicolor image forming apparatus with tension controlled image transfer belt, March 1 1994. US Patent 5,291,252. 8

[32] Kayahara S. Minbu R. Sawai Y. Takahashi M. Uchida S. Kamiyama H. Ogiyama H., Kawagoe K. Image forming apparatus including an intermediate image transfer belt and high resistance contact member, May 31 2005. US Patent 6,901,234. 8

[33] Kuroda M. Shigemori K. Takano K. Takayama S. Nishi N. Hokari N. Hoshino T. Tagawa K. Yamashina S., Sato I. et al. Method and apparatus for correcting running state and tension for an endless belt in an image-forming apparatus, November 20 2001. US Patent 6,321,052. 8

[34] David P. Bujese. Electrostatic color printing system utilizing an image transfer belt, February 4 1994. US Patent 5,285,244. 8

[35] Yasunori Kawaishi Katsuya Kawagoe, Shin Kayahara. Image transferring method and image forming apparatus for transferring toner image from image carrier to recording medium either via or carried on intermediate image transfer belt, April 3 2001. US Patent 6,212,351 B1. 9

[36] Shinichi Sugiyama. Image forming apparatus having releasing mechanism for removable toner-image conveyance belt, November 22 2011. US Patent 8,064,797 B2. 10

[37] D.A. DeHollander, M.S. Roetker, S.J. Griffin, D.W. Martin, and J. Herko. Intermediate transfer belt and methods for making the same, June 7 2011. US Patent 7,957,684. 11

[38] M.A. Atwood, J.P. Calamita, and A. Podzorov. Intermediate transfer belt steering system, April 5 2011. US Patent 7,920,814. 12

[39] R. Maeyama and Y. Okamoto. Image forming apparatus and intermediate transfer belt module to efficiently accommodate additional image forming unit, January 13 2004. US Patent 6,678,493. 13

[40] N. Iwata, S. Katou, Y. Shio, and T. Yabuta. Registration control for an image forming apparatus having an intermediate transfer belt, October 27 1998. US Patent 5,828,926. 13

[41] H. Ishibashi, T. Maruta, Y. Sawai, T. Yoshikawa, and A. Takehara. Tandem color image forming apparatus with an image transfer belt and backup roller, February 6 2007. US Patent 7,174,124. 13

[42] T. Sasamoto, K. Miyawaki, M. Obu, M. Suzuki, and Y. Aoyama. Belt device and unit device including belt device and image forming apparatus using the belt device and unit device, November 27 2001. US Patent 6,324,374. 13

[43] T. Ueno, K. Murayama, and N. Hoshi. Developing device and process cartridge comprising first and second sealing members and electrophotographic image forming apparatus comprising a developing device comprising first and second sealing members, November 23 2004. US Patent 6,823,153. 13

[44] G.A. Denton and S.C. Tungate. Method of setting laser power and developer bias in an electrophotographic machine based on an estimated intermediate belt reflectivity, February 28 2006. US Patent 7,006,250. 13

[45] Y. Natori and M. Matsuo. Intermediate transfer belt and image forming apparatus and image forming method using the same, September 9 2008. US Patent 7,424,256. 13

[46] J. J. Shah T. C. Kraver, G. W. Fan. "complex modal analysis of a flat belt pulley system with belt damping and coulomb-damped tensioner". *Journal of Mechanical Design*, vol. 118:pp. 306–311, 1996. 13

[47] Yang Y. L. Barker C. "dynamic analysis of an automotive belt drive system". *Proceedings of the First international Applied Mechanical Systems Design Conference*, page No. 75, June 11-14, 1989. 14

[48] Breig W. F. Barker C. R., Oliver L. R. "dynamic analysis of belt drive tension forces during rapid engine acceleration". *Proceedings of SAE Conference*, pages pp. 239–254, 1991. 14

[49] Allebach Jan P. Burningham Norman Bang Yousun, Pizlo Zygmunt. "discrimination based banding assessment". *Proceedings of 2003 International Conference on Digital Printing Technologies*, pages pp. 745–750, 2003. 15

[50] J.E. Roddy, B. Narayan, and E.M. Granger. Scanning apparatus for halftone image screen writing, October 23 1990. US Patent 4,965,599. 15

[51] Robert P. Loce, William L. Lama, and Martin S. Maltz. "modeling vibration-induced halftone banding in a xerographic laser printer". *Journal of Electronic Imaging*, vol. 4:pp. 48–61, 1995. 15

[52] Je-Ho Lee and J.P. Allebach. "inkjet printer model-based halftoning". *Image Processing, IEEE Transactions on*, vol. 14:pp. 674–689, May 2005. 15

[53] Sang Ho Kim and J.P. Allebach. "impact of hvs models on model-based halftoning". *Image Processing, IEEE Transactions on*, vol. 11:pp. 258–269, Mar 2002. 15

[54] F.A. Baqai and J.P. Allebach. "halftoning via direct binary search using analytical and stochastic printer models". *Image Processing, IEEE Transactions on*, vol. 12:pp. 1–15, Jan 2003. 15

[55] F.A. Baqai, Je-Ho Lee, A.U. Agar, and J.P. Allebach. "digital color halftoning". *Signal Processing Magazine, IEEE*, vol. 22:pp. 87–96, Jan 2005. 15

[56] Cheng-Lun Chen and G.T.-C. Chiu. "banding reduction in electrophotographic process". In *Advanced Intelligent Mechatronics, 2001. Proceedings. 2001 IEEE/ASME International Conference on*, volume vol. 1, pages pp. 81–86, 2001. 16

[57] Cheng-Lun Chen and G.T.-C. Chiu. "incorporating human visual model and spatial sampling in banding artifact reduction". In *American Control Conference, 2004. Proceedings of the 2004*, volume vol. 3, pages pp. 2642–2647, June 2004. 16

[58] Mikkilineni Aravind K. Delp Edward J. Allebach Jan P. Chiu George T.-C. Chiang Pei Ju, Ali Gazi N. "extrinsic signatures embedding using exposure

modulation for information hiding and secure printing in electrophotography". *Proceedings of 2004 International Conference on Digital Printing Technologies*, vol. 6:pp. 295–300, 2004. 16

[59] Allebach Jan Pizlo Zygmunt, Bang Yousun. "banding assessment with controlled halftoning: The ten printer experiment". *Journal of Imaging Science and Technology*, vol. 50:pp. 522–529, 2006. 16

[60] M.H. Rahnavard and M. Zomorrodi. Suppression of banding due to vibration in imagers with laser drivers, August 10 2004. US Patent 6,774,925. 16

[61] Cheng-Lun Chen, G.T.-C. Chiu, and J.P. Allebach. "robust spatially sampled controller design for banding reduction in electrophotographic process". In *Robotics and Automation, 2003. Proceedings. ICRA '03. IEEE International Conference on*, volume vol. 2, pages pp. 2622–2627, Sept 2003. 16

[62] J. P. Allebach C.-L. Chen, G.T.-C. Chiu. "banding reduction in ep processes using human contrast sensivity function shaped photocnoductor velocity control". *Journal of Imaging Science and Technology*, May 2003. 16

[63] J. P. Allebach C.-L. Chen, G.T.-C. Chiu. "robust spatial-sampling controller design for banding reduction in electrophotographic process". *Journal of Imaging Science and Technology*, Nov 2006. 16

[64] C.-P. Weng C.-L. Chen. "modeling and simulation of a laser printing system". *Journal of Engineering*, Nov 2007. 16

[65] C.-P. Weng S.-H. Lin Y.-H. Yang, C.-L. Chen. "spatial domain adaptive repetitive controller design for uncertain variable-speed rotational motion systems". *Journal of the Chinese Society of Mechanical Engineers*, Feb 2008. 16

[66] G. Chiu C.-L. Chen. "spatially periodic disturbance rejection with spatially sampled robust repetitive control". *Journal of Dynamic Systems, Measurement and Control*, Mar 2008. 16

[67] G. Chiu C.-L. Chen. "banding artifact reduction for a class of color electrophotographic printers with under-actuated motor/gear configuration". *IEEE Trans. Control Systems Technology*, July 2008. 16

[68] J. P. Allebach C.-L. Chen, G. Chiu. "halftone banding reduction for a class of electrophotographic systems – part i: characterization and modeling". *Journal of Mechatronics*, Oct 2008. 16

[69] C.-L. Chen and G. Chiu. "halftone banding reduction for a class of electrophotographic systems – part ii: closed-loop control". *Journal of Mechatronics*, Oct 2008. 16, 18

[70] C.-P. Weng C.-L. Chen. "on modeling and simulation of digital laser printing: an integrated model from binary image to toner image". *Journal of the Chinese Institute of Engineers*, May 2009. 16

[71] Y.-S. Yang C.-L. Chen. "position-dependent disturbance rejection using spatial-based adaptive feedback linearization repetitive control". *Journal of Robust and Nonlinear Control*, Aug 2009. 16

[72] S.-H. Lin C.-L. Chen. "formulating and solving a class of optimization problems for high-performance gray world automatic white balance". *Journal of Applied Soft Computing*, Jan 2011. 16

[73] S.-H. Lin C.-L. Chen. "intelligent color temperature estimation using fuzzy neural network with application to automatic white balance". *Journal of Expert Systems with Applications*, June 2011. 16

[74] C.-L. Chen Y.-H. Yang. "spatial-based adaptive iterative learning control of nonlinear rotary systems with spatially periodic parametric variation". *Journal of Innovative Computing, Information and Control*, June 2011. 16

[75] C.-L. Chen C.-P. Weng. "optimal parameter design for a laser printing system using fuzzy multi-objective genetic algorithm". *Journal of the Chinese Institute of Engineers*, June 2011. 16

[76] C.-P. Weng C.-L. Chen. "a multi-objective problem based on fuzzy inference with application to parametric design of an electrophotographic system". *Journal of Expert Systems with Applications*, July 2011. 16

[77] C.-Y. Chiu C.-L. Chen. "a fuzzy neural approach to design of a wiener printer model incorporated into model-based digital halftoning". *Journal of Applied Soft Computing*, Apr 2012. 16

[78] C.-L. Chen Y.-H. Yang. "spatial domain adaptive control of nonlinear rotary systems subject to spatially periodic disturbances". *Journal of Applied Mathematics*, July 2012. 16

[79] Li C. "a short bibliography of pontrjagin's maximum principle of the theory of optimal control". *Automatic Control, IRE Transactions on*, vo. 7:pp. 74–75, Jan 1962. 21

[80] Groginsky Herbert L. "on a property of optimal controllers with boundedness constraints", May 1961. 21

[81] Kalman R. "on the general theory of control systems". *Automatic Control, IRE Transactions on*, vol. 4:pp. 110, Dec 1959. 21

[82] Pan X. Todorov E., Li W. "from task parameters to motor synergies: A hierarchical framework for approximately optimal control of redundant manipulators". *Journal of Robotic Systems*, vol. 22:pp. 691–719, 2005. 22

[83] Beheshti M.T. H. Farhoodi M. "extended linear matrix inequality approach to multiobjective output feedback controller design". In *India Conference, 2008. INDICON 2008. Annual IEEE*, volume vol. 2, pages pp. 542–547, Dec 2008. 24

[84] Takehiro Oishi Yimei Yu Jie Yu, Hiroshi Yamaura. "vibrations suppression control of image transfer belt system with flywheel or dynamic vibration absorber". *Journal of Advanced Mechanical Design Systems and Manufacturing*, Jan 2013. 29

[85] Ian Postlethwaite Sigurd Skogestad. *Multivariable Feedback Control Analysis and Design*. John Wiley and Sons Press, Chichester, New York, second edition, 2001. 43

[86] Samad T. *Variable Structure and Sliding Mode Control*. Wiley-IEEE Press, New York, first edition, 2001. 45

[87] Mitsuda H. Murakami K., Komori M. "flywheel energy storage system using smb and pmb". *Applied Superconductivity, IEEE Transactions on*, vol. 17:pp. 2146–2149, June 2007. 47

[88] U. Schaper, O. Sawodny, T. Mahl, and U. Blessing. "modeling and torque estimation of an automotive dual mass flywheel". In *American Control Conference, 2009. ACC '09.*, pages 1207–1212, June 2009. 47

[89] Makan Fardad Mihailo R. Jovanovic. "h2 norm of linear time-periodic system: A perturbation analysis". *Journal of Automatica*, Mar 2008. 53

[90] K. Glover K. Zhou, J. C. Doyle. *Optimal and Robust Control*. Prentice Hall Press, New York, second edition, 2001. 54

[91] Toscano R. *Structured Controllers for Uncertain Systems: A Stochastic Optimization Approach*. Springer Press, New York, second edition, 2013. 54

[92] Pramod P. Khargonekar Mario A. Rotea. "h2-optimal control with an h-inf constaint: The state feedback case". *Journal of Automatica*, vol. 2:pp. 307–316, 1991. 58

[93] Sayed A. *Linear Algebra*. Wiley-IEEE Press, New York, first edition, 2008. 58

[94] Eric Feron Venkataramanan Balakrishnan Stephen Boyd, Laurent EI Ghaoui. *Linear Matrix Inequalities in System and Control Theory*. SIAM Press, New York, first edition, 1994. 59

[95] Denis Arzelier Yoshio Ebihara, Dimitri Peaucelle. *S-Variable Approach to LMI-Based Robust Control*. Springer Press, Kyoto, Toulouse, second edition, 2014. 60, 63

[96] Theodor Y. Shaked U. "h infin;-optimal estimation: a tutorial". In *Decision and Control, 1992., Proceedings of the 31st IEEE Conference on*, 1992. 76

[97] Pierre R. Belanger. *Control Engineering: A Modern Approach*. Oxford University Press, New York, first edition, 1995. 76

[98] Pierre Bernhard Tamer Basar. *H-Infinity Optimal Control and Related Minimax Design Problems: A Dynamic Game Approach*. Springer Science and Business Media Press, U.S.A, France, second edition, 1995. 77

[99] Keith Glover. H-infinity control. In John Baillieul and Tariq Samad, editors, *Encyclopedia of Systems and Control*, pages 1–9. Springer London, 2014. 77

[100] Hara S. Iwasaki T. "generalized kyp lemma: unified frequency domain inequalities with design applications". *Automatic Control, IEEE Transactions on*, vol. 50:pp. 41–59, Jan 2005. 79

[101] Guo K.-H. Chen H., Sun P.-Y. "constrained h-infinity control of active suspensions: an lmi approach". In *Control and Automation, 2002. ICCA. Final Program and Book of Abstracts. The 2002 International Conference on*, pages pp. 157–157, June 2002. 81

[102] Mary A. D. "robust lmi based control of wheeled mobile robots". In *Computer Science Education (ICCSE), 2011 6th International Conference on*, pages pp. 1404–1409, Aug 2011. 83

[103] Tay E. B. Ang E.L. Ho W. K., Gan O. P. "performance and gain and phase margins of well-known pid tuning formulas". *Control Systems Technology, IEEE Transactions on*, vol. 4:pp. 473–477, Jul 1996. 90

[104] T. Hagglund K. J. Astrom. "revisiting the ziegler-nichols step response method for pid control". *Journal of Process Control*, Sep 2004. 90

[105] Uy-Loi Ly Ewald Schoemig, Mario Szanier. "mixed h2/h-infinity control of multimodel plants". *Journal of Guidance, Control, and Dynamics*, May-June 1995. 97

[106] Issac Yaesh Eli Gershon, Uri Shaked. *H-Infinity Control and Estimation of State-Multiplicative Linear Systems*. Springer Science and Business Media Press, Israel, first edition, 2005. 97

[107] Rotea M. A. Khargonekar P. P. "mixed h2/h infin; control: a convex optimization approach". *Automatic Control, IEEE Transactions on*, vol. 36:pp. 824–837, Jul 1991. 97

[108] Arturo Molina Cristobal. *Multiobjective Control: Linear Matrix Inequality Techniques and Genetic Algorithms Approach*. PhD thesis, The University of Sheffield, Department of Automatic Control and System Engineering, 2005. 101

List of Publications

Academic Journal

(1) Jie Yu, Hiroshi Yamaura, Takehiro Oishi, and Yimei Yu, "Vibrations Suppression Control of Image Transfer Belt System with Flywheel or Dynamic Vibration Absorber", *Journal of Advanced Mechanical Design, Systems, and Manufacturing*, Vol. 7, No. 1, pp. 52-64, 2013 *refer to Chapter 2*

(2) Jie Yu, and Hiroshi Yamaura, "Vibration Reduction Design for Image Transfer Belt System with H_∞ Optimal Control Configuration", *Journal of Microsystem Technologies*, submitted in Sept. 2014, under review. *refer to Chapter 4*

(3) Jie Yu, and Hiroshi Yamaura, "Optimal State Feedback Controller Design for Vibration Attenuation in a Class of Image Transfer Belt", *Journal of Applied Mechanics and Materials*, accepted in Nov. 2014, in press. *refer to Chapter 3*

International Conference Proceeding

(1) Jie Yu, Hiroshi Yamaura, Takehiro Oishi, and Yimei Yu, "Vibration Suppression Control of Image Transfer Belt System", *CD-ROM Proceedings*, 2012 ASME-ISPS/JSME-IIP Joint International Conference on Micromechatronics for Information and Precision Equipment (MIPE 2012), Santa Clara University, Santa Clara, California, U.S.A, June 18-20, 2012. *refer to Chapter 2*

(2) Jie Yu, and Hiroshi Yamaura, "Optimal Mixed H_2/H_∞ Controller Design for Vibration Suppression in a Class of Image Transfer Belt", *Proceedings of Control and Automation (MED), 2014*, pp. 1383-1387, *IEEE*, the 22nd Mediterranean Conference on Control and Automation (MED'14), University of Palermo, Palermo, Italy, June 16-19, 2014. *refer to Chapter 5*

(3) Jie Yu, and Hiroshi Yamaura, "Vibration Reduction for Image Transfer Belt System with H_∞ Optimal Control Configuration", *Proceedings of 2014 Conference on Information Storage and Processing Systems*, pp. V001T08A001, *ASME Proceedings*, the 23rd ASME Conference on Information Storage and Process Systems (ISPS 2014), Santa Clara University, Santa Clara, California, U.S.A, June 23-24, 2014. *refer to Chapter 4*